23RD HYDRONAV 2023

INTERNATIONAL SYMPOSIUM ON HYDRODYNAMICS IN SHIP DESIGN, SAFETY, MANOEUVRING AND OPERATION

MAY 24-26TH, 2023, SOPOT, POLAND

SCIENTIFIC COMMITTEE

- Prof. PhD, DSc., Eng. Teresa Abramowicz-Gerigk – Gdynia Maritime University
- Prof. PhD, DSc., Eng. Zbigniew Burciu – Gdynia Maritime University
- Prof. PhD, DSc., Eng. Paweł Dymarski – Gdańsk University of Technology
- Prof. PhD, DSc., Eng. Iwona Kochańska – Gdańsk University of Technology
- Prof. PhD, DSc., Eng. Przemysław Krata – Gdańsk University of Technology
- PhD, DSc. Tomasz Marcinkowski – Maritime Institute of the Gdynia Maritime University
- Prof. PhD, DSc., Eng. Jerzy Matusiak – Aalto University School of Engineering (Emeritus Professor)
- Prof. PhD, DSc., Eng. Jacek Misztal – Gdańsk University of Technology
- PhD, DSc., Eng. Jacek Nowicki – Foundation for Safety of Navigation and Environment Protection
- PhD, DSc., Eng. Maciej Reichel – Foundation for Safety of Navigation and Environment Protection
- PhD, DSc., Eng. Wojciech Sulisz – Institute of -Engineering of the Polish Academy of Sciences
- Prof. PhD, DSc., Eng. Tadeusz Szelangiewicz – Maritime University of Szczecin
- PhD, DSc., Eng. Zbigniew Szozda – Maritime University of Szczecin
- Prof. PhD, DSc., Eng. Jarosław Tęgowski – University of Gdańsk
- PhD, DSc. Monika Warmowska-Gadzińska – Polish Register of Shipping

ORGANIZING COMMITTEE

Polish Register of Shipping

- Monika Warmowska-Gadzińska
- Kinga Lowińska-Neumann
- Marek Narewski
- Karolina Kruszewska
- Agnieszka Iwan-Rząska

Gdańsk University of Technology

- Paweł Dymarski
- Hanna Pruszko

TABLE OF CONTENTS

Teresa Abramowicz-Gerigk, Zbigniew Burciu, Jacek Jachowski, Henryk Pepliński
MULTI-FUEL TWIN-HULL YACHT WITH A HYDROGEN CELL 5

Sebastian Bielicki
MODELLING THE HULL-THRUSTER INTERACTION IN MANOEUVRING SIMULATIONS 9

Sebastian Bielicki, Michał Kalbarczyk
MODERN REGRESSION TECHNIQUES IN HULL RESISTANCE PREDICTIONS 15

Ewelina Ciba, Paweł Dymarski
MODELING OF DISPLACEMENTS OF AN OFFSHORE WIND PLATFORM
IN THE ANSYS AQWA PROGRAM EXTENDED WITH THE INFLUENCE OF VISCOSITY 25

Patryk Dobreńko, Marek Kraskowski and Tomasz Bugalski
VALIDATION OF THE CFD ANALYSIS FOR AN OLYMPIC CANOE WITH TAKING
INTO ACCOUNT ACCURATE ANALYSIS OF THE AERODYNAMIC RESISTANCE................................ 26

Bartosz Dombrzalski, Janusz Narewski
APPROACHES AND CHALLENGES TO DETERMINING POWER-SPEED
CHARACTERISTICS AND REFERENCE SPEED FOR THE CALCULATION
OF EEXI ENERGY EFFICIENCY INDICATORS.. 31

Radosław Kołodziej
INVESTIGATION OF THE TUG INDIRECT MODE ESCORT MANEUVERS
WITH THE USE OF MODEL TESTS.. 32

Krzysztof Jacek Kołwzan
NEW 2023 IMO REQUIREMENTS ON VESSELS ENERGY EFFICIENCY. METHODOLOGY
OF IN-SERVICE PERFORMANCE MEASUREMENTS TO DETERMINE REFERENCE
SPEED TO CALCULATE AN ENERGY EFFICIENCY EXISTING SHIP INDEX EEXI 38

Arun Krishnan, Tomasz Hinz and Grzegorz Mazerski
BULK CARRIER WITH RIGID SAILS – COMBINED EFFECTS
OF REALISTIC WEATHER CONDITIONS.. 44

Król Przemysław
NUMERICAL ASPECTS OF LIFTING FOIL SYSTEMS DESIGN AND ANALYSIS.................................. 53

Leszek Kwapisz, Jan Andrzej Szantyr, Marek Narewski
DETERMINATION OF THE VORTEX WAKES BEHIND OFFSHORE WIND TURBINES 58

Karol Listewnik
OVERVIEW OF CALIBRATION METHODS FOR UNDERWATER ACOUSTIC
AND PRESSURE SENSORS FOR SHIP MEASUREMENT 64

Zbigniew Macikowski, Artur Karczewski and Przemysław Krata
TOWARDS DEFINING OF A CORRELATION BETWEEN EXPERT TRIAL
IN OPERATIONAL CONDITIONS AND HYDRODYNAMIC CHARACTERISTICS OBTAINED
USING CFD SIMULATION FOR A WINDSURFING FOILING CLASS FRONT WING............................. 65

Anna Miller, Andrzej Rak
MODELING OF THE LAKE WAVES FOR THE ENVIRONMENTAL DISTURBANCES
SIMULATION OF THE SCALE SHIP MODEL.. 70

Marek Narewski
UNDERWATER RADIATED NOISE REDUCTION IN LIGHT
OF CLASS SOCIETIES INITIATIVES 76

Hanna Pruszko, Maciej Reichel, Krzysztof Czerski, Marek Necel
NUMERICAL OPTIMISATION OF POD PROPELLER REVOLUTION FOR A CONTAINER SHIP
WITH A HYBRID TWIN-CRP-POD PROPULSION SYSTEM 80

Piotr Pruszko Maciej Reichel
OPEN WATER MODEL TESTS OF BRASS AND 3D-PRINTED COMPOSITE
PROPELLER: FDM AND SLS 86

Emil Roch and Krzysztof Woloszyk
SIMPLIFIED METHOD TO ANALYSE THE WHIPPING-INDUCE VIBRATIONS
IN CONTAINER SHIPS 87

Mohammad Sadeghi, Hamid Zeraatga, Mohammad Hossein Ghaemi, Mojtaba Barjasteh
TIME-DOMAIN NUMERICAL EVALUATION OF SHIP RESISTANCE AND MOTION
IN REGULAR WAVES BY USING THE CFD URANS METHOD 91

Aleksander M. Schmidt
HYDROACOUSTICS TESTING LABORATORY – RESEARCH CAPABILITIES
AND COMPETENCES 100

Prashant Singh
INVESTIGATION OF MEWIS DUCT AS ENERGY SAVING DEVICE
USING COMPUTATIONAL FLUID DYNAMICS -AN OVERVIEW 101

Jarosław Soliwoda, dsc eng.
SECURING CARGO IN CONTAINERS IN RELATION TO THE REQUIREMENTS
OF THE CSC CONVENTION 107

Sebastian Sorek, Wojciech Sulisz
A 3D ANALYTICAL MODEL FOR THE INTERACTION OF WATER WAVES
WITH AN OSCILLATING BREAKWATER 113

Jarosław Tęgowski, Karolina Trzcińska
UNDERWATER NOISE GENERATED BY SHIP TRAFFIC IN THE POLISH BALTIC
WATERS – RESULTS OF THE BIAS EU PROJECT 115

Monika Warmowska-Gadzińska, Krzysztof Wołoszyk
NUMERICAL MODELING OF CONTAINERSHIP BEHAVIOUR ON WAVES TAKING
INTO ACCOUNT THE WHIPPING AND SPRINGING PHENOMENA 119

Mateusz Weryk
UNDERWATER NOISE ISSUES 127

MULTI-FUEL TWIN-HULL YACHT WITH A HYDROGEN CELL

Teresa Abramowicz-Gerigk[1], Zbigniew Burciu[2], Jacek Jachowski[3] and Henryk Peplinski[4]

[1, 2, 3] Gdynia Maritime University, Department of Ship Operation, Faculty of Navigation, POLAND.

(E-mail: t.gerigk@wn.umg.edu.pl, z.burciu@wn.umg.edu.pl, j.jachowski@wn.umg.edu.pl)

[4] HIGH-FLIER Sp. z o.o., POLAND.

(E-mail: henryk.pelplinski@galliot.pl)

Keywords: catamaran, hydrogen cell, multi-fuel yacht,

ABSTRACT

The paper presents investigations on the implementation of an eco-efficient multi-fuel propulsion system on a double-hull yacht with four types of power sources including diesel oil, liquefied petrol gas (LPG), compressed natural gas (CNG), photovoltaic panels and hydrogen cell. The initial design with the hull form for which the resistance calculations were optimized using the CFD method. The most important issues related to the safe operation of the designed propulsion system on the background of the applicable regulations of classification societies are discussed.

1 INTRODUCTION

According to EU Directive 2014/94/EU the emission of CO2 from vessels should be reduced by 40% by 2050 compared to 2005 levels. Thanks to research on the use of green energy on ships, we can observe the continuous development of environmentally friendly solutions [1,4,5,8].

Eco-friendly yachts as means of transport and recreation become important elements of modern forms of ecotourism preventing negative impacts on nature and encouraging tourists to promote nature conservation and socio-economic development. The access to green energy sources is still very limited however the transitional hybrid solutions combining conventional and ecological drives are emerging. The ecological source is usually an additional element with limited application possibilities. The proposed solution is a combination of innovation and safety, through the use of proven and alternative sources. It combines classic duel-fuel diesel engines generators, fuel cells and photovoltaic panels with a developed methodology for using these power sources in various configurations. The possibility of using hydrogen as a source of green energy, included the latest hydrogen technologies, was recently confirmed by research conducted on experimental and prototype boats “Energy Observer” [9], “HYNOVA” [10] and “Aquon One” [11] and the conclusions drawn from their operation were considered in the presented study.

The elements of the multi-fuel system and their configuration were selected depending on their function and expected operational limitations of the yacht - resistance and propulsion properties, and stability. Design constraints included: emission of harmful compounds of carbon dioxide and monoxide, hydrocarbons, nitrogen oxides and particulate matter in exhaust gases as well as noise emission. The most important issue of the presented study was the safety of operation of the multi-fuel system with hydrogen cells and the related development of classification rules.

2 METHODOLOGY

The main design objective was development of the twin-hull yacht with eco-effective electrically-powered propulsion system with 20 m maximum length. It was assumed that it will be an experimental catamaran for testing hybrid drives, with three independent engine rooms.

Each engine room can work alone or in combination with the others. The innovative approach in designing involved the use of ecological energy sources combined with the wide range of yacht operation tests. The idea of a multi-fuel propulsion system was to enable the yacht to operate using various energy sources.

When selecting the fuels, the impact on the environment was taken into account followed by the safety of use, due to significant price fluctuations on the market and the lack of green hydrogen on the domestic market, the criteria of fuel unit consumption were adopted in economic considerations.

The marine low sulphur diesel oil (MDO), liquified petrol gas (LPG), compressed natural gas (CNG) and hydrogen (H2) were considered as the main energy sources. Photovoltaic panels, wind turbine converting wind energy into electricity and hydrogenator were considered as auxiliary energy supply sources. The main design assumptions were as follows: maximum overall dimensions of the catamaran – length and breadth no greater than 20 m and 8 m respectively, cruising range of 200 nautical miles (Nm), cruising speed of 10 knots (kn), in the zero-emission mode in various operating conditions and reduction of pollutant emissions.

A block diagram of a developed plug-in series hybrid multi-fuel propulsion system using individual and independent energy sources is presented in Figure 1.

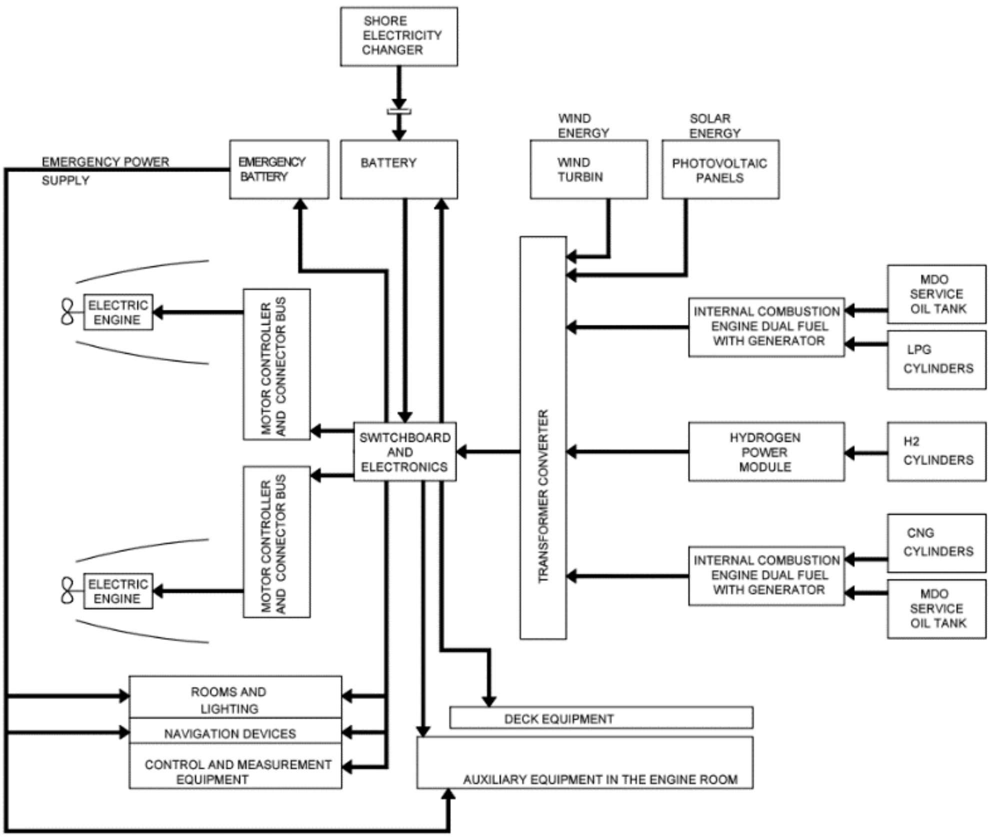

Figure 1 Block diagram of a plug-in series hybrid multi-fuel propulsion system.

3 RESULTS AND DISCUSSION

Resistance analysis using the CFD method was carried out for five versions of the catamaran hull form in the speed range from 6 to 15 kn for two drafts T=1 m and T=1.2 m taking into account the variable trim and draft during the simulation for the given displacement. The calculations were carried out on the principle of reversed flow.

The geometry of the first version of the catamaran used for calculations and results of simulation – curve of hydrodynamic resistance as a function of speed v and free surface elevation at speed of 10 kn and 1 m designed draft is presented in Figure 2.

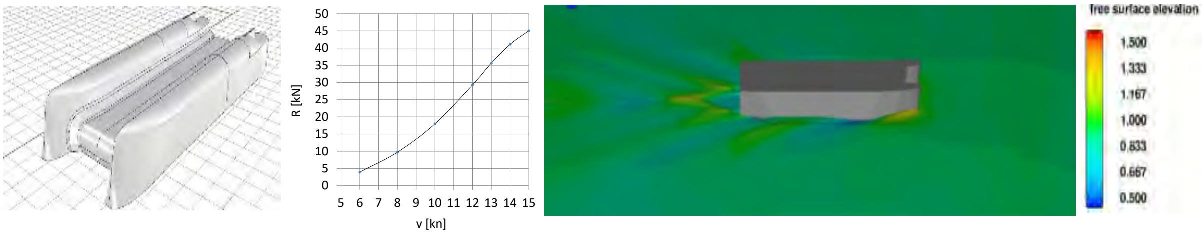

Figure 2 The geometry of the catamaran, resistance curve at 1m draft and free surface elevation at 10 kn.

For a range of 200 nautical miles and an operating speed of 10 knots, the energy reserve provided by the fuel cell and hydrogen stored in the tanks should amount to 1000 kWh. This corresponds to 63 kg of hydrogen, in 8 standard cylindrical tanks at a pressure of 350 bar. The weight of the cell and hydrogen tanks per 1 kWh of energy is 1.7 kg, hence the weight of the hydrogen-powered module is 1700 kg. The production of 1 kWh of electricity is accompanied by 1 kWh of thermal energy, which can be used to heat water. The unit weight of lithium-ion batteries per 1 kWh of stored energy is 12.5 kg. It is more than 6 times higher than for the fuel cell and hydrogen tanks.

In the designed system, energy storage in the form of batteries is provided only for the purposes of starting the aggregates, heating the fuel cell to the operating temperature of 80°C and emergency power supply. The yacht's drive will be adapted to work in automatic mode and starting the fuel cell will not require an external power supply, but it is also possible to use energy from an external power source.

The principles of using compressed hydrogen are similar to those for compressed natural gas (LNG) [3]. However, the range of issues and threats resulting from safe use is definitely larger and requires a wider application of appropriate security systems. The high permeability of hydrogen and the property to quickly and easily enter into chemical reactions, in the event of large or uncontrolled leaks, poses a risk of explosions in contact with oxygen or obtaining toxic chemical compounds when in contact with nitrogen. Monitoring of installations and rooms with sensors alone is not sufficient. It is also necessary to constantly check with thermal imaging cameras because the flame during the reaction of hydrogen with oxygen is invisible to the human eye.

Appropriate security procedures are necessary, launched automatically in the event of a failure or other reasons causing damage to the instance.

It is also very important to prepare appropriate procedures and fire extinguishing systems, especially since hydrogen cells power the electrical installation, energy receivers as well as lithium-ion batteries [6]. It is an interconnected system and in the event of a fire it is very important to consider the interactions.

4 CONCLUSIONS

The base emission value for a classic drive with two combustion engines is 6300 g/Mm, the target value for the drive proposed in the project: fuel cells, diesel and LPG or CNG generators was 2200 g/Mm. The base value of diesel fuel consumption at the speed of 10 knots is 120 dm^3/100 km (222 dm^3/100 Nm). The target value of fuel consumption should be 40 dm^3/100 km (74 dm^3/100 Nm) using energy from combustion generators (including diesel and LPG or CNG) and a hydrogen cell, i.e. three times less compared to the basic solution.

Classification Societies are currently working on developing Regulations on the use of hydrogen. The analysis of the entire process related to safety and technical functionality design, should also take into account the time of planned operation of the system and its individual devices [7]. DNV has published Handbook for Hydrogen-Fuelled Vessels [2] with the aim of more effective alternative design approval process while developing the knowledge base for future approval according to DNV and IMO rules.

ACKNOWLEDGMENT

The research presented in the paper was supported by The National Centre for Research and Development grant POIR.01.04.01.00-0067/20 and Gdynia Maritime University Grants: WN/2023/PZ/03, WN/2023/PZ/08 and WN/PI/2023/04.

REFERENCES

[1] Alfonsín, V., Suarez, A., Cancela, A., Sanchez, A., Maceiras, R., Modelization of hybrid systems with hydrogen and renewable energy oriented to electric propulsion in sailboats. Int. J. Hydrogen Energy, 39, 2014, 11763–11773.

[2] Handbook for Hydrogen-Fuelled Vessels. DNV, MarHySafe JDP, Maritime Hydrogen Safety Joint Development Project, Phase 1, 1st Edition (2021-06).

[3] Klebanoff, L.E., Pratt, J.W., LaFleur, C.B., Comparison of the safety-related physical and combustion properties of liquid hydrogen and liquid natural gas in the context of the SF-BREEZE high-speed fuel-cell ferry. International Journal of Hydrogen Energy, 42, 1, 2017, 757-774.

[4] Lebkowski, A., Analysis of the use of electric drive systems for crew transfer vessels servicing offshore wind farms. Energies, 13, 2020, 1466.

[5] Lesniewski, W., Piatek, D., Marszalkowski, K., Litwin, W., Small Vessel with Inboard Engine Retrofitting Concepts; Real Boat Tests, Laboratory Hybrid Drive Tests and Theoretical Studies, Energies, 13, 2020, 2586, doi:10.3390/en1310258.

[6] Mylonopoulos, F., Boulougouris, E., Trivyza, N.L., Priftis, A.; Cheliotis, M., Wang, H., Shi, G., Hydrogen vs. Batteries: Comparative Safety Assessments for a High-Speed Passenger Ferry. Applied Science, 12, 2022, 2919. https://doi.org/10.3390/app12062919

[7] Safe use of hydrogen as a fuel in commercial industrial applications, Information publication 11/I, June 2021, PRS.

[8] Shi, G., Priftis, A., Xing-Kaeding, Y., Boulougouris, E., Papanikolaou, A.D., Wang, H., Symonds, G., Numerical Investigation of the Resistance of a Zero-Emission Full-Scale Fast Catamaran in Shallow Water. J. Mar. Sci. Eng. 2021, 9, 563. https://doi.org/10.3390/jmse906056363.

[9] https://www.energy-observer.org/about/vessel.

[10] https://www.hynova-yachts.fr/hynova-40/.

[11] https://newatlas.com/marine/aquon-one-solar-hydrogen-yacht/.

MODELLING THE HULL-THRUSTER INTERACTION IN MANOEUVRING SIMULATIONS

Sebastian Bielicki[1, 2]

[1] Ship Hydromechanics Division, Maritime Advanced Research Centre, POLAND.

(E-mail: sebastian.bielicki@cto.gda.pl)

[2] Faculty of Mechanical Engineering and Ship Technology, Gdansk University of Technology, POLAND.

(E-mail: sebastian.bielicki@pg.edu.pl)

Keywords: Azimuth thrusters, hydrodynamic forces, manoeuvring, mathematical model, wake fraction

ABSTRACT

The experimental based method for evaluation of the steady forces acting on the azimuth thruster in oblique flow are presented in this paper. The origin of method is based on momentum equation for quasi-stationary, incompressible flow where the rotational velocity induced by propeller is neglected. The experiments were conducted in homogeneous flow conditions with wide variation of inflow angles and couple sets of advance ratio. The flow angle corrector was estimated basing on these experiments which is the main outcome of this method. This factor can be applied on commonly exploited open water characteristics of azimuth thrusters and adopted as a parameter to evaluate thrust and side force in manoeuvring simulations. Further the method was evaluated on azimuth thrusters working in behind the hull conditions, thus the axial velocity flow correction (wake fraction) was estimated by simplified formula. The parameters of proposed wake fraction correction formula was found by regression analysis of experimental data taken out from planar motion mechanism (PMM) tests conducted on hull propelled by propeller driven azimuth thrusters and towed with various drift angles and yawing speeds.

1 INTRODUCTION

Azimuth thrusters have become more popular propulsion system installed not only on service or ferry vessels but also on small and medium size chemical tankers [7] in recent years. The manoeuvring properties of vessels are important features in ship design [2], [5] and their manoeuvrability is typically assessed using free running, scaled models. Alternatively, manoeuvrability can be assessed through simulations [9], in which the parameters of the equations of motion are identified using captive model tests. One of these parameters is the forces acting on thrusters, which must be formulated by a mathematical model to ensure flexibility in simulations approach. Another parameter is the mathematical formula used to estimate the velocity of water inflow to the thrusters. The authors' method for identifying the aforementioned parameters is presented in this paper. The forces on thrusters and the formula for estimating water inflow velocity are evaluated through model tests. The tests are conducted on a free-running thruster, as well as in conditions behind the hull. The inflow velocity in behind-hull conditions is evaluated using wake fraction formulae proposed by the author.

2 THRUSTER FORCES

The reaction forces acting on azimuth thruster in oblique flow conditions, can be found by free running model tests carried out in variety of thruster angles δ and advance ratios, J. This approach is cost and time consuming thus this paper is introducing quasi empirical method for evaluation of side and thrust force in oblique flow conditions. The coordinate system and sign conventions are presented in **Figure 1**

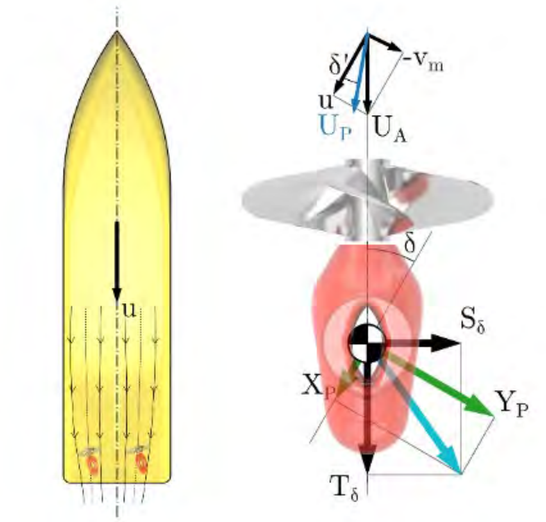

Figure 1 Coordinate system

The origin of this method was originally proposed by Matusiak in [5], which proposed the evaluation of reactions to oblique flow inflow velocities by momentum theory. The thrust from open water curves $K_T - J$ is derived in straight flow conditions as follows:

$$T_\delta = K_{T\delta}\rho D^4 n^2$$

where $K_{T\delta}$ is the thrust coefficient derived from open water curves at advance ratio J_δ, which is repersented by formula:

$$J_\delta = \frac{u_P}{nD}$$

and n is the propeller rate of revolutions and D is the propeller diameter. Side force S_δ can be found, by the momentum theory, as a resultant hydrodynamic reaction to velocities acting on thruster by formula:

$$S_\delta = \rho A_p\left(\Delta u_p + u_p\right)v_p$$

The propeller-induced velocity Δu_p in the propeller plane, which is represented by the expanded area $A_p = 1/4\pi D^2 A_E/A_0$ is determined using Bernoulli's principle as shown in equation below:

$$\Delta u_p = \frac{1}{2}u_P\left(-1 + \sqrt{1 + \frac{8K_{T\delta}}{\pi J_\delta^2}}\right)$$

The inflow velocity components in propeller plane are found by (according to [2], [7]):

$$u_p = u\left(1 - w_p\right)\cos(c_\delta \delta)$$

$$v_p = u(1 - w_p)\sin(c_\delta \delta)$$

The effective wake fraction w_p in the aforementioned equations is impacted by both the drift angle β and the yaw rate r. The relationship between w_p and the wake fraction w_T, which is evaluated through self-propulsion tests, can be determined using equation:

$$\frac{1 - w_p}{1 - w_T} = 1 + \alpha_1 \left(1 - e^{-\left|\frac{\beta_p}{\alpha_2}\right|^{\frac{9}{4}}}\right)$$

This equation expresses the ratio of $1 - w_p$ to $1 - w_T$ as a function of geometrical inflow to the thruster β_p, where α_2 represents the rate of effective axial velocity change with respect to β_p. The value of α_2 is such that the left-hand side of above equation reaches $1 + \alpha_1$. The geometrical inflow to the thruster is defined as:

$$\beta_P = \beta - \gamma r \frac{x_T}{L}$$

where x_T is the distance location of thruster relative to the midship, while the reference length ship is L and γ is the flow straightening coefficient, proposed originally by Kose et al. in [4] for conventional propeller rudder vessels and earlier by Tuda and Fuji in [1], however the physical meaning is very similar.

3 EXPERIMENTS

Model tests of azimuth thrusters in homogeneous oblique flow conditions were carried out in the CTO large towing tank, and the complete results of the tests were published by Reichel in [9]. The scaled model of the azimuth thruster, which was propelled by a propeller with the geometry shown in Table 2, was towed at speeds of 0.67m/s, 1.33m/s, and 2.00m/s, and then at zero speed with deflection angles δ ranging from 0° to 55° on both sides, with a step of 5°. The propeller revolution was kept constant at 15.0 1/s, which ensured that the Reynolds number was high enough to consider turbulent flow conditions.

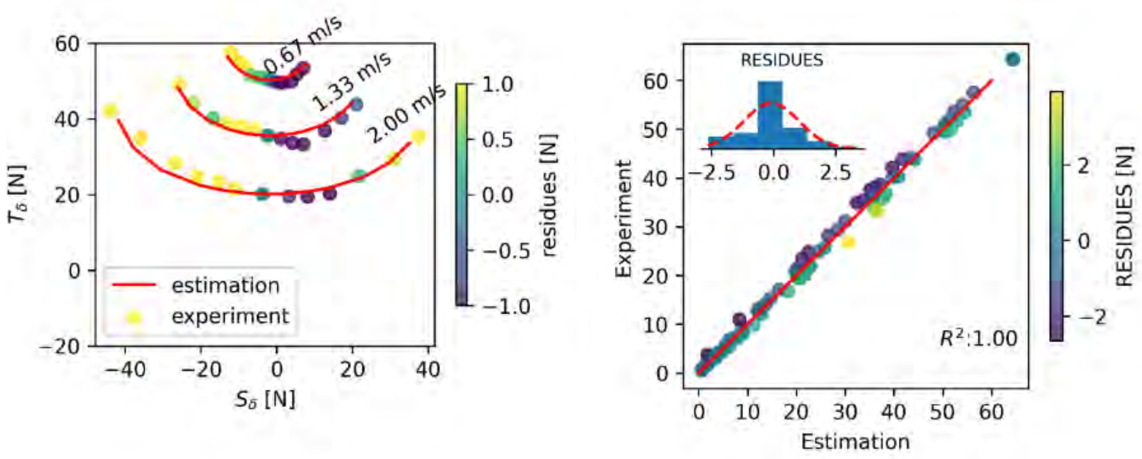

Figure 2 Hydrodynamic forces on thruster in homogeneous, oblique flow.

Model tests for thrusters working in the behind-hull conditions were tested on towed hull model equipped by two azimuth thruster propelled by propeller models. The geometry particulars of the hull and propeller models are presented in Table 1 and Table 2 respectively. These tests were conducted at a towing speed of $1.46m/s$ and with two propeller revolutions: 14.8 $1/s$ and 15.8 $1/s$. The thruster was deflected on both sides within the range of angle δ from 2° to 40°.

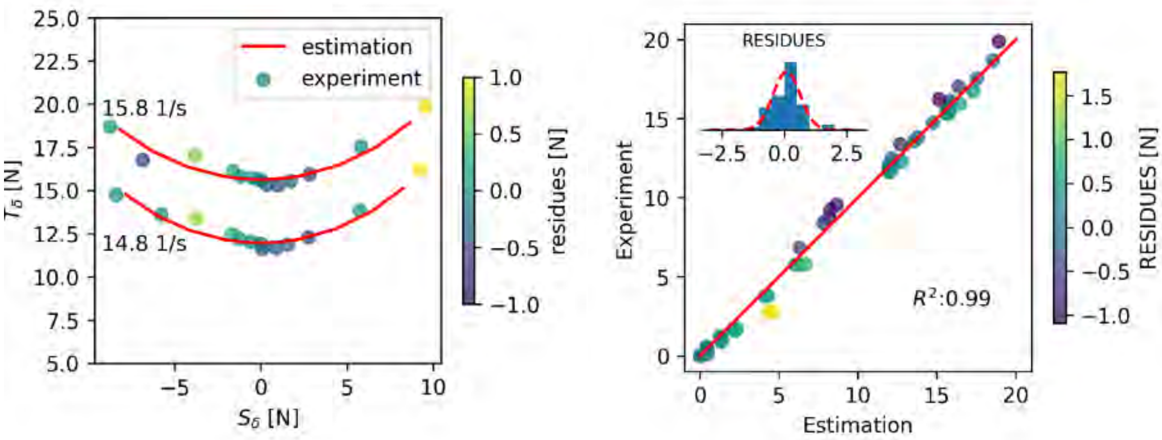

Figure 3 Hydrodynamic forces on thruster in behind the hull, oblique flow conditions.

The relationship between open water curves (POC) and oblique flow conditions was established through tests that involved measuring the hydrodynamic reactions on the entire unit, consisting of the propeller and body. The results presented in **Figure 2** showed good agreement with the proposed model. This agreement was further confirmed by the Person's R^2 coefficient of 1, and the residues demonstrated a normal distribution with maxima not exceeding 2.5N. Similar discrepancies were observed in the behind-hull conditions (BHC), as shown in **Figure 3**. However, the Person's R^2 is lower in this case, at 0.99, with residues following the same distribution pattern.

Table 1
Hull model particulars

L [m]	3.50
B [m]	0.75
T_A [m]	0.25
T_F [m]	0.19
CB	0.78
x_T/L	-0.45

The average axial flow velocity change behind the hull due to the geometrical inflow angle during the planar motion of the hull was evaluated from model tests in which the hull was towed by a planar motion mechanism (PMM) at different drift angles β and yaw rates r. The thrusters were in the position to generate thrust along the longitudinal axis of the hull. The axial inflow velocity was estimated by advance ratio shift evaluated from POC based thrust coefficient and behind the hull in motion thrust coefficient calculated from measured reactions on thruster-propeller system.

Table 2
Propeller models particulars

	POC	**BHC**
D [m]	0.125	0.161
P/D	1.100	0.785
A_E/A_0	0.635	0.550
z	4	4

The ratio $1 - w_P/1 - w_T$ was evaluated from direct measurements and approximated using a non-linear least squares trust region reflective algorithm to fit the empirical formula. The model was trained on 33% of the measured data, excluding outliers. Yasukawa and Yoshimura (H. Yasukawa 2015) revealed that the velocity behind the hull in planar motion is higher than in a straight run, and therefore, the outliers were mainly ratios below 1, which are non-physical. The quality of approximation, confirmed by $R^2 = 0.62$ and normal distribution of residues with most probable value between ± 0.05 is found to be enough for correction of inflow velocity in proposed model.

Table 3
Parameters of mathematical models

	BHC	**POC**
$c_{\delta\,(+)}$	0.70	0.99
$c_{\delta\,(-)}$	0.65	1.22
α_1	0.17	
α_2	0.48	

4 CONCLUSIONS

The method and regression formula proposed in this paper can be successfully applied in simulations when considering the planar motion of a ship's hull. The minor discrepancies between the theoretically predicted hydrodynamic reactions on the thruster, based on momentum theory, and empirically evaluated inflow correction coefficients lead to the conclusion that this approach can accurately predict forces. The main advantage of this method is that the simulator can be fed with POC thrust coefficients only, derived in axial inflow (typical thruster characteristics used in predicting ship's performance) and the c_δ coefficient. This good agreement is probably achieved due to the relatively small size of the azimuth thruster gondola. To further verify this, investigation of thrusters with larger units is necessary.

Another conclusion is that the behind-the-hull axial velocity of the flux while the ship is manoeuvring can be estimated using the proposed regression formula, which includes α_1 and α_2 empirical coefficients derived from PMM model tests. The approximation factors revealed worse correlation quality; however, the velocity drop of azimuth-thruster-driven ships is usually very small (below 10% of the ship's speed). Thus, the model applied in simulations will generate a small absolute error in water inflow velocity correction while manoeuvring.

REFERENCES

[1] H. Fuji, T. Tuda. 1961. “Experimental Research on Rudder Performance 2.” Journal of the Japan Society of Naval Architects and Ocean Engineers 110: 31–42.

[2] H. Yasukawa, S. Tanaka et al. 2009. “Study on Maneuverability of a Ship with Azimuthing Propellers.” Journal of the Japan Society of Naval Architects and Ocean Engineers 9: 155–65.

[3] H. Yasukawa, Y. Yoshimura. 2015. “Introduction of Mmg Standard Method for Ship Maneuvering.” Journal of Marine Science and Technology 20: 37–52.

[4] K. Kose, Y. Yoshimura, A. Yumuro. 1981. “Concrete of Mathematical Model for Ship Manoeuvring.” In Proceedings of the 3rd Symposium on Ship Maneuverability, III:27–80. The Society of Naval Architects of Japan.

[5] Matusiak, J. 2003. “Momentum Equation Applied to the Problem of a Propeller in Oblique Flow.” *Ship Technology Research, Shiffstechnik* 50 (3): 103–5.

[6] M. Woodward, M. Atlar, D. Clarke. 2003. “On the Manoeuvring Prediction of Pod Driven Ships.” In Proc. Of the International Conference on Marine Simulation and Ship Maneuverability, 7–1–7–9. MARSIM’03. Kanazawa, Japan: The Society of Naval Architects of Japan.

[7] N. Harata H. Yasukawa, S. Tanaka. Improving course stability of a ship with azimuthing propellers. Journal of the Japan Society of Naval Architects and Ocean Engineers, 10:123–133, 2009.

[8] Reichel, M. 2017. “Prediction of Manoeuvring Abilities of 10000 Dwt Pod-Driven Coastal Tanker.” Ocean Engineering 136: 201–8.

[9] Reichel, Maciej. 2007. “Manoeuvring Forces on Azimuthing Podded Propulsor Model.” Polish Maritime Research 14 (2): 3–8. https://doi.org/doi:10.2478/v10012-007-0006-0.

[10] Sasaki, Noriyuki, Jaap H. Allema, Mehmet Atlar, Se-Eun Kim, Valery Borusevich, Antonio Sanchez-Caja, Francesco Salvatore, and Chen-Jun Yang. 2008. “The Final Report of Specialist Committee on Azimuthing Podded Propulsion.” In 25th International Towing Tank Conference, 2:563–604. United Kingdom: University of Newcastle upon Tyne.

MODERN REGRESSION TECHNIQUES IN HULL RESISTANCE PREDICTIONS

Sebastian Bielicki[1, 2], Michał Kalbarczyk[1]

[1] Ship Hydromechanics Division, Maritime Advanced Research Centre, POLAND.

(E-mail: sebastian.bielicki@cto.gda.pl)

[2] Faculty of Mechanical Engineering and Ship Technology, Gdansk University of Technology, POLAND.

(E-mail: sebastian.bielicki@pg.edu.pl)

Keywords: ship's resistance, ship's performance prediction, machine learning, artificial intelligence, deep neural network

ABSTRACT

Machine learning (ML) and artificial intelligence (AI) becomes very popular approach in scientific data analyses recently. This paper tries to apply this techniques on database of ship resistance evaluated on model tests conducted in the towing tank. First part of work presents results of couple most common linear regression models, from the simplest Ridge and Lasso toward the more complex Random Forest and Gradient Boosting Regressor. Further in the paper the deep neural network approach for prediction of ship's resistance was studied. The analyses were carried out on the fishing vessel types to maximize accuracy of tested models. The residuary resistance coefficients is predicted basing on presented methods and further evaluated by standard ITTC methodology to achieve main goal which is the total resistance of ship. Accomplished results are evaluated basing on standard metrics such as Pearson correlation coefficient (coefficient of determination R^2) and mean square error (MSE). The results of presented study seems to be very practical on early stage design and may be used for primary estimation of engine power based on resistance results.

1 INTRODUCTION

Until today, the Holtrop-Mennen method [1] has been widely used as an empirical method for predicting the resistance of a ship's hull. This approach is based on a statistical analysis of data from model tests and has undergone several revisions and updates over the years to improve its accuracy and applicability to different types of ships [2]. Recently, machine learning (ML) and artificial intelligence (AI) have gained popularity as approaches for scientific data analysis, particularly for predicting a ship's performance based on resistance estimates. These techniques were applied by Khan [3] and later by Grabowska [4] to a database of ship resistance evaluated on model tests conducted in a towing tank . AI is used not only for estimating a ship's resistance in ideal conditions but also for predicting its performance in ice (see Sun et al. [5] or Milaković et al. [6]). The ML and AI models are not only built on the database of model tests but also on the database of the total resistance of ships currently designed and in operation. Yu Ao et al. [7] utilized a multiple-input neural network to develop a solution based on AI and data analysis. This solution can calculate hydrodynamic performance in real-time and predict the hydrodynamic performance of ship hulls by considering their modification parameters related to geometry. Tarelko and Rudzki [8] have applied artificial neural networks (ANN) successfully in modelling speed and fuel consumption basing on data set obtained from diesel driven tall ship Pogoria during sea trials. Yang et al. [9] verified Radial Basis Function Neural Network (RBFNN) and compared to the machine learning algorithms predicting performance of 13500TEU container ship. The comparable set of machine learning techniques as presented in this paper was used by Uyanık et al. in [10] for estimation of fuel consumption and based on actual ship data.

This paper employs the deep neural network preceded by two machine learning techniques using the results of model tests recently carried out on fishing vessels type. The first part of the work presents the comparison of six regression models. Later in the paper, the deep neural network approach was studied for predicting a ship's resistance. The analyses were carried out on fishing vessel types to maximize the accuracy of the tested models. The residuary resistance coefficients were predicted using the presented methods and further evaluated by the standard ITTC methodology to achieve the main goal of determining the total resistance of the ship. Finally the achieved results were evaluated based on standard metrics such as the Pearson correlation coefficient (coefficient of determination R^2) and mean square error (MSE).

2 MACHINE LEARNING MODELS

This section introduces short description of regression method applied in study. The independent variables presented in formulas are x as a scalar or X as a vector, whilst dependent variables is assigned to y.

2.1 Linear Support Vector Regression

Linear Support Vector Regression (LSVR) is a type of regression analysis technique that uses support vector machines (SVMs) to perform linear regression. In contrast to traditional linear regression, which tries to minimize the mean squared error between the predicted and actual values, SVR tries to minimize the generalization error ε of the model while still staying within a certain margin around the target variable. The linearized formula describing this problem according to Smola and Schölkopf [11]

$$\min_{w,b} \frac{1}{2} w^T w + C \sum_{i+1}^{n} m\,ax(0, |y_i - (w^T \phi(x_i) + b)| - \varepsilon)$$

where x_i $(i = 1, \dots, n)$ is the training vector and ϕ is the linear kernel function, w, b are the vector of regression parameters and $y_i \in \{1, -1\}^n$.

2.2 Lasso and Ridge

Least Absolute Shrinkage and Selection Operator (Lasso) is a linear regression model which simply adds a penalty term $\alpha||w||_1$ to the ordinary least squares (OLS) objective function in the equation above, which is a measure of the sum of squared errors between the predicted values and the actual values. This penalty term is proportional to the absolute value of the coefficients of the regression model, which encourages the model to produce coefficient values that are as close to zero as possible [12].

$$\min_{w} \frac{1}{2n} ||Xw - y||_2^2 + \alpha||w||_1$$

Similar to Lasso is the Ridge regression technique which adds a penalty term to the standard linear regression objective function in the equation above, which forces the coefficients to shrink towards zero, while still allowing all of the variables to contribute to the model. The objective function, proposed by Hoerl and Kennard [13]

$$\min_{w} ||Xw - y||_2^2 + \alpha||w||_2^2$$

The parameter α is an input constant, $||w||_1$ is the L1-norm and $||w||_2$ is L2-norm of coefficient w vector.

The L1-norm penalty encourages sparsity in the model, meaning that some of the coefficients will be exactly equal to zero, resulting in a simpler model with fewer predictors, whilst the L2-norm penalty forces the coefficients to shrink towards zero, but it doesn't force any of them to be exactly zero. These properties was selected as useful for feature selection and for dealing with data due to irrelevant or redundant features found in model tests data used in regression.

2.3 Extreme Gradient Boosting

Extreme Gradient Boosting is an algorithm that uses a combination of multiple weak decision trees to make predictions. Although it is commonly used for classification tasks, the focus of this paper is on its regression version, as formulated by Chen and Guestrin [14]:

$$y_i = \widehat{y}_i + \sum_{m=1}^{M} f_m(x_i),$$

where y_i is the true target value (dependent variable) of the i-th observation, $\widehat{y}_i$ is the initial prediction for the i-th observation, f_m is the m-th decision tree model, M is the total number of decision trees, and x_i is the feature vector (independent variable) of the i-th observation. The goal of XGBoost is to minimize a loss function, L, that measures the difference between the true target values and the predicted target values [14]:

$$L = \sum_{i=1}^{n} l(y_i, \widehat{y}_i) + \sum_{m=1}^{M} \Omega(f_m),$$

where n is the total number of observations, l is the loss function (mean squared error here), and Ω is the regularization term that penalizes complex models (large values of the decision tree coefficients). To prevent overfitting, XGBoost adds a regularization term to the loss function that penalizes complex models. The regularization term is defined as:

$$\Omega(f_m) = \gamma T + \frac{1}{2}\lambda \sum_{j=1}^{T} w_j^2,$$

where T is the total number of leaves in the decision tree, w_j is the weight associated with the j-th leaf, γ is the complexity parameter that controls the number of leaves in the tree, and λ is the regularization parameter that controls the magnitude of the weight penalty. The first term in the regularization penalty, γT, encourages simpler trees by penalizing trees with more leaves, while the second term, $\frac{1}{2}\lambda \sum_{j=1}^{T} w_j^2$, encourages small weights by penalizing large values of the weights w_j.

2.4 Gradient Boosting Regressor

Gradient Boosting Regressor (GBR) works by combining multiple weak learners to form a strong learner. The general idea of boosting is to sequentially add models to the ensemble, where each model is trained to correct the errors made by the previous models. Friedman in [15] gave set of algorithms for this technique which can be simplified as follows:

Algorithm 1 Gradient Boosting Regressor

Input: Training set $(x_1, y_1), \ldots, (x_n, y_n)$, number of iterations M, learning rate η, maximum depth of weak learner, minimum number of samples per leaf node

Output: Prediction function $F(x)$

$F_0(x_i) \leftarrow \bar{y}$ ▻ Initialize model

for $m = 1$ to M **do**

$r_{im} \leftarrow y_i - F_{m-1}(x_i)$ ▻ Compute residual errors

$h_m(x_i) \leftarrow$ *Fit weak learner to* (x_i, r_{im}) ▻ Fit weak learner

$w_m \leftarrow \min_{w} L(y_i, F_{m-1}(x_i) + w_m \cdot h_m(x_i))$

$F_m(x_i) \leftarrow F_{m-1}(x_i) + \eta \cdot w_m \cdot h_m(x_i)$ ▻ Update model

end for

where L is the loss function (mean squared error in this paper) and w is a scalar weight.

2.5 Random Forest decision trees

Another commonly used classification technique for regression analyses selected for the purpose of current work is Random Forest Regressor (RFR). The Random Forest model can be used for regression tasks by building decision trees based on a random vector Θ, where the predictor $y_i(x, \Theta)$ outputs numerical values instead of categorical labels. Assuming that the training set is randomly sampled from the distribution of the random vector y, X, the output values of the predictor are numerical. In this case, the mean-squared generalization error of any numerical predictor $y_i(X)$ can be calculated as the expected value of the squared difference between the true response variable Y and the predicted value $y_i(X)$ over the entire joint distribution of Y and X. The mean-squared generalization error is given by the following equation (Breiman [16]):

$$E_{X,Y}[(Y - y_i(X))^2]$$

This formula calculates the expected value of the squared difference between the true response variable Y and the predicted value $y_i(X)$ over the entire joint distribution of Y and X. RFR then is an ensemble learning technique that uses multiple decision trees to make a prediction. The final prediction is made by aggregating the predictions y_i of all the trees in the forest. The formula for RFR can be expressed as:

$$\hat{y} = \frac{1}{T} \sum_{i=1}^{T} y_i$$

where $\hat{y}$ is the predicted value of the response variable, T is the total number of trees in the forest and y_i is the predicted value of the response variable for the i-th tree.

3 ARTIFICIAL NEURAL NETWORK

The artificial neural network used in this paper is based on the Deep Neural Network (DNN) algorithm, which consists of multiple layers of neurons. Each layer transforms the input data to produce an output. This section briefly overviews the key components of a DNN model.

Input layer: This is the first layer of the network, which receives the input data. with specified the shape of the input data (the number of features).

Output layer: This is the final layer of the network, which produces the output. There may be multiple output types, such as binary classification, multi-class classification, or regression. In this particular layer, a linear activation function and a mean absolute error (MAE) loss function were used for regression.

Hidden layers: These are the intermediate layers of the network, which transform the input data to produce an output.

Activation functions: These are functions applied to the outputs of each neuron in the hidden layers, to introduce non-linearity into the network.

Dropout regularization: This is a technique used to prevent overfitting in the network, by randomly dropping out some of the neurons during training.

Loss function: This is a function that measures the error between the predicted output and the true output. For regression type of analysis, the mean squared error is used.

Optimization algorithm: This is an algorithm used to update the network weights during training, in order to minimize the loss function. The one selected here among the severity of loss functions was Adaptive Moment Estimation (Adam). It was proposed by Kingma and Ba in [17].

Overall, the DNN model implemented here involves specifying the number and type of layers, activation functions, regularization techniques, loss function, and optimization algorithm, and then training the model on a dataset obtained from resistance model experiments conducted on trawlers tested in a large CTO towing tank. The trained model can then be used to make predictions on new data.

4 ANALYSIS AND RESULTS DISCUSSION

The ML model was built using a database of trawlers tested in the CTO in recent years. The database comprises 28 ships that were tested under at least one loading condition. The features (independent variables) were determined through a correlation analysis, and the best ones were selected as inputs for the ML model. The density plots for each of selected features are presented in **Figure 4**.

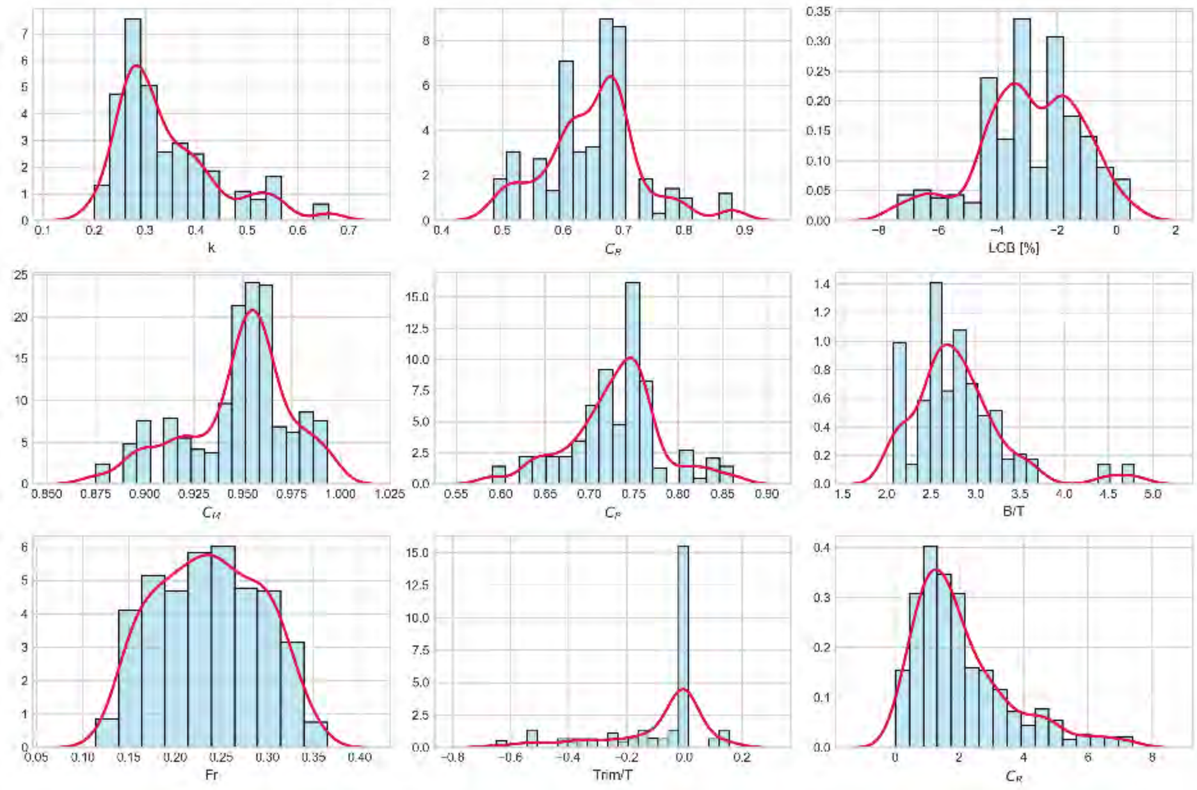

Figure 4 Density histograms of data with KDE (red line)

[fig:feat_hist]

The bag of features describing typical parameters of ships includes characteristics such as the form factor (k), longitudinal buoyancy (LCB), prismatic (C_P), block (C_B), and midship (C_M) coefficients, as well as ratios such as breadth to draught (B/T) and trim to draught ($Trim/T$), and finally the Froude number (Fr). These quantities are used to characterize the trawlers tested in the CTO. The goal of the prediction is the residuary resistance coefficient C_R, which is an independent variable in this case.

4.1 Total ship's resistance

The final prediction of the total resistance of the ship in calm water follows the ITTC'78 [18] method, including ML and AI predicted residuary coefficient C_R. The total resistance coefficient is calculated according to the formula:

$$C_T = (1+k)C_F + \Delta C_F + C_A + C_R + C_{AA}$$

where friction resistance coefficient C_F is found by ITTC'57 friction line:

$$C_F \cdot 10^3 = \frac{75}{(log_{10}(Re) - 2)^2}$$

and roughness allowance coefficient ΔC_F is calculated:

$$\Delta C_F \cdot 10^3 = 44\left[\left(\frac{k_s}{L}\right)^{1/3} - 10 \cdot Re^{-1/3}\right].$$

Correlation allowance C_A is found by Bowden and Davidson [19]:

$$C_A \cdot 10^3 = 105 \cdot \left(\frac{k_s}{L}\right)^{1/3} - 0.64$$

where k_s is standard hull roughness. Air resistance coefficient C_{AA} is simply calcualted as:

$$C_{AA} \cdot 10^3 = \frac{A_T}{S}$$

where A_T is transverse projected area, and S is wetted surface area. Finally the total resistance of ship is calculated by formula:

$$R_T = \frac{1}{2} \cdot \rho \cdot C_T \cdot S \cdot V^2$$

4.2 Machine learning outcome

The methods described in Section 2 were used to predict the C_R values of a new trawler. The scikit-learn [20] Application Programming Interface (API) was used for most of the ML techniques, except XGB which was based on the dmlx XGBoost API [14]. The metrics used for the quantification of predictions are presented in Figure [fig:ML_met].

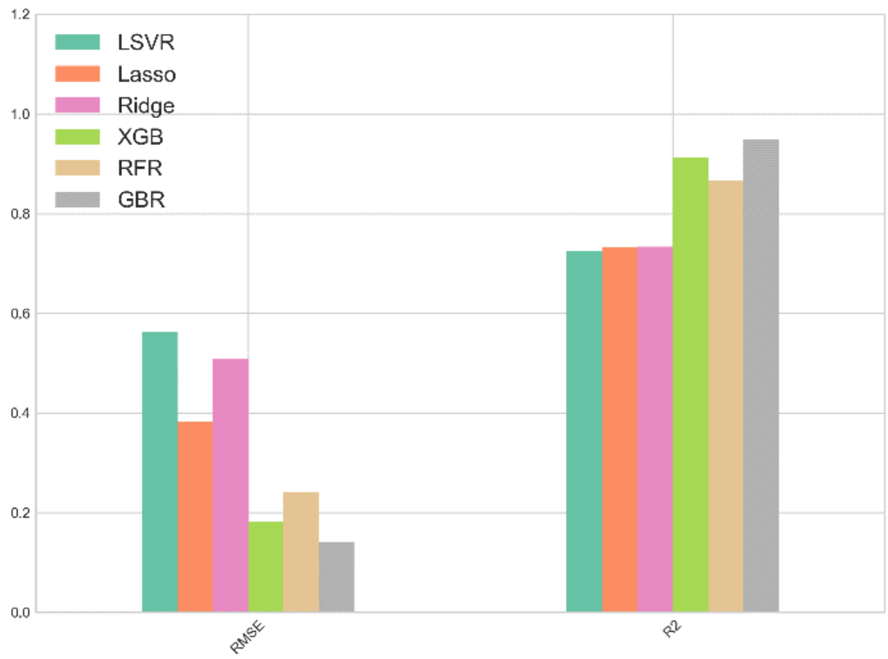

Figure 5 The metrics quantifying the performance of the applied ML techniques

The Person's R^2 metric presented in **Figure 5** shows the lowest values of this metric in LSVR, Lasso, and Ridge models, which are linear. Thus, these methods were rejected for the kind of prediction needed. The highest values were achieved for the ensemble method, with the highest R^2 and concurrently lower $RMSE$, revealing the best performance of the GBR method.

4.3 Deep Neural Network outcome

The artificial neural network applied in ship's resistance prediction, presented in this paper and compared with the best-performing machine learning techniques, is shown in Figure [fig:RT_pred]. The DNN was built on eight input layers referring to features used in ML process, six hidden and one output layer. The Rectified Linear Unit (ReLU) activation functions for input and hidden layers was selected and loss function was mean absolute error (MAE). The keras package from tensorflow API was used in the predictions.

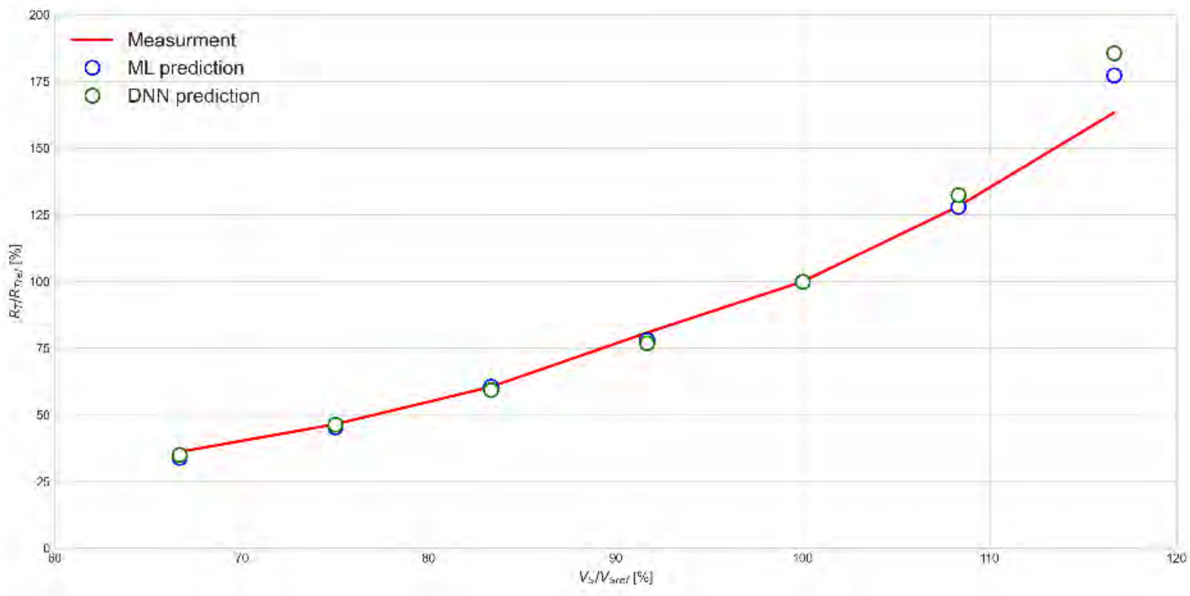

Figure 6 Comparison of ML and DNN predictions with model tests results

The reference resistance R_{Tref} in **Figure 6** is equivalent to the contract speed, which is the reference value for speed V_{Sref}, where R_T and V_S are equal to 100%, respectively. The ML and AI approaches have very similar accuracy in the whole range of vessel speeds; however, at the highest speed, the ML-predicted resistance was closer to the experimental value.

5 CONCLUSIONS

There are no major differences between ML and AI methods for the prediction of resistance based on a trained database of trawler vessels. In general, both methods seem to be equivalent in their predictions on the database. However, the number of data inputs considered by the models is relatively small and may be relevant in the final decision of selecting a method for prediction. This work is only the first step in building a tool that uses both regression techniques for fast prediction of ship performance, utilizing the CTO towing tank database.

REFERENCES

[1] M. G. Holtrop J., "An approximate power prediction method," *International Shipbuilding Progress*, vol. 29, pp. 166–170, 1978.

[2] L. Nikolopoulos and E. Boulougouris, "A Study on the Statistical Calibration of the Holtrop and Mennen Approximate Power Prediction Method for Full Hull Form, Low Froude Number Vessels," *Journal of Ship Production and Design*, vol. 35, no. 1, pp. 41–68, Feb. 2019, doi: 10.5957/JSPD.170034.

[3] H. Khan, "Artificial neural networks based prediction and validation tool (annpvt) for ship model powering tests in towing tanks," in *2021 international conference on artificial intelligence (icai)*, 2021, pp. 113–118. doi: 10.1109/ICAI52203.2021.9445251.

[4] K. Grabowska and P. Szczuko, "Ship resistance prediction with artificial neural networks," in *2015 signal processing: Algorithms, architectures, arrangements, and applications (spa)*, 2015, pp. 168–173. doi: 10.1109/SPA.2015.7365154.

[5] Q. Sun, M. Zhang, L. Zhou, K. Garme, and M. Burman, "A machine learning-based method for prediction of ship performance in ice: Part i. Ice resistance," *Marine Structures*, vol. 83, p. 103181, 2022, doi: https://doi.org/10.1016/j.marstruc.2022.103181.

[6] A.-S. Milaković, F. Li, M. Marouf, and S. Ehlers, "A machine learning-based method for simulation of ship speed profile in a complex ice field," *Ships and Offshore Structures*, vol. 15, no. 9, pp. 974–980, 2020, doi: 10.1080/17445302.2019.1697075.

[7] Y. Ao, Y. Li, J. Gong, and S. Li, "Artificial Intelligence Design for Ship Structures: A Variant Multiple-Input Neural Network-Based Ship Resistance Prediction," *Journal of Mechanical Design*, vol. 144, no. 9, Jun. 2022, doi: 10.1115/1.4053816.

[8] W. Tarelko and K. Rudzki, "Applying artificial neural networks for modelling ship speed and fuel consumption," *Neural Computing and Applications*, vol. 32, no. 23, pp. 17379–17395, Dec. 2020, doi: 10.1007/s00521-020-05111-2.

[9] Y. Yang, H. Tu, L. Song, L. Chen, D. Xie, and J. Sun, "Research on accurate prediction of the container ship resistance by rbfnn and other machine learning algorithms," *Journal of Marine Science and Engineering*, vol. 9, no. 4, 2021, doi: 10.3390/jmse9040376.

[10] T. Uyanık, Ç. Karatuğ, and Y. Arslanoğlu, "Machine learning approach to ship fuel consumption: A case of container vessel," *Transportation Research Part D: Transport and Environment*, vol. 84, p. 102389, 2020, doi: https://doi.org/10.1016/j.trd.2020.102389.

[11] A. J. Smola and B. Schölkopf, "A tutorial on support vector regression," *Statistics and Computing*, vol. 14, no. 3, pp. 199–222, Aug. 2004, doi: 10.1023/B:STCO.0000035301.49549.88.

[12] R. Tibshirani, T. Hastie, and J. Friedman, "Regularized paths for generalized linear models via coordinate descent," *Journal of Statistical Software*, vol. 33, Feb. 2010, doi: 10.1163/ej.9789004178922.i-328.7.

[13] A. E. Hoerl and R. W. Kennard, "Ridge regression: Biased estimation for nonorthogonal problems," *Technometrics*, vol. 12, no. 1, pp. 55–67, 1970, doi: 10.1080/00401706.1970.10488634.

[14] T. Chen and C. Guestrin, "XGBoost: A scalable tree boosting system," in *Proceedings of the 22Nd acm sigkdd international conference on knowledge discovery and data mining*, in KDD '16. New York, NY, USA: ACM, 2016, pp. 785–794. doi: 10.1145/2939672.2939785.

[15] J. H. Friedman, "Greedy function approximation: A gradient boosting machine." *The Annals of Statistics*, vol. 29, no. 5, pp. 1189–1232, 2001, doi: 10.1214/aos/1013203451.

[16] L. Breiman, "Random Forests," *Machine Learning*, vol. 45, no. 1, pp. 5–32, 2001, doi: 10.1023/A:1010933404324.

[17] D. P. Kingma and J. Ba, "Adam: A method for stochastic optimization," *CoRR*, vol. abs/1412.6980, 2014.

[18] *ITTC quality system manual: Recommended procedures and guidelines: Procedure 1978 ittc performance prediction method*. International Towing Tank Conference, 1978.

[19] B. Bowden and N. Davison, "Resistance increments due to hull roughness associated with form factor extrapolation methods," NPL Ship TM 3800, 1974.

[20] F. Pedregosa *et al.*, "Scikit-learn: Machine learning in Python." https://scikit-learn.org, 2011.

MODELING OF DISPLACEMENTS OF AN OFFSHORE WIND PLATFORM IN THE ANSYS AQWA PROGRAM EXTENDED WITH THE INFLUENCE OF VISCOSITY

Ewelina Ciba, Paweł Dymarski [1,2]

[1, 2] Institute of Ocean Engineering and Ship Technology, Gdańsk University of Technology.

(E-mail:)

Keywords: FOWT, AQWA, spar, viscous drag

ABSTRACT

The Ansys Aqwa program is a very good tool for analyzing offshore structures. It is easy to lead the analyzed structure in the form of surface models to it. It has various anchor modeling options, from linear models, through anchor chains with defined parameters, to any stiffness matrices entered by the user. It allows you to determine the response of the structure in the frequency domain as well as the time response. It provides the hydrostatic data of the structure in transcendental form, and also allows for stability calculations. It is equipped with the ability to present the frequency of natural movements. It has various forms of introducing external inputs - wave, wind, current and user-defined forces, constant or time-varying, and also defined in the form of a spectrum. Calculation results can be both observed on the screen and exported to a .csv file. It is also possible to export the pressure on the structure to the module of the Ansys program that enables strength calculations.

However, Aqwa is based on the diffraction theory, therefore in its basic form it does not take into account the influence of viscosity. For calculations of the behavior of the platform on the wave, this is too much of a simplification and the influence of viscosity in the form of additional coefficients should be taken into account. The program allows you to enter additional matrices of linear damping or Morison resistance coefficients and added water mass. However, the input values are constant, while in reality they depend on both the frequency of the oscillations and their amplitude.

There are various methods for determining the hydrodynamic coefficients. Most often, free or forced oscillation tests are used in the form of model tests or RANSE-CFD calculations.

The results of calculations of the platform motion on the wave obtained in the Anaya Aqwa program may be very similar to those obtained from model tests, but much depends on the appropriate selection of additional hydrodynamic coefficients related to viscosity. The popular and easy to perform free oscillation test gives values only for natural frequencies, so the best solution is to perform forced oscillation tests to understand the broader response characteristics of the structure. It is also very important to know the influence of the displacement amplitude on the value of the coefficients and to select their values for the expected amplitude of the platform movements on the wave. The work will discuss the methods of determining these coefficients and the impact of their values on the final results.

VALIDATION OF THE CFD ANALYSIS FOR AN OLYMPIC CANOE WITH TAKING INTO ACCOUNT ACCURATE ANALYSIS OF THE AERODYNAMIC RESISTANCE

Patryk Dobreńko[1], Marek Kraskowski[2] and Tomasz Bugalski[3]

[1, 2] Centrum Techniki Okrętowej, Ośrodek Hydromechaniki Okrętu, POLAND.

(E-mail: patryk.dobrenko@cto.gda.pl, marek.kraskowski@cto.gda.pl)

[3] Water Sport Equipment Group, POLAND.

(E-mail: tomasz.bugalski@gmail.com)

Keywords: scale model tests, CFD, canoe, resistance, aerodynamics

ABSTRACT

The results of the scale model tests are the most reliable reference data for the validation of CFD analyses in marine applications. One of the drawbacks of the towing tank measurements is the lack of possibility of direct evaluation of aerodynamic component of the resistance. In many cases, it is simply neglected in validation studies due to relatively low speed of the hull models and their small frontal windage area. However, in case of olympic canoes, reaching the speeds above 6m/s, the aerodynamic component of the measured resistance is considerable and it is no longer justified to compare the computed resistance in water or total resistance of simplified geometry with total resistance measured in the towing tank. Moreover, the blockage introduced by the carriage construction accelerates the air flow around the upper part of the hull. This paper presents the validation study for an olympic canoe with taking into account fully detailed geometry of the upper part of the hull and the actual air speed measured below the towing carriage.

1 INTRODUCTION

The shapes of modern Olympic canoes are very well optimized in respect of resistance. For that reason, the differences between the resistance of the canoes of the same class is very small, usually within 1%, even between different brands. Nevertheless, the search for further improvement still goes on [1] and requires reliable tools. RANS CFD is the most natural choice, however, the computational models should be carefully validated before applying them to optimisation studies. Towing tank tests are the best reference, especially that the resistance reference for canoes are rare case of experimental predictions at full scale which do not require recalculations for sea water. However, due to large speed of Olympic canoes, the aerodynamic resistance must be accurately accounted for. This study presents this kind of validation, with taking into account the actual flow speed under the towing carriage.

2 MEASUREMENTS OF THE VELOCITY BELOW THE TOWING CARRIAGE

Despite its truss construction, the carriage used in the primary towing tank of CTO S.A. introduces considerable blockage of the space above the water surface (Figure 1). For that reason, it can be expected that the velocity of the air flow around the above-water part of the towed model is not equal to the velocity of the water flow.

Figure 1 Towing carriage

For the purpose of quantitative evaluation of the velocity in the gap between the water surface and the bottom of the towing carriage, a dedicated experiment was realized, consisting in measuring the velocity in specified locations above the water for given speeds of the carriage. The Schmidt probe (a sensor using the constant temperature anemometry technique) was used for the measurements. Two carriage speeds were considered: 4m/s and 6m/s. Figure 2 presents the air velocity as a function of the height above water.

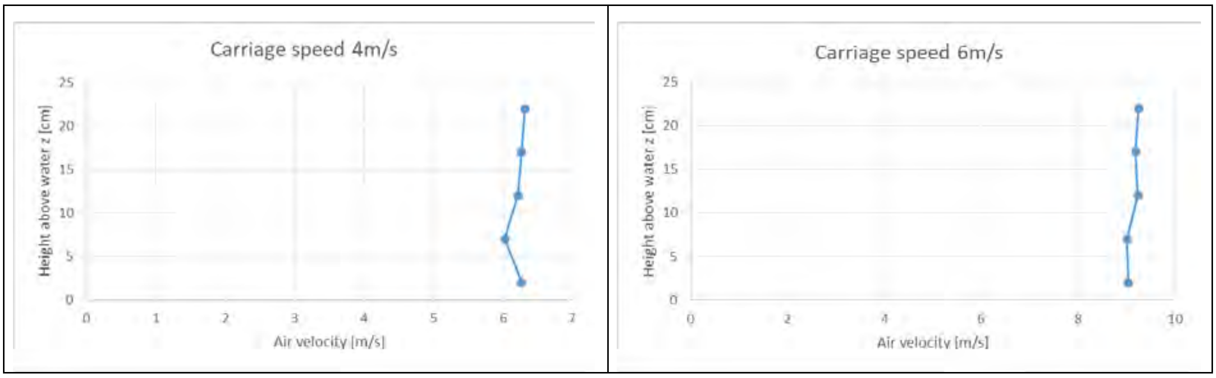

Figure 2 Results of measurements

It was found that within the range of 0-25 cm above the water surface, the air speed is approximately constant and almost independent of speed (1.55 of carriage speed for 4m/s and 1.52 for 6m/s).

3 COMPUTATIONAL METHOD AND TEST CASE

The analysed case was a K2-men canoe – CTO's model No. M705. Total mass of the model was 188 kg. The resistance was measured and computed for the speed of 5.75 m/s. The water temperature in the computations was set exactly to the temperature in the towing tank during the measurements.

The computational mesh of app. 2 500 000 cells was used. Single domain was used for the compuations of water resistance and air resistance. The water speed was set to 5.75 m/s and the air speed was set to 8.83m/s. Realizable k-epsilon turbulence model was applied. Visualization of the mesh and the convergence of resistance are presented in figures below.

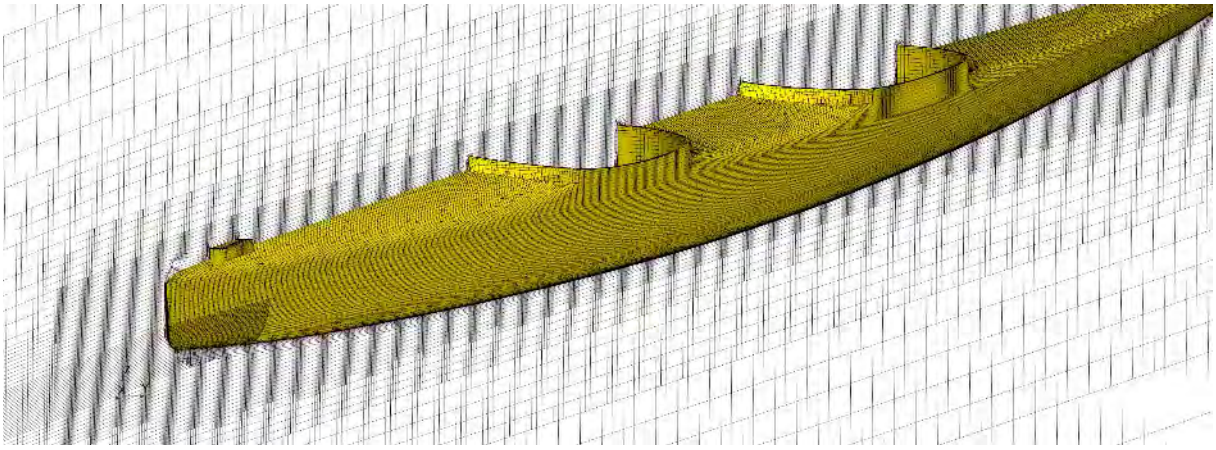

Figure 3 Computational mesh

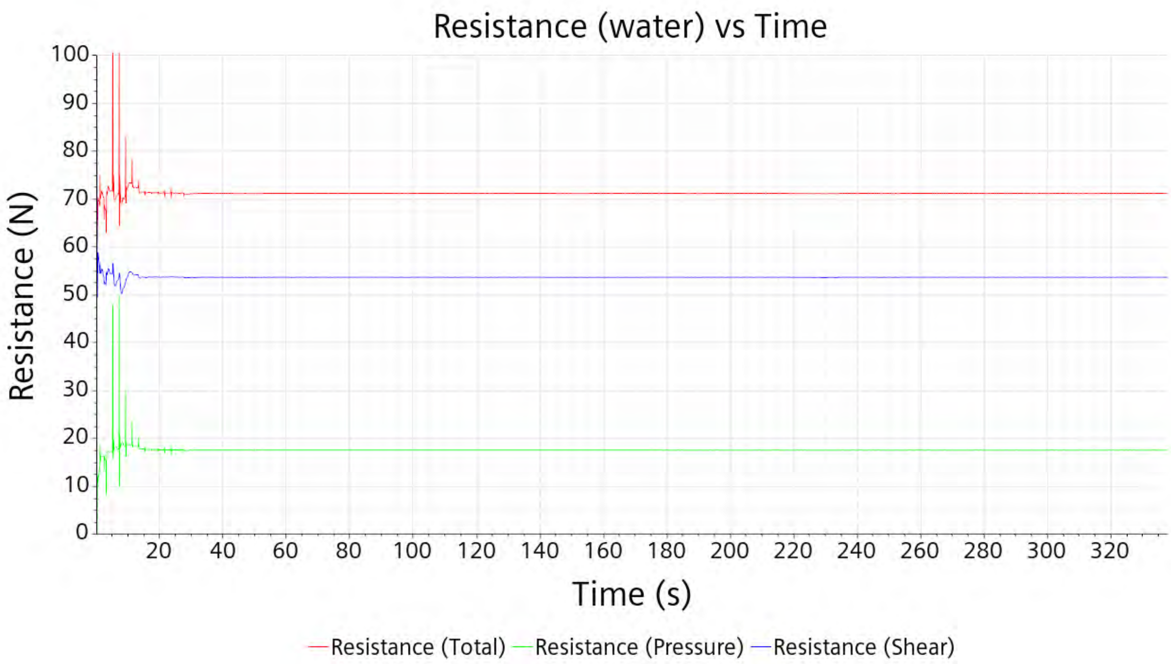

Figure 4 Convergence of resistance (water)

4 RESULTS

The computed resistance values are presented in the table below [2].

Pressure resistance [N]	35.02
Friction resistance [N]	107.22
Aerodynamic resistance [N]	2.16
Total resistance [N]	144.40
Measured resistance [N]	146.13

The visualizations of the results are presented in figures below.

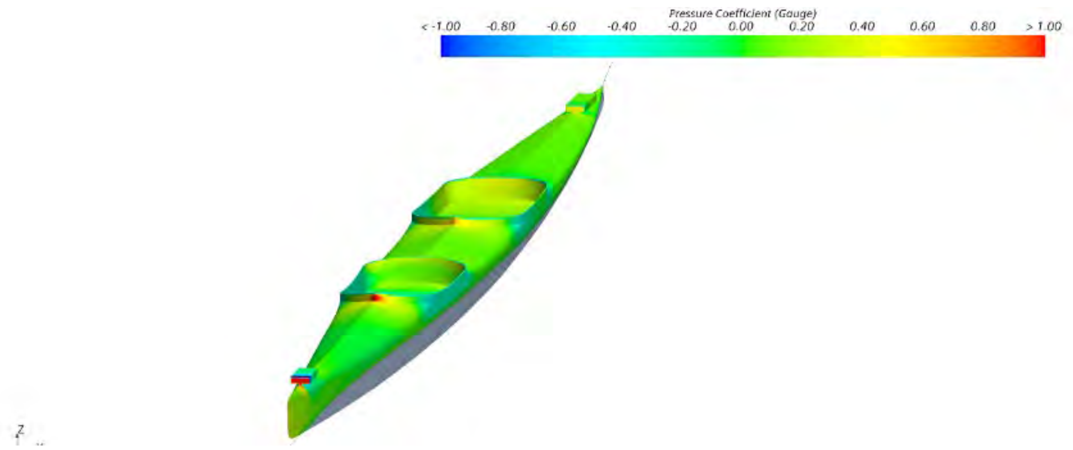

Figure 5 Pressure distribution – upper part of the hull

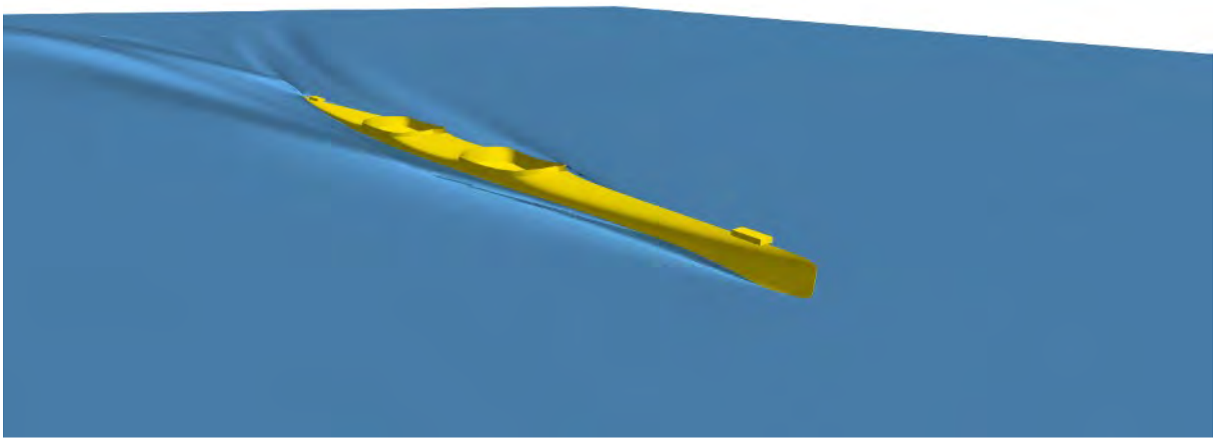

Figure 6 Wave pattern

5 CONCLUSIONS

The presented work yields the following conclusions:

1. The aerodynamic resistance of the canoe itself, evaluated with taking into account the air flow acceleration under the towing carriage, approximates 1.5% of total resistance.
2. Taking into account that the differences in resistance between well optimized shapes are usually below 1%, this shows how important it is to assure that the aerodynamic resistance of compared shapes is equivalent for all cases. This means e.g. using exactly the same equipment for mounting the model to the carriage for the resistance tests.
3. In case of using the model tests for CFD validation with taking into account the aerodynamic resistance, the presented effect of flow acceleration must be obligatory taken into account. Exact speed value should be evaluated for specific facility.
4. The accuracy of the resistance prediction for the selected K2 canoe is 1.2%. This shows that the computational model captures correctly the flow phenomena and can be used for relative comparisons.

ACKNOWLEDGMENT

Presented paper was prepared within framework of project POIR.01.01.01-00-0103/19 “Innovative Olympic and Paralympic class boats for canoeing sprint events”.

REFERENCES

[1] Bugalski T.: Development of the New Line of Sprint Canoes for the Olympic Games, Proceedings of 10th Int. Conference of Fast Sea Transportation -FAST 2009, 1039-1049, Athens, 2009

[2] Raport badania nr RH-07/B-14265/14266, CTO S.A.

APPROACHES AND CHALLENGES TO DETERMINING POWER-SPEED CHARACTERISTICS AND REFERENCE SPEED FOR THE CALCULATION OF EEXI ENERGY EFFICIENCY INDICATORS

Bartosz Dombrzalski, Janusz Narewski [1,2]

[1, 2] Polish Register of Shipping (PRS).

(E-mail: Bartosz.Dombrzelski@prs.pl, Janusz.Narewski@prs.pl)

Keywords: EEXI, EEDI, Sea Trials , Tank Tests, Ship Energy Efficiency

ABSTRACT

From 01/01/2023, also ships built before 2013 must have a documented index similar to EEDI called EEXI (Energy Efficiency Existing Index). Although the EEDI and EEXI attained indicators have a physically identical interpretation, it was necessary to introduce additional ways to determine the key power-speed relationships for older ships, often several decades old, with lower quality or incomplete technical documentation, and what was significant was the weakness of the older sea standards trials. The article reviews the available routes for EEXI calculations based on different approaches, taking into account the practical experience of PRS, which was directly involved in the development and verification of the relevant calculation documentation in the form of EEXI Technical files.

INVESTIGATION OF THE TUG INDIRECT MODE ESCORT MANEUVERS WITH THE USE OF MODEL TESTS

Radosław Kołodziej[1]

[1]Maritime Advanced Research Centre

(radoslaw.kolodziej@cto.gda.pl)

Keywords: Ship model tests, Escort manoeuvre, Indirect mode, Escort tug, Ship handling

ABSTRACT

Navigating in restricted seaways or during heavy weather conditions poses a considerable risk for ships. When such situations occur, the safety of ship navigation can be increased by the assistance of escort tug. Fulfilling this task requires tug designers to take into account additional requirements during design process, which include stability against capsizing and increased towing force demand. Although there are currently no ITTC guidelines regarding escort manoeuvring, model tests can still be utilized in assessment of tug performance in this case. This paper presents an investigation of tug escort manoeuvres for a ship in indirect mode using captive model tests. The study focuses on measuring the forces generated on the azimuth thrusters as well as braking and pulling forces induced on the towing line with the use of dedicated measuring devices. As a result, the prognosis of pulling forces is presented on a butterfly diagram. The purpose of this study is to discuss the benefits and challenges of predicting escort tug performance with presented method.

1 INTRODUCTION

The workboat industry faces significant challenges when it comes to designing and operating tugs. The growing size of merchant vessels necessitates usage of tugs with increasingly higher bollard pull capabilities, which is usually achieved by implementation of propulsion unit with greater power [1]. Unfortunately, this trend presents several drawbacks. Ships may not be capable of withstanding high push forces exerted by larger tugs, nor the extremely high wire pulls required for bollard assistance. Moreover, large tugs are not always ideal for manoeuvring in restricted waters, and the high power and size of these vessels entail significant challenges for operators [2]. The development of effective hydrodynamic forces for steering and braking requires an integrated design approach that considers both hull form and propulsion system.

Following this trend, numerous research has been conducted in recent years in order to improve design process of escorting tugs. In 2004 Allan and Molyneux investigated hydrodynamic performance of different types of tug design with the use of planar motion mechanism [3]. In 2013 Artyszuk presented steady-state analytical model of ASD tug in escort push operations [4]. The integrated numerical and empirical method of tug manoeuvring prediction was introduced by Zhang et al. in 2023 [5]. Although intensified effort put into development of new ways of tug escorting performance prediction, no unified method is available as of now.

2 RESEARCH METHODOLOGY

In this study assisted ship is represented by towing carriage which is connected to model with captive mechanism. The measuring setup consists of 3 dynamometers. Two of them are measuring forces and moments induced on each of the thruster. The third one is located on towing carriage and is set to measure forces generated on towing line. This dynamometer is connected with captive mechanism and model at the height and longitudinal position of the towing staple of the tug. The model is free to move in every degree of freedom except for the surge and sway and the measurement of drift, roll and pitch angles is done. Prior to the experiment inclining tests were done in order to confirm the metacentric height of the model and for dynamometers mass roll and pitch corrections at 0 speed. The tests were done for propeller pitch ratio P/D = 0.935 and constant revolutions (F_D = 0). The reference systems, both for towing line tension and thruster forces are presented in Figure 1. The measurement of the forces takes place for the quasi-steady conditions for each tested thruster deflection angle and propeller revolutions after the model reach towing position.

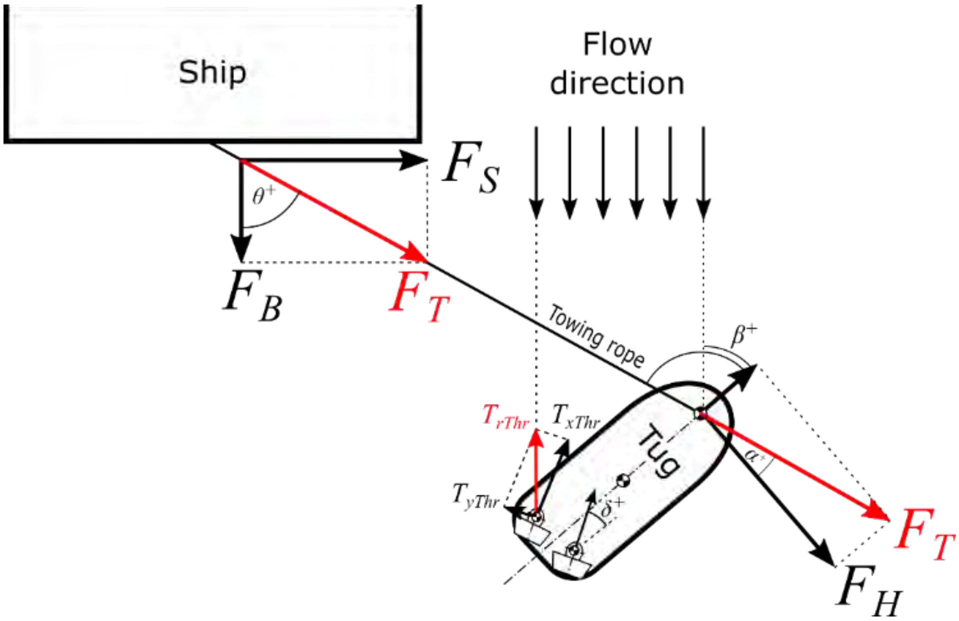

Figure 1. Reference system related to forces generated on the hull

The tug geometry developed for this study is typical representation of ASD type towing tug equipped with 2 azimuth thrusters with nozzle. The model was built with dedicated deck which allow for partial flooding, but preventing water from getting inside. This allow for observation of deck submergence when prominent heel angles are achieved. The geometry of the model is presented in Figure 2 and its main parameters are included in Table 1.

Figure 2. Geometry of tested ship model M1118 – „CTO tug"

Table 1
Main parameters of tested towing tug.

Parameter	symbol	unit	ship	model
scale	λ	[-]	1.000	10.849
Length between perpendiculars	L_{PP}	[m]	26.00	2.397
Breadth at waterline	B	[m]	11.18	1.031
Draught: fore	T_F	[m]	3.1	0.286
Draught: aft	T_A	[m]	3.1	0.286
Displacement volume	∇	[m3]	480.6	0.376
Relative longitudinal centre of buoyancy from midship section, "+" to fore	L_{CB}/L_{PP}	[%]	-0.31	
Block coefficient	C_B	[-]	0.533	
Propeller diameter	D_P	[m]	2.30	0.212
Wetted surface area of bilge keels	S_{BK}	[m]	12.00	0.102
Nozzle length to propeller diameter ratio	L_D/D_P	[-]	0.50	
Metacentric height	GM	[m]	2.56	0.24
Escorted ship speed	V_A	[kn], [m/s]	8.00	1.25

3 RESULTS AND DISCUSSION

The model tests conducted in this study were than for the speed of 1.25 m/s (the equivalent of 8 knots in full scale). The thrusters deflection angles ranged from 0:60° with 5° step oriented to starboard. The maximum deflection value of 60° was considered as maximum allowable value in order to prevent portside thruster water slip stream from flushing starboard thruster. The tests were complemented with direct mode manoeuvres. The critical thrusters deflection angle of 60° is presented in Figure 3.

Figure 3. Escort manoeuvre model test with both thrusters deflected 60°

The results obtained in the study suggest that the maximum steering force F_S generated by the tug can be noticed for thrusters angle deflected by approximately 45° above which the steering component start do drop. The braking force F_B is increasing in the entire tested range as a result of what the value of towing line tension F_T is still increasing above 45° of thruster deflection angles. The F_S / F_B diagram obtained during the tests is presented in Figure 4.

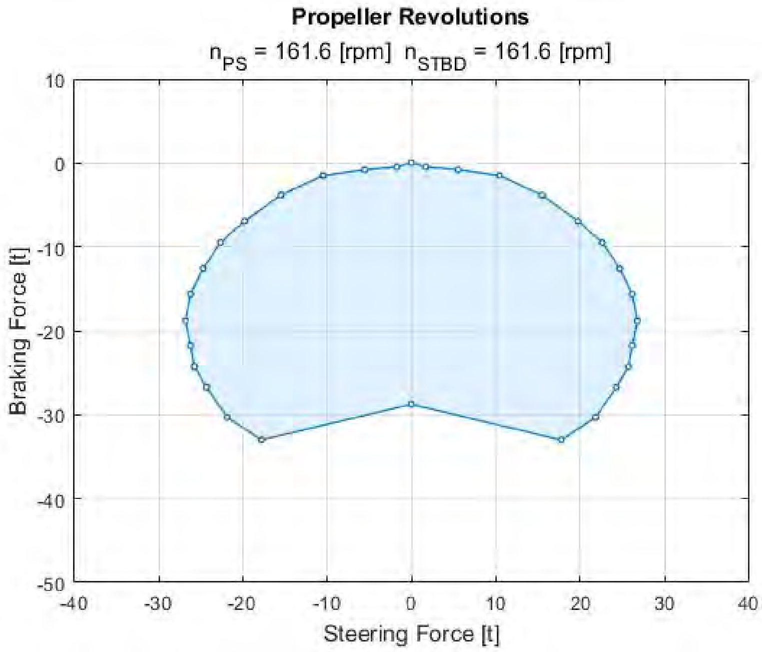

Figure 4. F_S / F_B diagram – full scale

The observed roll also has increasing trend with the increase of thruster deflection angle. Considering that this parameter is crucial where it comes to the tug navigation safety, the study of impact of additional starboard thruster deflection angles of 75° and 90° was done. As a result further increase of roll was noticed for 75° and a drop of roll was observed at 90°. This trend is not uniform and depend on thruster load. In general the higher propeller revolutions the lower thruster angle is necessary to counteract the excessive roll as shown in Figure 5.

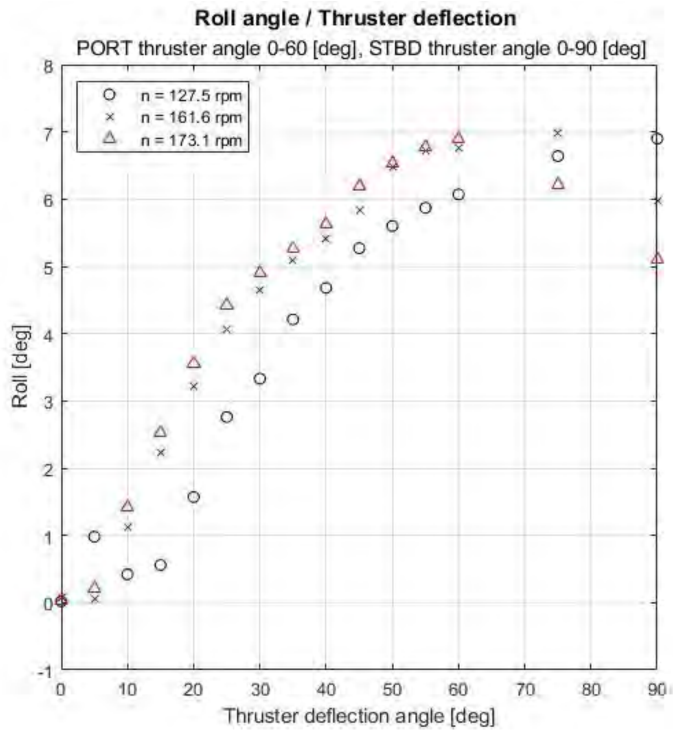

Figure 5. roll angle / thruster deflection – full scale

As expected, the thrust differ for starboard and portside thrusters as they operate in a different wake field. The water inflow to starboard thruster is slowed down significantly in case presented in this study and therefore its advance ratio is decreasing with thruster deflection. The portside thruster operates in more favourable conditions as presented in Figure 6.

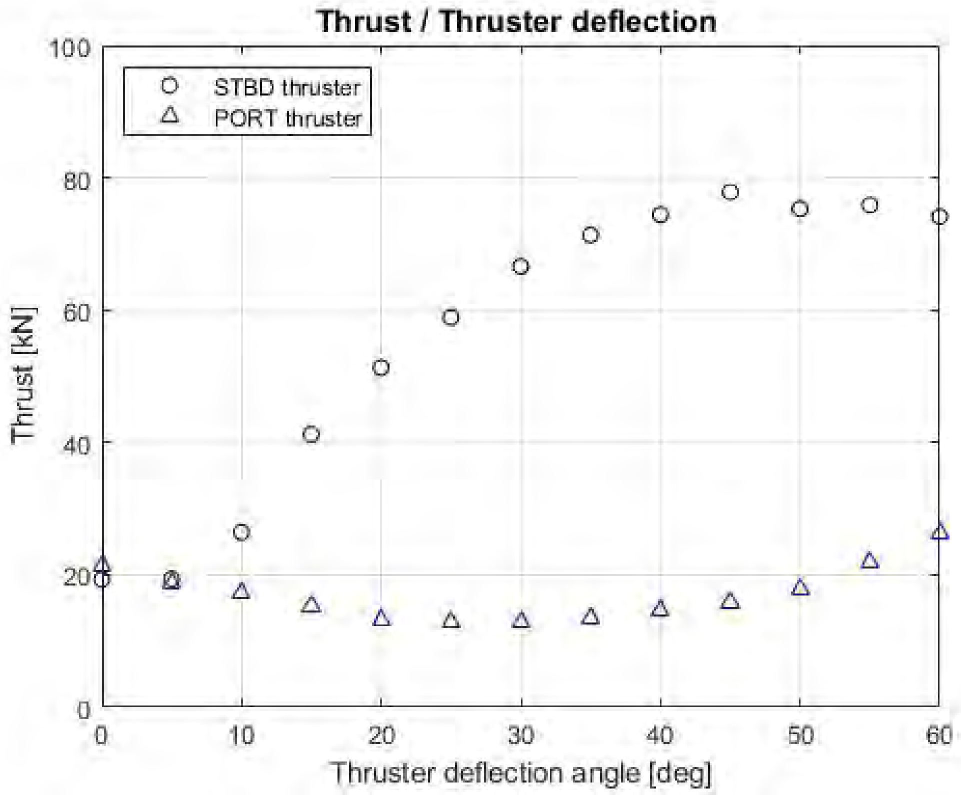

Figure 6. Comparison of thrust for different thrusters deflection – full scale

4 CONCLUSIONS

The study proves that model tests can be successfully implemented for determination of maximum steering forces as well as maximum towing line tension generated by the tug during escort manoeuvres. This methodology however, faces some challenges as the selection of thrusters revolutions should be done carefully and with the assistance of propulsion unit manufacturer. For instance, there can be two approaches to modelling of propulsion unit working load. One considers direct scaling of maximum allowable propeller revolutions. Second option is based on scaling of propeller thrust and require adjustment of propeller revolutions for each tested deflection angle. Another important aspect is determination of model scale. On one hand model should be large enough so that it is possible to model metacentric height correctly on the other small enough so that forces induced on model are within limits of measuring devices. Finally model should be manufactured with deck in order to fully observe its flooding. All this require careful planning at the very initial phase of the project.

Nevertheless, prediction of the escort tug performance with the use of model tests gives a lot of flexibility both in terms of selection of investigated scenarios and complex analysis of the propulsion performance. That is why future study is planned in order to fully systematize this method and compare the results with data obtained with the use of other means.

ACKNOWLEDGMENT

This paper has been elaborated within the framework of the internal research and support of the Maritime Advanced Research Centre (CTO S.A) in 2022.

REFERENCES

[1] Martelli, M., Figari, M., Piaggio, B., New Escort Tug Family Designed to Anticipate New Safety Requirements and Operational Needs, International Conference on Ships and Shipping Research, Trieste, Italy, 2018.

[2] Iglesias-Baniela, S., Vinagre-Ríos, J., Pérez-Canosa, J., Ship Handling in Unprotected Waters: A Review of New Technologies in Escort Tugs to Improve Safety, Applied Mechanics, Volume 2, Issue 1, 2021, DOI:10.3390/applmech2010004.

[3] Allan, R.G., Molyneux D., Escort tug design alternatives and a comparison of their hydrodynamic performance, Society of Naval Architects and Marine Engineers, 112, pp 191-205, 2004.

[4] Artyszuk, J., Simplified steady-state analytical model for manoeuvring and control of ASD tug in escort push operations, Scientific Journals of Maritime University of Szczecin, 36(108) z. 1 pp. 5–14, 2013.

[5] Zhang, S., Wu, Q., Liu, J., He, Y., Li, S., Twin-screw ASD tug maneuvering prediction based on integrated CFD and empirical methods, Ocean Engineering, vol. 269, 113489, 2023.

NEW 2023 IMO REQUIREMENTS ON VESSELS ENERGY EFFICIENCY. METHODOLOGY OF IN-SERVICE PERFORMANCE MEASUREMENTS TO DETERMINE REFERENCE SPEED TO CALCULATE AN ENERGY EFFICIENCY EXISTING SHIP INDEX EEXI.

K. Kolwzan[1]

[1] Centre for IMO Affairs, Polish Register of Shipping, POLAND.

(E-mail: krzysztof.kolwzan@prs.pl)

Keywords: Energy Efficiency Existing Ship Index (EEXI), In-Service Performance Measurements, Vessel Energy Efficiency, Vessel Reference Speed (Vref)

ABSTRACT

The International Maritime Organization (IMO) is implementing short-term measures to improve ship Energy Efficiency and reduce Fuel Consumption to minimize CO_2 emissions from shipping [1]. The IMO's Marine Environment Protection Committee (IMO MEPC) at 78th session in 2022, approved the *Guidance on Methods, Procedures and Verification of In-Service Performance Measurements* for the purpose of calculating Energy Efficiency Existing Ship Index (EEXI), as set out in resolution MEPC.350(78) [2]. In cases where the ship speed-power curve is not available or the sea test report does not include EEDI or draught under design load conditions, the speed of the vessel Vref may be obtained by the method of measuring the operating performance for the EEXI calculation, in accordance with the guidelines for the calculation of EEXI [2,4].

1 INTRODUCTION

The attained Energy Efficiency Existing Ship Index (EEXI) is a measure of ship's energy efficiency (g/t*nm) and calculated by the following formula:

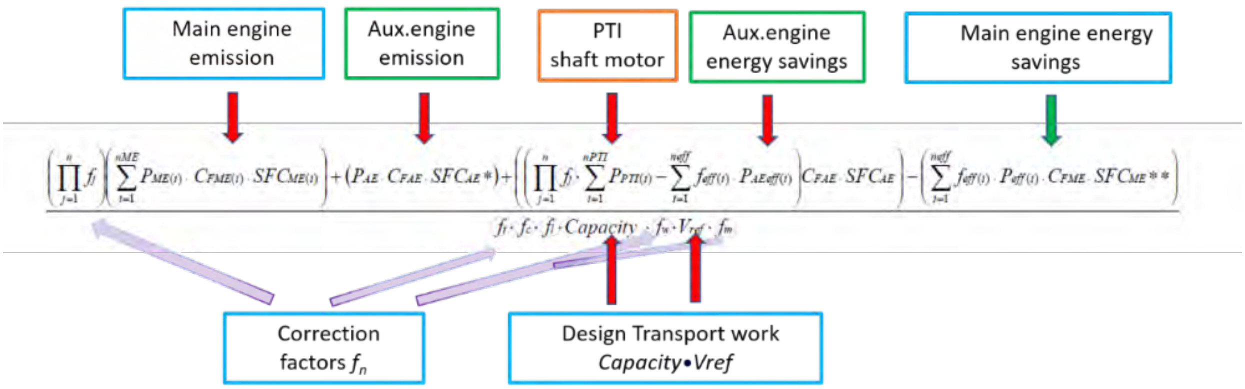

Figure 1 Formula for calculation of the vessel's Energy Efficiency Existing Ships Index (EEXI)

For the calculation of the EEXI, it is necessary to determine the reference speed (Vref) at a certain draft of the vessel.

2 METHODOLOGY OF IN-SERVICE PERFORMANCE MEASUREMENTS TO DETERMINE REFERENCE SPEED (VREF)

For many existing vessels subject to the EEXI, it is unlikely that compliant model tests or sea trials at the required draft exist or that a scale model still exists. Therefore, the EEXI calculation guidelines offers the option to calculate the Vref using an approximate formula for the ship type and installed power. With an included margin factor of 5%, this approximated reference speed will be conservative.

The EEXI rating can be improved by determining the Vref from model tests. However, building a new vessel's model to scale and conducting towing tank tests only for the purpose of evaluating the effect of improving the Vref is unreasonably expensive and time consuming, especially for conducting EEXI screenings of entire fleets. In cases where the energy-saving device is installed or there is lack of model test data and value of Vref [3, 4], model tests might be substituted by other methods approved by the verifier, based on the following methods in accordance with defined quality and technical standards:

.1 sea trials after installation of the device; and/or
.2 in-service performance measurement method; and/or
.3 dedicated model tests; and/or
.4 numerical calculations.

3 IN-SERVICE PERFORMANCE MEASUREMENTS

This paper is concentrated on the in-service performance measurements. When carrying out the in-service performance measurements, common international standards (such as ITTC quality procedures, ISO 15016:2002, ISO 15016:2015 and/or ISO 19030:2016) should be referred to, unless explicitly specified in this guidance. An overview of preparations and procedures are outlined in the Table 1 below [4].

Table 1
In-service performance sea trial preparations and procedures

IN-SERVICE PERFORMANCE MEASUREMENT ANALYSIS			
STEP 1: PREPARING SENSORS	• Speed log / GPS • Echosounder • Heading control • Fuel flow meter • Shaft torsion meter • Draft measurement • Gyro compass	**STEP 2:** PRE-TRIAL PARAMETERS	• Displacement • Forward/Aft draughts • Water depth • Air/Sea temperature • Seawater density • Anemometer height • Fuel density • Fuel LCV
STEP 3: IN-SERVICE PERFORMANCE MEASUREMENT	• Sea state • Wind • Water depth • Currents	**STEP 4:** DURING TRIAL PARAMETERS	• Reported data • System prints • Equipment control • Fuel analysis
STEP 5: DOCUMENTATION		• Shaft RPM/Power • Heading • Ship's speed and distance • Wind and current speed/direction • Wave height /period/direction	

4 PREPARATIONS TO IN-SERVICE PERFORMANCE TRIALS

The preparation is one of the most important aspects of a successful in-service performance measurement procedure. All relevant instruments should be calibrated and their operational conditions prior to the commencement of the trials should be confirmed by the verifier. The Verifier is the flag Administration, or a competent organization delegated by the flag Administration.

The list below in Table 2 indicates the primary instruments to be used for collecting the data.

Table 2
Sensors for in - service performance trials

Sensor	Remarks
Shaft torque meter	The measurement system should be certified for power measurements with a bias error as small as practicable. Zero setting checked before and after test.
GPS	The GPS system should operate in the differential mode to ensure sufficient accuracy.
Anemometer	It should be clear of possible obstructions (superstructure, masts, funnel, etc.) and its height from sea level recorded.
Draft measurements	Draft measurement system (if available and calibrated): Otherwise, physical observation is required.
Speed log	The sensor should have been cleaned recently.
Echo sounder	Important for checking water depth for safety and ensuring there are no effects from shallow water on the ship performance.
Course recorder	Should be checked before the trial and be able to provide a course printout following each trial run.
Fuel flow meter	Either volume flow or mass flow meters to be fitted to ships. Both should be calibrated and cleaned or maintained as per manufacturer’s recommendations.
Gyro compass	Record the ship's heading during the voyage and should be calibrated prior to the trials.

The Guidelines [4] described environmental conditions that should be met for in-service performance measurements presented in the Table 3:

Table 3
Environmental conditions for in-service performance measurements

Parameter	Remarks
Sea state	Conditions as specified in ISO 15016: 2015
Wind speed	Conditions as specified in ISO 15016: 2015
Water depth	Conditions as specified in ISO 15016: 2015
Currents	Avoid areas with known high current values and variations. During the trials, the following condition should be met: $V_{GPS} - V_{STW} < 0.3\ knots$ or conditions as specified in ISO 15016: 2015
Trials period	Trials should be conducted in daylight
Duration	The run duration should be the same for all speed runs with a minimum of 10 minutes, see figure 1 below

Before the start of each performance measurement run, the following data, listed below in the Table 4 should be noted in the Data Reporting Form (see below on Figure 2):

Table 4
In-service environment and conditions

Parameter	Remarks
Displacement	Speed trials should be performed at displacement and draught conditions, which are comparable to those of the delivery sea trials or model tests or assumed ballast conditions. The trim shall be maintained within very narrow limits. For the even keel condition, the trim shall be less than 0.1 % of the length between perpendiculars. For the trimmed trial condition, the fore draught shall be within ± 0.1 m of the ship's ideal condition.
Draught forward, mid and aft	
Water depth	No remarks
Air temperature	Air temperature and pressure should be measured using a calibrated thermometer and barometer.
Air pressure	
Sea water temperature	The local seawater temperature and density at the trial site should be recorded to enable the calculation of the ship's displacement and corrections with regards to viscosity. The water temperature should be taken at the waterline level.
Sea water density	
Anemometer height	Its height from sea level should be recorded.
Fuel density	The fuel's density and LCV to be obtained from a laboratory's analysis report.
Fuel LCV	

The following data presented below in the Table 5 should be collected at the beginning and end of each performance measurement run:

Table 5
Data be collected at the beginning and end of each performance measurement run:

Data	Unit
Main engine supply flowmeter reading	[ltr/h] or [kg/h]
Main engine supply flowmeter temperature	[deg]
Main engine return line flowmeter reading*	[ltr/h] or [kg/h]
Main engine return line flowmeter temperature*	[deg]

* For ships fitted with flowmeter on return line

The following data should also be collected with a sampling rate of at least 1 Hz during the in-service performance measurement in accordance with list presented in the Table 6:

Table 6

Logged parameters during in-service performance measurements

Parameter	Unit
Date	dd-mm-yyyy
Time	hh:mm:ss
Revolution counter reading	[s^{-1}]
Shaft power	[kW]
Heading	[deg]
Ship's speed (GPS and Speed Log)	[knots]
Distance ("0" should be at the beginning of each run)	[nm]
Relative wind speed	[m/s]
Relative wind direction (coming from)	[deg]
Current speed	[knots]
Relative current direction (going to)	[deg]
Observed wave height	[m]
Observed wave period	[s]
Observed wave direction (going to)	[deg]

Apart from power, rpm and consumption, average prevailing values for the following main engine parameters should be provided for each run for the following as shown in the Table 7:

Table 7

The main engine parameters during in-service performance measurements

Parameter	Unit
Scavenge air temperature	[deg]
Scavenge air pressure	[kg/cm^2]
Blower air inlet temperature	[deg]

All data related with in-service performance measurements should be noted in the Data reporting shown on Figure 2:

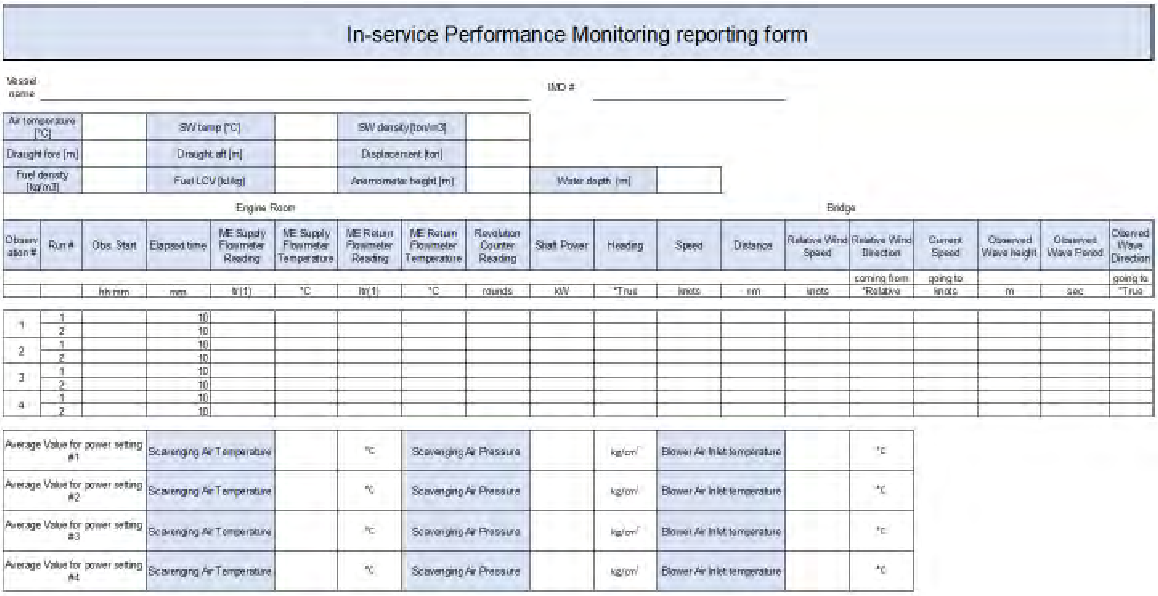

In-service Performance Monitoring reporting form

Vessel name ____ IMO # ____

Air temperature [°C]		SW temp [°C]		SW density [ton/m3]	
Draught fore [m]		Draught aft [m]		Displacement [ton]	
Fuel density [kg/m3]		Fuel LCV [kJ/kg]		Anemometer height [m]	
Water depth [m]					

Observation #	Run #	Obs. Start	Elapsed time	ME Supply Flowmeter Reading	ME Supply Flowmeter Temperature	ME Return Flowmeter Reading	ME Return Flowmeter Temperature	Revolution Counter Reading	Shaft Power	Heading	Speed	Distance	Relative Wind Speed	Relative Wind Direction	Current Speed	Observed Wave height	Observed Wave Period	Observed Wave Direction
		hh:mm	mm	ltr(1)	°C	ltr(1)	°C	rounds	kW	°True	knots	nm	knots	coming from °Relative	going to knots	m	sec	going to °True
1	1		10															
	2		10															
2	1		10															
	2		10															
3	1		10															
	2		10															
4	1		10															
	2		10															

Average Value for power setting #1	Scavenging Air Temperature		°C	Scavenging Air Pressure		kg/cm²	Blower Air Inlet temperature		°C
Average Value for power setting #2	Scavenging Air Temperature		°C	Scavenging Air Pressure		kg/cm²	Blower Air Inlet temperature		°C
Average Value for power setting #3	Scavenging Air Temperature		°C	Scavenging Air Pressure		kg/cm²	Blower Air Inlet temperature		°C
Average Value for power setting #4	Scavenging Air Temperature		°C	Scavenging Air Pressure		kg/cm²	Blower Air Inlet temperature		°C

Figure 2 Example of the In-Service Performance Measurements Reporting Form

5 DISCUSSION - AFTER THE IN-SERVICE PERFORMANCE MEASUREMENTS

All information collected should be checked by the verifier and any errors/typos should be noted in supplementary documentation, including any corrected/replaced values clearly marked in the form. Data which is continually recorded should be provided "as is" and non-variable data should be noted at the beginning and the end of the in-service performance measurements in order to confirm that any changes are set to a minimum.
For each run the following should be submitted:

.1 one filled-in soft copy of the "In-service performance monitoring reporting form";
.2 printouts and/or soft copies from the performance monitoring system output;
.3 printouts and/or soft copies from the loading computer calculations representing the loading condition at which the run took place; and
.4 printouts and/or soft copies from the course recorder for the period covering the run.

A copy of the fuel oil analysis for the fuel used during the in-service performance measurements also should be submitted.
Any comments about the in-service performance measurements, including any large variations in environmental conditions, should be noted.

6 CONCLUSIONS

The Energy Efficiency Existing Ship Index is a new measure under Annex VI to IMO's MARPOL Convention to reduce the Greenhouse Gases (GHG) emissions of ships and is related to the technical design of a ship. The required EEXI value is determined by the ship type, the ship's capacity and principle of propulsion and is the maximum acceptable attained EEXI value. The attained EEXI should be calculated for the individual ship, which falls under the regulation. The paper present IMO's approved methodology to obtain the speed of the vessel Vref for the EEXI calculation when the ship speed-power curve is not available, by the method of measuring the operating performance [4], in accordance with the dedicated IMO guidelines for the calculation of EEXI [2].

REFERENCES

[1] International Maritime Organization, Initial IMO Strategy on reduction of GHG emissions from ships, Resolution MEPC. 304(72), London, 2018.

[2] International Maritime Organization, 2022 Guidelines on the method of calculation of the attained energy efficiency existing ship index (EEXI), Resolution MEPC.350(78), London, 2022.

[3] International Maritime Organization, 2021 Guidance on treatment of innovative energy efficiency technologies for calculation and verification of the attained EEDI and EEXI, MEPC.1/Circ.896, London, 2021.

[4] International Maritime Organization, Guidance on methods, procedures and verification of in-service performance measurements, MEPC.1/Circ.901, London, 2022.

BULK CARRIER WITH RIGID SAILS – COMBINED EFFECTS OF REALISTIC WEATHER CONDITIONS

Arun Krishnan[1], Tomasz Hinz[2] and Grzegorz Mazerski*[2]

[1] Deltamarin Ltd., FINLAND

[3] Deltamarin sp. z o.o., POLAND

(E-mail: Grzegorz.mazerski@deltamarin.com)

Keywords: rigid sail, weather, hullform, bulkcarrier

ABSTRACT

Alternative propulsion technology in form of rigid sails is investigated. Application of two such sails onboard a bulk carrier is simulated. Three different hullforms are developed and their resistance in calm water and in waves is studied. Weather database is sampled for a variety of routes to provide actual power demand. Effects of sails is accounted for, additional corrections for other fuel-saving technologies are also applied. A force balancing routine is also developed to determine the effects of drift generated by sails and counteracted by the rudder. Approx 5% savings from hullform modifications are presented. Improvements from rigid sails were also tested and shown to provide 9 –14 % benefit.

1 INTRODUCTION

The main challenges to the shipping industry nowadays are rising fuel prices and the requirement to significantly reduce CO_2 and other emissions. Such reductions may be achieved by optimizing several design and operational aspects. These can include alternative technologies like rigid wind wings, dual fuel engines, waste heat to power conversion, air lubrication. Such solutions will contribute to the reduction of resistance, generation of additional thrust or recuperation of the energy. The combined effects of these pieces of equipment are addressed in CHEK project that proposes to reach zero emission shipping by disrupting the way ships are designed and operated today.

2 METHODOLOGY

2.1 Hull surface modelling

The hull lines for Kamsarmax bulkers were developed in CATIA. A Kamsarmax vessel developed by DM in the past was used as a reference hull form. This reference hull form was then further developed to improve the calm water resistance of the hull. Kamsarmax bulkers have standardized basic particulars and hull forms of different vessels are similar. Hence, it was more straightforward arriving at the hull form matching the particulars of the actual vessel.

2.2 Hydrostatics

The hydrostatic data were calculated in the NAPA program with verification of the results by CATIA scripts. The hulls used for these calculations were imported from CATIA.

2.3 Calm-water resistance

The calm water resistance is calculated using high-fidelity full-scale CFD simulations that are based on the RANS equations. The CFD simulations are performed using commercial CFD package Simcenter STAR-CCM+ [1] that has an add-on package Estimating Hull Performance (EHP) dedicated for simulations of ship hull in calm water. With this approach there are smaller uncertainties in scaling effects compared to model scale simulations. According to several similar types of reference vessels, Deltamarin Star-CCM+ full scale CFD results also have a good correlation with the model test results.
In the RANS-CFD simulations the ship hull is free to sink and trim. The fluid flow is modelled as a turbulent viscous flow. A Volume of Fluid (VOF) approach is adopted that accounts for the free surface effects and captures the air/water interface. Due to the symmetry condition of the hull and the motions, only one half of the ship is modelled in the CFD simulations. A trimmed cartesian mesh is used to discretize the fluid domain into finite volumes. Volumetric refinements are provided on the free surface to capture the waves dissipated from the ship.
Model tests result of a reference hull form are used to compare the results simulations and the measurements and arrive at the correlation factor. Firstly, CFD simulations were conducted on the reference hull form and the effective power (PE) was predicted using HSVA calculation procedure [2]. The reason being that the model tests were conducted in HSVA. Then the difference between the predictions and the actual measurements can be used to assess the accuracy of the results and the correlation factor between the measurements and the simulations. This constant correlation factor is further used in the all the future simulations.

2.4 Air resistance and Added resistance in waves

Wind and wave resistance is calculated using ITTC recommended procedures and guidelines for analysis of speed trails [3] for the bulker. The wind resistance coefficients for angle of attack are obtained from the same guidelines report for a representative hullform. The true wind speed and direction is transformed to apparent wind conditions using the vessel speed. The apparent wind conditions are used in the formula for calculating the air resistance values in kN.
Wind resistance due to the apparent wind is:

$$R_{AA} = \frac{1}{2}\rho_A V_{WR}^2 C_X(\psi_{WR}) A_T$$

where A_T is maximum transverse section exposed to the wind, C_X is wind coefficient (-C_A), V_{WR} is the apparent wind speed, ψ_{WR} is apparent wind direction where 0 means head wind and ρ_A is the air density. If the wind speed is measured by the anemometer (in the case of historic data) it was corrected for the wind speed profile considering, the height of the anemometer and the reference height for the wind resistance coefficients (normally 10 m) according to ITTC recommendations.
The wave resistance is calculated using the STA-WAVE2 method. Irregular waves can be represented as linear superposition of the components of regular waves. Furthermore, the mean resistance increases in short crested irregular waves. R_{AW} is calculated by linear superposition of the directional wave spectrum E and the response function of mean resistance increase in regular waves R_{wave}:in this method. The relationship can be represented as:

$$R_{AW} = \int_0^{2\pi}\int_0^{\infty} \frac{R_{wave}(\omega, \alpha; V_s\,)}{\varsigma_a^2}\, E(\omega, \alpha) d\omega d\alpha$$

R_{AW} mean resistance increase in short crested irregular waves, R_{wave}:mean resistance increases in regular waves, ς_a: wave amplitude, ω: circular frequency of regular waves, α: angle between ship heading and incident regular waves; 0 means heading waves, V_S: ship speed through the water, E: directional spectrum which relates to the angular distribution function and frequency spectrum as:

$$E = S_f(\omega)G(\alpha)$$

The modified Pierson-Moskowitz frequency spectrum of ITTC 1978 is used for definition of $S_f(\omega)$ The total resistance of the vessel in wind and waves is then represented as:

$$R_T = R_{calm} + R_{AW} + R_{AA}$$

Then the total shaft power in weather is calculated in the following way:

$$P_s = \frac{R_T V_S}{\eta_D \eta_s}$$

Each route and voyage periods are processed as a time series data with the wave and weather conditions. The speed is assumed constant for this process of comparing the performance of the hull forms. For each time series data point the calm water resistance, wind and wave resistance is calculated as per the procedure described above. The final total shaft power is then estimated for each data point and for the routes analysed.

2.5 Sail Effect

The effect of having sails on the shaft power demand of the bulker is studied for all the routes. It is assumed that the ship is fitted with two sails that assist in the propulsion. To accurately predict the savings it is crucial to perform a 4DOF analysis of a ship and conduct a force balancing optimization routine to determine the yaw, heel moments, thrust and leeway of the ships. It can be assumed that the effect of heel moments could have a small effect on the vessel performance as can be concluded from various research publications. However, the effect of yaw and leeway or drift should be fundamental when calculating the performance. The drift and yaw would also influence the performance of air bubble (air lubrication) technology. The model for such force balancing is being developed now and the initial calculations show satisfactory results. The thrust provided by the sails and the preliminary savings due to the same provide a good understanding of the performance of the ship with and without sails. A detailed comparison will be shown between the shaft power demand and the percentage savings along various routes for the variants of bulker.

The apparent wind conditions are calculated using the true wind data and the vessel speed. The apparent wind conditions will be used in calculating the lift and drag forces produced by the sails. The lift and drag coefficient for one sail was provided by BAR Technologies. This data is used to calculate the local lift and drag forces produced by the sails for various angles of attack. In the calculation it is assumed that the sails perform best around 40 to 135 deg relative wind angles and at this angular range the sails produce maximum lift. Basically, the angle of attack in this interval is optimized to produce the maximum lift force and this is around 38 deg. In the range of 0-20 deg the sails are adding a small drag, and this is same for following winds for angles greater than 140 deg. The effect of boundary layer is also included in the calculations. The calculated thrust and drag forces are then transformed to the ship coordinate system.

$$F_T = L.sin\alpha - D.cos\alpha$$
$$F_L = L.cos\alpha + D.sin\alpha$$

where F_T and F_L are thrust/driving force and side force on the vessel assuming no heel, L and D are sail's lift and drag forces and α is the apparent wind angle. When the thrust and side forces for the effect of two sails are calculated the forces do not exactly double but there is an interaction between the sails.

Finally, the propeller thrust that the ship must generate to achieve an equilibrium is:

$$T(1-t) = (Calm\ water\ resistance + added\ resistance\ in\ waves + added\ resistance\ due\ to\ wind + hull\ induced\ resistance) - wind\ assist\ thrust$$

The hull induced resistance is not calculated in this analysis (see section 2.3.). This effective thrust is used in conjunction with the propulsion data to calculate the shaft power demand.

2.6 Hull fouling

The increase in shaft power demand due to hull fouling has been estimated as an addition to the standard frictional resistance coefficient ΔCFR as per the well-known ITTC method. The standard HSVA extrapolation method is employed for the calculation of this increase in frictional coefficient. In this method a hull roughness of 150 micros is considered as clean hull and for roughness values other than 150 microns the propulsion data for the full-scale ship is corrected to include the added frictional resistance ΔCFR due to fouling.

$$\Delta C_{FR} = C_{FR} - C_{FR.\ KR=150}$$

$$C_{FR} = 0.075/[\log(Rn/(1+0.0011\frac{K_R}{L}\ Rn)) - 2]^2$$

where K_R is the average hull roughness.

[4] is referred to estimate the value average coating roughness for different forms of hull fouling. The calculations are made for light slime, heavy slime, and small calcareous conditions.

2.7 Air Lubrication

The effect of air lubrication provided by Silverstream Technologies is considered simply by using a percentage reduction in final shaft power demand at this stage. In the later stage of the project the hydrodynamic interactions of sails and air lubrication will be treated more comprehensively. As stated earlier, wind-assisted ship sails with leeway or drift angles. The leeway angles will result in the flow lines not aligned parallel to the flat bottom resulting in an oblique flow along it. The air lubrication system is designed to have the air carpet propagating and covering the flat bottom to reduce friction. Nevertheless, the oblique flow under the flat bottom could result in the bubble carpet to be carried away partially. This effect can be estimated using CFD simulations at various drift angles and considering the percentage wetted surface area covered by the flow lines. The estimated frictional resistance will be then corrected using the lower flat bottom area covered.

2.8 Gate rudder

The effects of gate rudder are not accounted for in this report except for regular rudder interactions due to effects of wind. Any manoeuvring or reduced resistance benefits are not analyzed or included. Also, the influence of the gate rudder on the hull shape in the stern area is not analyzed.

2.9 Bulker hullform development

CHEK project concentrates on two ship types, one of them being Kamsarmax-size bulk carrier (approx. 80 000 dwt). A base bulk carrier hull form and its variants are developed from this data.

Table 1
Basic particulars of Kamsarmax bulk carrier

LOA	229.00 m
LPP	225.06 m
Breadth	32.26 m
Deadweight and draft	80900 MT at 14.475 m
MCR and rpm	8880 kW at 86.5 rpm
Laden- service speed and shaft power	14 knots at 80% MCR

A standard ship design practice is followed for the development of alternative hull forms, which includes the following steps:

- Identify the selection criteria
- Select variables and decide how to achieve them,
- Recognize the constraints that have been identified and that impose limits on design changes,
- Generate an alternative hull shape,
- Conduct the calculations.
- Compare the results

Several potential selection criteria have been identified. Based on these, the following two have been chosen:

- low calm water resistance
- low added resistance in waves

In preparing the alternative hull forms, changes to the following elements were considered:

- width of stern bulb
- angle of frames forward of propeller
- radius of frame shape between flat bottom and stern bulb
- angle of frame at waterline
- transverse and vertical location of bulb
- widest point o entrance angles of waterlines at bow
- width of deck and deck knuckle lines

In the process of the creation of alternative hull forms, there has been an assumption that there will be no change in main dimensions incl. displacement, no reduction of stability, location of propeller/propulsors are the same and propeller tip clearance for all hull is the same.

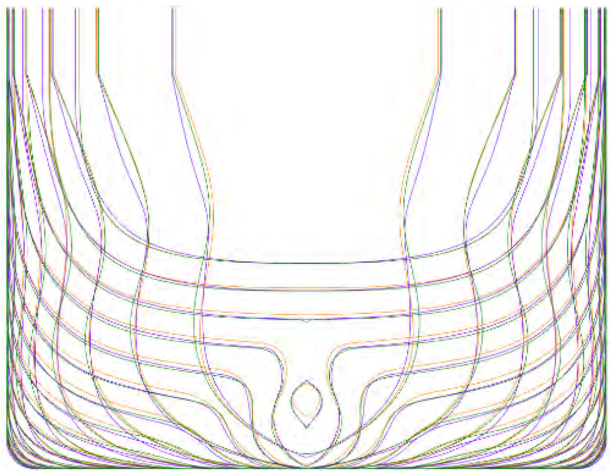

Figure 1 Hull form comparison

The hullform development process is concluded by obtaining three different hullforms, as presented in Figure 1 and Table 2.

Table 2
Basic particular of three bulk carrier hull forms in full load

		BR1	BA1	BA2
lpp	[m]	225.06	225.06	225.06
beam	[m]	32.26	32.26	32.26
draft	[m]	12.20	12.20	12.20
block coefficient	[-]	0.876	0.873	0.874
lcb	[m]	114.73	119.01	114.73
wetted surface	[m^2]	11700	12883	11485
metacenter	[m]	11.98	13.61	13.57

2.10 Routes and weather

Based upon information provided by the ship charterer (and partner in CHEK project) six different routes were selected as a realistic sample of operations for this size of bulk carrier. These are presented in Table 3 below.

Table 3
Routes tested

	Departure	Arrival	Via	Length
A	Brazil	China	Cape of Good Hope	11220 nm
B	China	Australia (Newcastle)		4812 nm
C	Australia (Newcastle)	Brazil	Cape Horn	7243 nm
D	Australia (Newcastle)	Brazil	Cape of Good Hope	8698 nm
E	Rotterdam	Baltimore		3646 nm
F	Baltimore	Brazil		5002 nm

A navigations routing software Wartsila FOS coupled with an interpolation algorithm is used to generate a set of geographical coordinates with fixed distance interval.

In order to account for a seasonal weather variability, it is assumed that the ship sails along each of the routes 12 times, starting on the first day of each month. Based on the vessel's position and assumed time the wind and wave parameters are gathered from the weather database. Data extraction algorithm is presented in Figure 2 below.

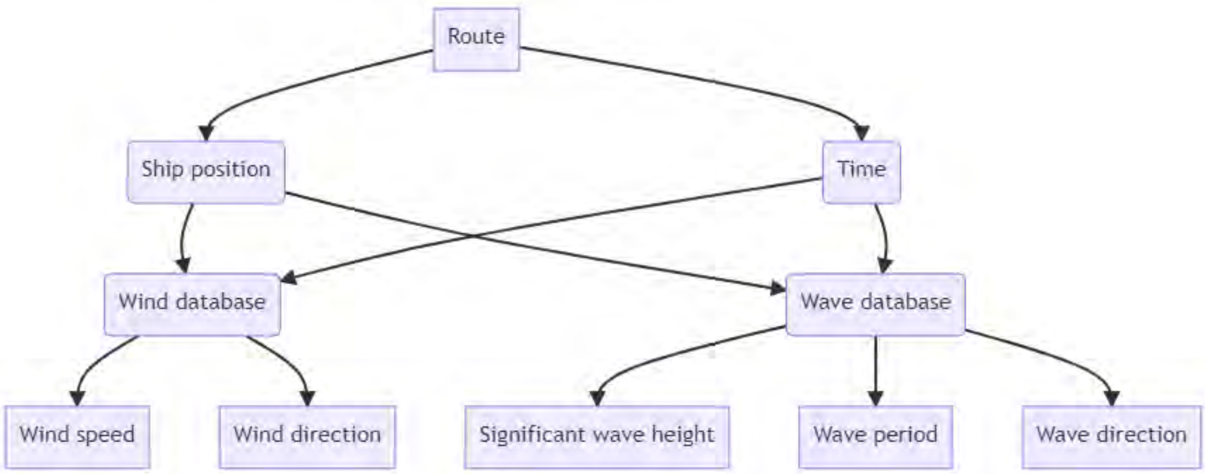

Figure 2 Algorithm for extraction and processing of data for added resistance

The main databases used in the project are those provided by the European Commission initiative called Copernicus ([5] and [6]). This initiative aggregates data provided by European meteorological institutes. This data is based on information provided mainly by satellite observation. The main source of data for the marine environment is the Copernicus Marine Environment Monitoring Service. Information about winds can also be obtained from Copernicus Climate database.

3 RESULTS AND DISCUSSION

A summary of the results is presented in this section.

3.1 Calm water resistance

Table 4
Effective power [kW] for design draft for various speeds and hull forms

hull form	11,5 kn	%	12,5kn	%	14,5kn	%
Reference hull form BR1	2416	100,00	3041	100,00	4791	100
Alternative hull form BA1	2282	94,45	2919	96,00	4683	97,74
Alternative hull form BA2	2305	95,40	2926	96,23	4619	96,40

For further calculations (covering only alternative hull forms) of added resistance in waves and effects of sails delivered power (Pd) is used:

Table 5
Delivered power [kW] for design draft for various speeds and hull forms

hull form	11,5 kn	12,5kn	14,5kn
Alternative hull form BA1	3104	3987	6264
Alternative hull form BA2	3043	3914	6164

3.2 Added resistance in waves

Table 6
Delivered power [kW] including effects of waves along the routes for design draft of T=12,2 m for alternative hull forms

hull form	Calm water @ 12,5 kn	Yearly average power in waves	Average increase in waves
BA1	3987	4773	19,71 %
BA2	3914	4680	19,56 %

3.3 Effects of sails

Table 7
Delivered power [kW] including effects of waves and sails averaged across all routes, for design draft of T=12,2 m for alternative hull forms

hull form	In waves, without sails	In waves, with sails	Reduction with sails
BA1	4773	4198	12,04 %
BA2	4680	4117	12,02 %

4 CONCLUSIONS

Hull form of case vessel (reference hull form) was re-created as far as practically possible. Alternative hull forms were developed by modifying certain hull areas, while retaining the values of constraint factors.

Results suggest that an improvement of between 2,2% to 5,5% are possible by modifications of the hull form alone. Similar improvements are valid both for calm water as well as in realistic weather conditions. Improvements from rigid sails were also tested and shown to provide 9 – 14 % benefit (for two sails). It should be noted that the methodology presented in this report for analyzing the effect of sails does not include 'searching for weather'. It is expected that weather routing to find better winds would increase the savings due to sails optimistically. Importance of fouling seems to be quite high.

ACKNOWLEDGMENT

The research presented in the paper was conducted under EU Horizon 2020 project deCarbonising sHipping by Enabling Key (CHEK – Contract No. 955286).

REFERENCES

[1] STAR-CCM+. (2012). STAR-CCM+ version 13.02 manual.

[2] Bugalski, Tomasz, Streckwall, Heinrich and Szantyr, Jan A.. "Critical review of propeller performance scaling methods, based on model experiments and numerical calculations" Polish Maritime Research, vol.20, no.4, 2013, pp.71-79

[3] ITTC. (2014). Analysis of Speed/Power Trial Data. *ITTC-Recommended Procedures and Guidelines*. https://doi.org/7.5-04-01-01.2

[4] Schultz, M. P. (2007). Effects of coating roughness and biofouling on ship resistance and power. Biofouling, 23(5), 331–341.

[5] *Global Ocean Waves Analysis and Forecast,* Mercator Ocean International, https://doi.org/10.48670/MOI-00017

[6] *Global Ocean Wind L4 Near real Time 6 hourly Observations*. Mercator Ocean International, https://doi.org/10.48670/MOI-00184

NUMERICAL ASPECTS OF LIFTING FOIL SYSTEMS DESIGN AND ANALYSIS

Król Przemysław[1]

[1] Centrum Techniki Okrętowej, Ośrodek Hydromechaniki Okrętu, POLAND.

(E-mail: przemyslaw.krol@cto.gda.pl)

Keywords: Hydrodynamics, propeller, vortex method, design, lifting blade

ABSTRACT

The paper summarizes efforts towards development of numerical methods dedicated for lifting blade of screw propeller design and analysis. Core aspect is connected with analysis of a given blade geometry in known kinematic conditions for determination of its hydrodynamic properties. Complementary task is defined to design blade geometry to realize required loading for known operating profile. Both aspects are covered both for stand-alone propeller and for propulsor unit, consisting of rotor – propeller and stator – guide vane.

1 INTRODUCTION

Vortex theory is wide-known and well-documented tool for lifting blade design and analysis. Its theoretical background is formed by ideal fluid model and hydromechanics singularities (vortex filament, source/sink, doublet) used to model the flow pattern.

Generally, vortex models applied for lifting blade may be divided into three main groups. Lifting line models replace actual blade geometry with a straight-line vortex filament of variable intensity hence it is followed by a vortex wake of so called 'trailing' of 'free' vortices. Determination of radial loading distribution require additional knowledge on blade section profile's dynamic characteristics.

More sophisticated model – and adopted in this paper – is a lifting surface. Entire blade is reproduced with its outline in numerical domain. It is however assumed to have zero thickness. Thus loading of the blade is modelled via radial and chordwise distribution of so calles 'bound' vortices, while finite thickness – if not ignored – is modelled via distribution of sinks and sources.

Most realistic of vortex models is a boundary elements method, in which singularities are distributed over entire surface of the object's body. It allows to get separate circulation distribution over lifting and pressure sides of a lifting foil.

Lifting surface model was selected for most of works discussed here due to its optimum – in Author's opinion – balance between accuracy and computational cost. While it allows quite precisely reproduce radial and chordwise loading distribution for most cases, it requires only one set of singularities to cover entire blade – instead of two separate systems for both its sides.

This paper is divided into four theoretical parts: describing vortex model application for determination of screw propellers hydrodynamic characteristics and for the design of blade. Third part deals with additional features of the model, when propulsor system, consisting of rotor and stator, is to be analysed. Fourth, last part gives a few comments on strength calculations with FEM.

2 LIFTING BLADE ANALYSIS

In its basic form lifting surface model assumes that only propeller blades are modelled, while kinematic boundary condition on the hub may be ignored. Mentioned condition is one of tangent flow, stating that vector sum of external inflow – which may be uniform or not – and velocities induced by singularities system, has to be tangent to the blades surface. This statement forms a base for construction of linear equations system, allowing to track down circulation distribution.

Various approaches are met in the literature according shape of the vortex wake. For some cases, especially for lightly loaded propeller or when agreement between advance ratio and determined loading is not a goal of calculations, it is sufficient to assume it as rigid helical surface. In such case its shape – mainly vortex wake pitch, sometimes its contraction also – is determined based on blade's pitch and kinematic conditions. In most cases however it is necessary to incorporate more advanced model. There are known semi-empirical formulas for this however best approach (from reliability of the results) seems to be vortex wake relaxation. It is an iterative process of determination of vortex wake shape according to the velocity field induced by the operating propeller. As wake's shape impacts directly on the propeller's loading and thus – its induced velocities – it makes the process iterative. For highly loaded propellers (i.e. high angles of attack) it is even recommended to include leading edge separation and leading edge trailing vortices (this is rare case however for models met in literature and was not implemented by the Author).

Total blade hydrodynamic reactions may be determined variously. Two basic approaches are determination of surface pressure distribution by means of Bernoulli theorem and determination of local lifting forces, by means of Zhoukovsky law. These forces are then integrated over the blade surface. By its nature, the vortex models do not include fluids viscosity, hence the resistance has to be accounted for by other means. Most popular approaches include determinations of surface friction forces by local kinematic conditions and/or by use of section profile's resistance data.

3 LIFTING BLADE DESIGN

Lifting surface method as outlined above may be (almost) directly used for design task. In such case one has to determine spatial circulation distribution, satisfying demanded loading conditions (like target thrust force at given advance velocity and rate of revolution). The singularities are placed on some surface, which is treated as initial iteration of final blade shape. This is obtained via determination of induced velocities and adjustment of the geometry to fulfil kinematic boundary condition.

4 ROTOR – STATOR INTERACTION

Vortex model can easily incorporate interaction between the propeller and some kind of stator – let it be downstream rudder or, what was widely studied by the Author, upstream guide vane. In such case each of them are calculated separately. Only second objects mean induced velocities in given position are taken into account, e.g. mean guide vane – induced velocities in propeller position, when the propeller is analysed.

Such approach is justified as in most cases propellers rate of revolution is quite high and it proved sufficiently exact for determination of time-averaged dynamic properties of propulsor system.

5 STRENGHT CALCULATIONS

Vortex model can easily incorporate interaction between the propeller and some kind of stator – let it be downstream rudder or, what was widely studied by the Author, upstream guide vane. In such case each of them are calculated separately. Only second objects mean induced velocities in given position

6 SUMMARY

Methods outlined above were widely utilized by the Author for several tasks. Important example of standalone propellers design, were single-screw vessel propellers P759 and P766. Their models were manufactured and tested in model scale in CTO-Gdańsk.

Figure 1 Propeller P759 during cavitation tests

Figure 2 Propeller P766 during cavitation tests

Another important case was design of propeller cooperating with the guide vane stator object. First attempt was propeller CP745 with guide vane ST001. These were designed with preliminary version of vortex model, which was later developed when system CP753+ST002 was designed:

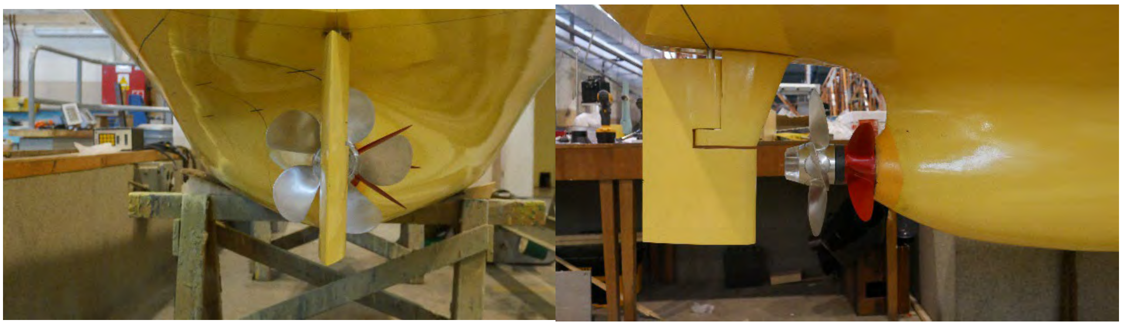

Figure 3 Propeller P753+ST002 before self-propulsion tests

Mature version of mentioned algorithm was utilized for the design of two systems, with propeller CP790 cooperating with two different guide vanes: CP790+ST003 and CP790+ST004.

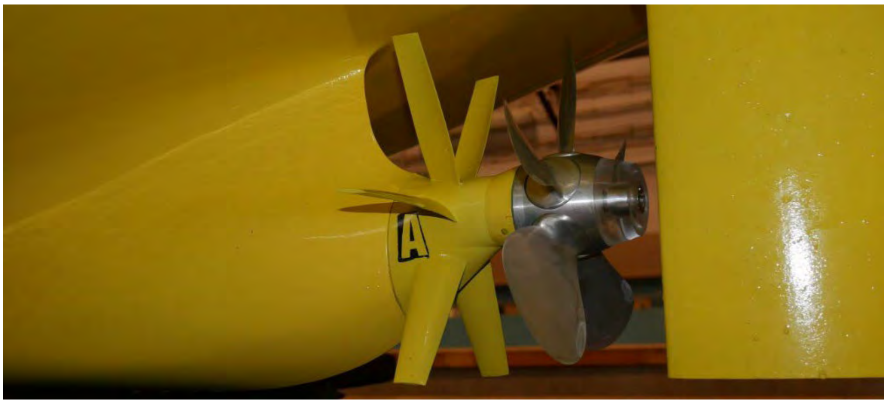

Figure 4 Propeller CP790+ST003 before self-propulsion tests

Figure 5 Propeller CP790+ST004 before self-propulsion tests

ACKNOWLEDGMENT

Some results presented in this paper were obtained within following projects:

- Internal Research Fund of CTO Gdańsk,
- European Project INRETRO – 'Support of improvement methods for propellers and propulsion tests by use of numerical analysis for propeller and ship hull interaction" MARTEC II/1/2015,
- Energy Saving Techniques for Energy Efficient Vessels and Emission Reduction towards Green Shipping, POLTUR3/ESTHETICS/1/2019, NCBiR
- NextProp – Next Generation of Propeller B-1466-GEM1-GP, European Defence Academy.

REFERENCES

[1] Król P. „Vortex Model of Ideal Guide Vane and its Application to the Real Guide Vane" Sixth Symposium on Marine Propulsors SMP'19, Rome 2019.

[2] Król P., Bugalski T. "Application of vortex flow model in propeller – stator system design and analysis" Polish Maritime Research No 1(97) 2018 Vol 25.

[3] Król P., Tesch K. „Experimental and numerical validation of the improved vortex method applied to CP745 marine propeller model" Polish Maritime Research No 2(98) 2018 Vol 25.

[4] Król P., Tesch K. "Pre-swirl energy saving device in marine application" XXIII Krajowa Konferencja Mechaniki Płynów, Zawiercie 2018.

[5] P. Król, 'Blade section profile array lifting surface design method for marine screw propeller blade', *Polish Maritime Research,* vol. 26, no. 4, 2019, doi: 10.2478/pomr-2019-0075

[6] Koronowicz T. "Model teoretyczny strumienia śrubowego oparty na formie skupionej wirowości z rdzeniem kawitacyjnym oraz charakterystyki hydrodynamiczne układów wirów swobodnych w przestrzeni ograniczonej" Zeszyty Naukowe IMP PAN w Gdańsku, Gdańsk 1979

[7] Bugalski T., Streckwall H., Szantyr J. "Critical review of propeller performance scaling methods, based on model experiments and numerical calculations" Polish Maritime Research No 4(80) 2013 Vol 20

[8] Bugalski T., Szantyr J. „Numerical Analysis of the Unsteady Propeller Performance in the Ship Wake Modified By Different Wake Improvement Devices" Polish Maritime Research No 3(83) Vol. 21, 2014

DETERMINATION OF THE VORTEX WAKES BEHIND OFFSHORE WIND TURBINES

Leszek Kwapisz[1], Jan Andrzej Szantyr[2], Marek Narewski[3]

[1,] Institute of Fluid-Flow Machinery of the PAS, Poland.

(E-mail: kwapi@imp.gda.pl)

[2]Gdańsk University of Technology, Poland.

(E-mail:jan.szantyr@pg.edu.pl)

[3]Polish Register of Shipping, R&D Department, Poland.

(E-mail: marek.narewski@prs.pl)

Keywords: aerodynamics, wind turbine, vortex ,wake

ABSTRACT

The article presents a simplified method for determination of the vortex wakes behind wind turbines which can be used when designing the arrangement of turbines on a wind farm in terms of maximum farm efficiency.

The calculation method is based on surface distribution of vorticity on the blades of the turbines and employs a model for dissipation of the shed wake vortices, which is controlled by the assumed turbulent viscosity coefficient.

There is a discussion on the typical wake angle behind a wind turbine.

1 INTRODUCTION

Tip vortices are generated behind the tips of lifting foils. They are result of the lift forces generation process. These vortices carry high energy and they may interact negatively with other bodies located in the flow stream. A well-known example is that vortex wakes behind large aircraft can extend up to 8 kilometers and entering these wakes by other, especially smaller aircraft, should be avoided. Similar problems can appear in the wakes generated behind offshore wind turbines, where the vortices can interact with all other kind of objects including neighboring wind farm towers or servicing waterborne crafts, helicopters, inspection drones and possibly offshore farm serviceman or even SAR rescue personnel.

The problem of the windmill wake expansion angle is a classical problem [8] when designing the lay-out of windmills in offshore as well as on land wind farms, taking into account the prevailing wind direction. For planning arrangement of wind towers, the wake analysis guidance is provided in IEC-61400-1 std and particularly in Annex H [15]. Determination of turbines lay-out is an important part of wind farm design process, being essential for optimisation electrical energy produced by wind farm. Finally, optimal wind turbines lay-out at can be subject of verification during wind farm documentation approval as a part of further certification process for IEC-61400 std.

2 METHODOLOGY

2.1 Calculation according to the original algorithm

The algorithm is based on the lifting surface theory, which enables calculation of potential flow around a rotor of an arbitrary geometry. The rotor is modeled by the distribution of vortices and sources. The kinematic boundary condition on the lifting surface leads to the equation:

$$\frac{1}{4\pi}\left[\int_{S_P}\bar{n}\,\bar{\gamma}_P\nabla\left(-\frac{1}{r_P}\right)dS_P+\int_{S_W}\bar{n}\,\bar{\gamma}_W\nabla\left(-\frac{1}{r_W}\right)dS_W+\int_{S_P}q_P\frac{\partial}{\partial n}\left(-\frac{1}{r_P}\right)dS_P\right]=-\left(\bar{V}+\varpi R\right)\bar{n} \qquad (2.1)$$

where:

$\bar{n}$ – unit vector normal to the surface

$\bar{\gamma}_P$ – vorticity distribution on the rotor blades

$\bar{\gamma}_W$ – vorticity distribution in the wake

q_P – source distribution on the rotor blades

r_P, r_W – distance of the surface element from the computation point

S_P – blade area (lifting surface)

S_W – wake surface

$\bar{V}$ – wind velocity

ϖ – angular velocity of the rotor

R– promień na którym znajduje się punkt obliczeniowy

After the aerodynamic characteristics of the turbine are calculated from the above, the parameters of the wake behind the turbine are determined. In order to take into account the viscous phenomena such as turbulence, the tip and hub vortices are described using the Lamb/Rankine vortex model. Rankine model is based on the concept of the vortex kernel, which rotates as a solid body. Lamb model assumes additionally dissipation of this vortex. The circumferential velocity outside this dissipating kernel may be determined from the formula:

$$U_T=\frac{\Gamma}{2\pi r}\left[1-\exp\left(-\frac{r^2}{R_l^2}\right)\right] \qquad (2.2)$$

where:

$R_l=2\sqrt{\nu t}$ -- radius of the dissipating vortex kernel, increasing with time t (v - combined molecular and turbulent viscosity)

Γ - circulation of the vortex

Based on the theory of an ideal axial wind turbine the following formula for the radius of the vortex wake "far behind" the turbine (i.e. about 3D behind the rotor) may be developed:

$$R_S=R_W\sqrt{\frac{1-1/2m}{1-m}} \qquad (2.3)$$

where:

R_S – radius of the wake "far behind"

R_W – radius of the rotor

The parameter m is determined from the following quadratic equation:

$$m^2 - 2m - C_T = 0 \quad (2.4)$$

where C_T is the loading coefficient of the turbine.

$$C_T = \frac{T}{1/2 \rho V^2 S} \quad (2.5)$$

Where :

T – axial force on the turbine
V – wind velocity
P – density of the air
S – area of the turbine disc.

2.2 How the angle α may be determined

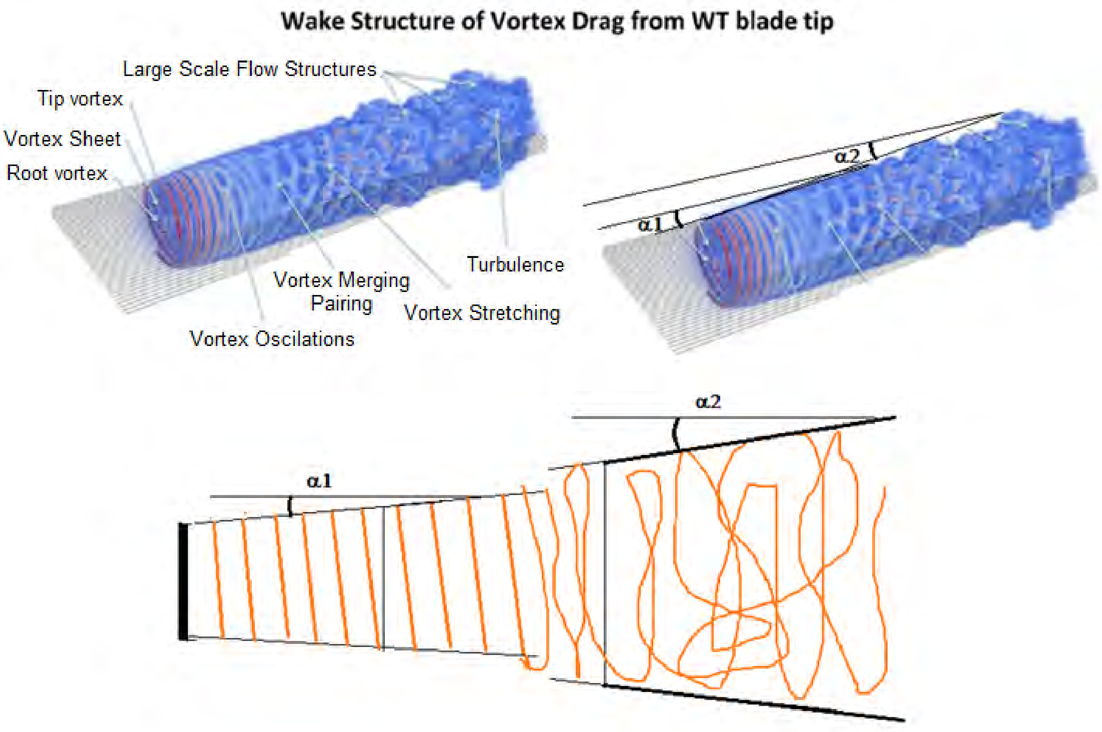

Figure 1 The wake expansion angle is smaller close to the turbine

In the first approximation the wake behind the turbine may be presented as a cone. The angle α is named below as the wake expansion angle. The angle α is equal to the half of the cone angle. The wake expansion angle should not be mistaken for the cone angle.

Experiments conducted in the wind tunnels, together with field observations, as well as numerous computer simulations based on different theoretical models, show that the wake expansion angle close to the turbine is rather low and is included in the range between 1.7 and 3 degrees.

According to Fig1, two different wake cones should be considered: one close to the turbine with an angle α1 and another at a larger distance from the turbine with an angle α2.

Analyzing the Fig. 1 it may be assessed that α1=0.5 α2. Consequently, for α2 =5.70 as in [8] α1= 2.850 and for α2= 4.2 [9] α1= 2.10. These values of α1 are realistic and they can be confirmed by the results quoted below.

The angle 5.70° is generally accepted in analysis of the problem of mutual interaction of turbines forming a wind farm.

3 RESULTS AND DISCUSSION

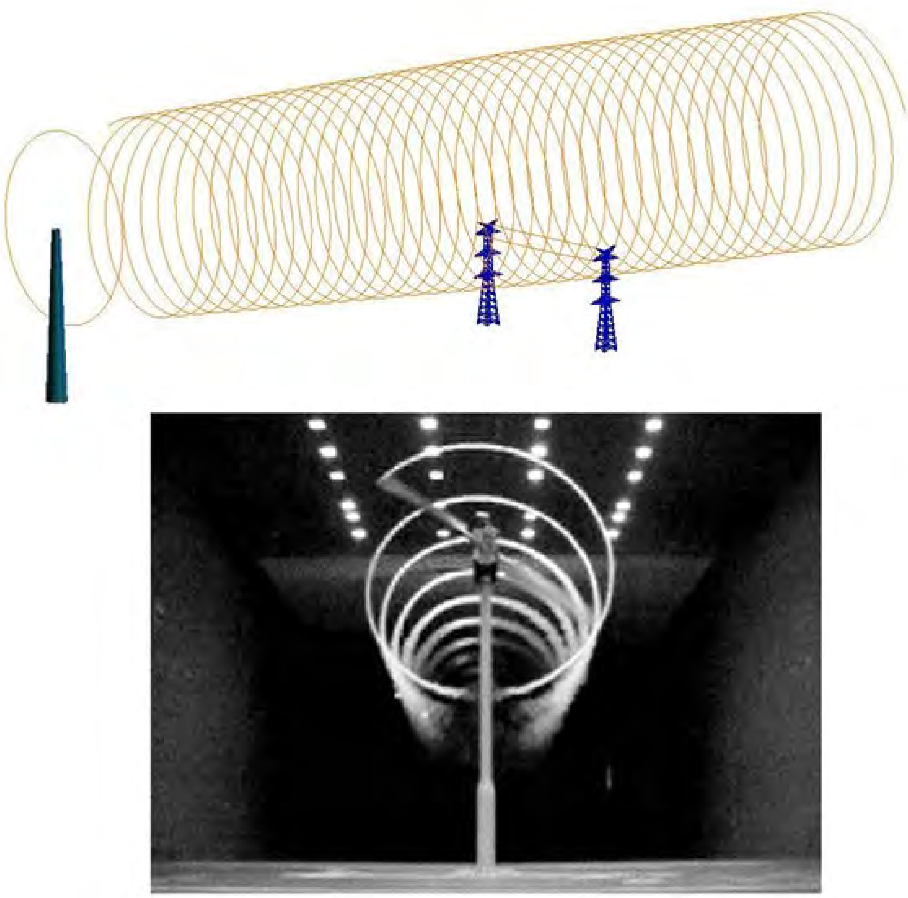

Figure 2 Helical vortex lines shed from the turbine: own calculation (up) versus experiment [1] (down).

Table 1
Example of the results: Calculation of the turbine wake diameter at 2D behind the turbine

Lp	V_0 [m/s]	C_T (our calc.)	Dw(Jensen) [m]	Dw(our calc.) [m]
1	10.0	0.536	127.8	126.1
2	15.0	0.148	123.7	121.5
3	20.0	0.074	122.0	120.8

where: V_0 – wind velocity; D = 120m diameter of the turbine; Dw – diameter of the wake (at 2D)

4 CONCLUSIONS

A simplified method of calculating the vortex wake behind a wind turbine has been presented. The proposed method creates possiblity to estimate the intensity of shed vortices and the vortex wake angle in the initial phase of the wake, where concentrated helical vortices occur. The discussion showed that the typical wake expansion angle in the initial phase is small (1.7-3 degrees), and is about 5.7 degrees in the further phase, according to Jensen's proposal of 1983.

REFERENCES

[1] Hand M, Simms D, Fingersh L, Jager D, Cotrell J,SchreckS, Larwood S. Unsteady aerodynamics experiment phase vi: Wind tunnel test configurations and available data campaigns. Technical report NREL/TP-500-29955, NREL, December 2001 (www address https://www.arising.com.au/aviation/windturbines/wind-turbine.html)

[2] A. van Garrel; Development Of A Wind turbine Aerodynamics Simulation Module; University of Twente, Enschede (UT)ECN-C--03-079 August 2003 NL
(www: https://www.researchgate.net/profile/Arne-Van-Garrel/publication/299643591_Development_of_a_Wind_Turbine_Aerodynamics_Simulation_Module/links/5703bb1c08aea09bb1a44b01/Development-of-a-Wind-Turbine-Aerodynamics-Simulation-Module.pdf)

[3] Paul Dvorak; CFD simulations give insight to rotor designs Wind Power Engeneering Development;11 August 2014; https://www.windpowerengineering.com/cfd-simulations-give-insight-rotor-designs/

[4] David MartenQBlade v0.9 Guidelines
QBlade@outlook.com ; Copyright 2015, TU Berlin
(www:https://www.scribd.com/document/319814553/QBlade-Guidelines-v09

[5] Pavithra Premaratne; "Analysis of wind turbine wake characteristics in atmospheric boundary layer winds"A dissertation submitted to the graduate faculty in partial fulfillment of the requirements for the degree of Doctor of Philosophy Iowa State University; Ames, Iowa; Copyright©Pavithra Premaratne, 2018.

[6] https://www.nigeq.com/#WT

[7] Stefan Ivanell; Wind Turbine Wakes and Wind Farms - Lecture 2: Flow behind the turbine, i.e. the wake; KTH Royal Institute of Technology Stockholm, 2015
www.ivanell.sestefani@mech.kth.se
(https://www.kth.se/social/files/56096af4f276542c937e5362/Wind Turbine Aerodynamics_L2_20150928_Wakes.pdf)

[8] Jensen, N. O. (1983); A note on wind generator interaction; Risø National Laboratory. Risø-M, No. 2411

[9] R. J. Barthelmie Sara, C Pryor; Automated wind turbine wake characterization in complex terrain; June 2019; Atmospheric Measurement Techniques 12(6):3463-3484 https://www.researchgate.net/figure/Schematic-of-wind-turbine-wake-expansion-downwind-and-the-scanning-volume-needed-grey_fig2_334104176

[10] Tadeusz Koronowicz, Jan A. Szantyr; Comparative analysis of the theoretical models of ideal propulsor, ideal fluid brake, ideal screw propeller and ideal axial wind turbine; Polish Maritime Research No 2 (78) 2013 Vol 20

[12] Paul van der Laan, Pierre-Elouan Réthoré, Alfredo Peña Diaz, Gunner Chr. Larsen, Søren Ott; Wind turbine wake models developed at the Technical Universityof Denmark: A review Tuhfe Göçmenn Technical University of Denmark, Department of Wind Energy, Risø campus, Roskilde, Denmark Renewable and Sustainable Energy Review; January 2016

[13] J.N. Sørensen, W.Z. Shen; Numerical modelling of wind turbine wakes; J. Fluids Eng, 124 (2) (2002), pp. 393-399

[14] Robert Jóźwiak and others "Badania eksperymentalne w tunelu aerodynamicznym i analizy numeryczne zjawisk przepływowych w śladzie turbiny wiatrowej"; Warszawa 2012, (Experimental Study and Numerical Analyses of the Flow Phenomena in the Wind Turbine Wake)

[15] IEC-61400-1 std: Wind turbines – Part 1: Design requirements

OVERVIEW OF CALIBRATION METHODS FOR UNDERWATER ACOUSTIC AND PRESSURE SENSORS FOR SHIP MEASUREMENT

Karol Listewnik [1]

[1] Gdynia Maritime University – Faculty of Electrical Engineering

(E-mail: k.listewnik@we.umg.edu.pl)

Keywords:

ABSTRACT

Due to the growing demand for research into the marine environment in the field of underwater noise, conducted in accordance with the requirements of Directive 2008/56/EC, and the need to study the underwater noise of ships and other floating objects for military purposes, there is a need to calibrate pressure and acoustic sensors. Ensuring the reliability and repeatability of recorded data starts with reliable calibration of the hydrophones and/or the entire recorder. The aim of the article is to discuss the calibration methods of pressure sensors and hydrophones used to test objects in the marine environment in the frequency range from 0.1 Hz to 1 MHz, along with examples. Standards containing a description of hydrophone calibration methods have also been referred to. Finally, activities in the field of construction of metrological infrastructure in the field of underwater acoustics in Poland were presented.

TOWARDS DEFINING OF A CORRELATION BETWEEN EXPERT TRIAL IN OPERATIONAL CONDITIONS AND HYDRODYNAMIC CHARACTERISTICS OBTAINED USING CFD SIMULATION FOR A WINDSURFING FOILING CLASS FRONT WING

Zbigniew Macikowski[1], Artur Karczewski[1] and Przemysław Krata[1]

[1] Gdańsk University of Technology,

ul. Gabriela Narutowiczan11/12, 80-233 Gdańsk, Poland.

(E-mail: zbigniew.macikowski@pg.edu.pl, artur.karczewski@pg.edu.pl, przemyslaw.krata@pg.edu.pl)

Keywords: Hydrofoil, CFD, sailing, operational conditions trial

ABSTRACT

In modern sailing, gear selection plays a major role in athlete performance. With the introduction of hydrofoil sailing classes competitors noticed that gear provided by manufacturers differ vastly in performance. This was even true for pieces produced within one production series. With this came demand for providing a viable way of testing and measuring gear to select the best one out of the available pool. This paper presents an initial approach for carrying out expert trials in operational conditions and searching for the correlation with hydrodynamic characteristics defined by CFD simulation. Testing was developed for the windsurfing foiling class front wing. During tests 4 hydrofoils were tested, which were produced by one manufacturer for the monotype racing class and are made out of carbon fiber.

During operational trial wings were compared to a reference wing. On each test, one of the wings was tested against the reference. Tests were done by professional sailors with matching capabilities. All runs were recorded (position and speed). During the test, sailors did several straight runs on different courses. Each wing was ranked based on the number of won runs. For the numerical part of the experiment, wings were 3D scanned and CFD simulations were performed for each wing. Later results of real-life and numerical experiments were compared. The paper presents the direction of future work and possible solutions to improve such trials.

1 INTRODUCTION

In modern sailing, gear selection plays a major role in an athlete's performance. With the introduction of hydrofoil sailing classes competitors have noticed that gear provided by manufacturers differ vastly in performance. It was even the case for pieces produced within one production series. With this came demand for providing a viable way of testing and measuring gear to select the best one out of the available.

Firstly, hydrofoil performance could be measured experimentally in controlled flow [3]. This approach is hard to apply widely because of the size of hydrofoils and resulting high costs of tests. Another way to determine hydrofoil performance could be using 3D scans of a wing to carry out CFD simulation. Such an approach was presented in developing velocity prediction for Nacra 17 catamaran by Knudsen [1]. Finally, they can be tested by comparison in operational conditions. Unfortunately it introduces many random variables including the human factor, on the other hand it reflects the full complexity of the associated phenomena

The First two methods give us clear numeric values that are easily comparable. The experimental approach is often used to validate CFD simulation results. The third method only provides qualitative type of information on the change in the performance of the watercraft. It means it is hard to compare it with the other ones.

This paper is presented an initial approach searching for a correlation between hydrodynamic characteristics defined using CFD and real-life trials in operational conditions for windsurfing foiling class front wing.

2 METHODS AND MATERIALS

2.1 Tested hydrofoils

For purpose of this paper, 4 hydrofoils were tested. They were serial hydrofoils approved by the racing class and were produced by the same manufacturer. Manufacturers do not publish specific hydrofoil specifications except for a wing span of 900 mm. Hydrofoils were not modified in any way for experiments. For 3D scanning dedicated stand was constructed to assure that scans are oriented in relation to the mounting points of the wing.

2.2 Operational trial

2.2.1 Trial procedure

The experiment was conducted as a series of races. Each wing was tested in 4 upwind and 4 downwind races. Sailors started on the sound signal at a distance of 10 meters from each other. Then they sailed for a set amount of time (60 seconds for upwind, 40 seconds for downwind course). After each race sailors change tack and align themselves back to a 10-meter distance. Each race tested wing gets set amount of points:

- 0 – lost against reference;
- 1 – tied against reference;
- 2 – won against reference.

2.2.2 Equipment used in trial

During the test sailors used the windsurfing gear used by them during a regatta. Each of the sailors was familiar with his gear and the only changed piece of equipment was one front hydrofoil. Gear wasn’t swapped between sailors which means one of them was always sailing the reference wing and the second one using the tested wing.

2.2.3 Sailors

Sailors selected for this test were selected by their coach as having as similar abilities as it is possible. Both of them are experts in windsurfing sailing and are active competitors on the top international level.

2.3 CFD simulation

CFD simulations were carried out using OpenFOAM (version 2206) software. As angles of attack in all cases are small, a steady-state solver was chosen (simpleFOAM). For Turbulence modeling k-Omega SST model was used. Validation of CFD simulation was done by comparing the results of CFD simulation with the experiment on a modified NACA0009 hydrofoil [3]. Hydrofoil in this experiment has similar sizes to the later examined wing, and they operate for similar Reynold’s number. During validation results for 5 angles of attack were compared.

Hydrofoil geometry was including the fuselage which was extended to the outlet of the domain. The maximum cell size on the surface is 0.00125 mm and the minimum is 0.000325 mm. All of the mesh parameters can be found in Table 1.

Table 1
Mesh dimensions.

Name	**Size [m]**	**Cell size [mm]**
Domain	2.88 x 2.84 x 1.28	0.32
Field refinement	1.6 x 1.92 x 1.28	0.08
Refinement box 1	1.42 x 1.28 x 0.48	0.02
Refinement box 2	0.8 x 1.08 x 0.24	0.005
Wing surface		0.00125 0.0003215
First inflation layer		0.00001

3 RESULTS AND DISCUSSION

3.1 Operational Trial results

Table 2 presents summarised points from the trials with a breakdown for upwind and downwind. In Table 3 result of each run during the trials are presented.

Table 2
Summarised trial results for each wing.

Wing No.	**Upwind**	**Downwind**	**Sum**
1	0	0	0
2	6	6	12
3	6	6	12
4	6	8	14

Table 3
Course results for each wing.

Wing No.	**1**	**2**	**3**	**4**
Upwind 1	0	2	1	2
Upwind 2	0	1	2	2
Upwind 3	0	2	1	1
Upwind 4	0	1	2	1
Downwind 1	0	2	1	2
Downwind 2	0	1	2	2
Downwind 3	0	2	1	2
Downwind 4	0	1	2	2

3.2 CFD results

3.2.1 Validation results

In Figure 1 results of validation simulations are presented. For lift coefficient values of the simulation are almost identical to the ones from an experiment. For Drag coefficient calculated values are higher but the error for different angles of attack is constant. As the values of coefficients for CFD simulations were close to the experimental ones and the error for drag coefficient is constant for shown range, we assume that the model is sufficient for calculating differences between hydrofoils.

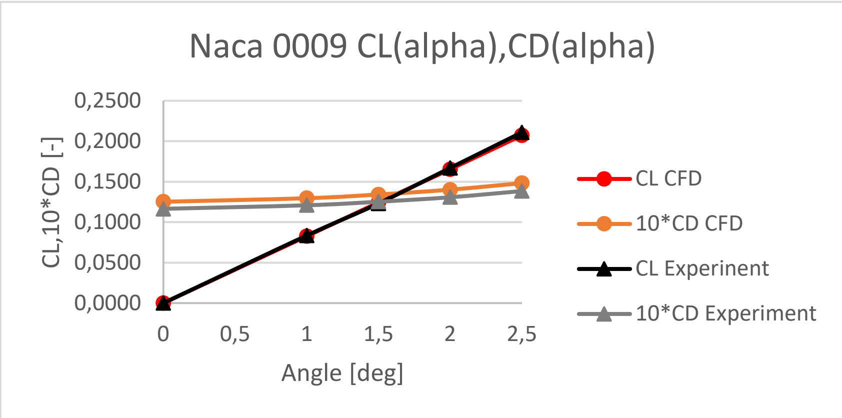

Figure 1 Results of lift and drag coefficients for validation simulations.

3.2.2 CFD simulation results

The results of CFD simulations for wings are presented in Table 4. Lift and drag are also presented for each side of the hydrofoils.

Table 4
Lift and drag results from CFD simulations.

Wing No.	L [N] left	L [N] right	L [N]	D [N] left	D [N] right	D [N]	L/D [-]
1	116.99	135.35	252.33	16.26	16.50	32.76	7.70
2	126.30	157.08	283.38	16.39	16.47	32.86	8.62
3	120.94	131.47	252.41	16.32	16.29	32.60	7.74
4	128.96	155.15	284.11	16.22	16.54	32.77	8.67

3.3 Result discussion

In the operational trial, the worst wing was Wing No. 1 and the best one was No.4. In CFD simulations Wing No. 1 had the lowest lift-to-drag ratio and No.4 had the highest. In the operational trial wings, 2-4 got very similar results but in CFD simulations results of wing No. 3 are closest to the worst one.

As a result of performed trials and experiments, the correlation between operational trials and the results of CFD simulation cannot be proven. The first issue is the sample size which is too small and should be expanded. Secondly operational trial in its current form is prone to the influence of human factor and condition changes. The main advantages of operational testing over CFD are a shorter time of testing and accessibility of this approach for coaches and competitors.

4 CONLUSIONS

The experiments aimed to find the correlation between operational trail and hydrodynamic characteristics calculated using CFD simulation. Based on the results presented in this paper such a correlation cannot be proven.

In future work first aspect which should be improved is a bigger number of tested hydrofoils. Secondly, the operational trial should be improved. Introducing a higher number of test runs and GPS tracking for velocity should improve the quality of results. Another idea was to increase the number of testers and tested wings in a single run. And after each run tester change the whole rig. This means each tester would have run on each gear. This could lead to reducing the influence of human factor during the trial.

REFERENCES

[1] Knudsen, S. S., Walther, J. H., Legarth, B. N., & Shao, Y. (2023). Towards Dynamic Velocity Prediction of NACRA 17. *Journal of Sailing Technology*, *8*(1), 1–23. http://onepetro.org/JST/article-pdf/8/01/1/3065319/sname-jst-2023-01.pdf/

[2] International IQFOIL Class Rules 2022-04-01, Sailing.org

[3] Zarruk, G. A., Brandner, P. A., Pearce, B. W., & Phillips, A. W. (2014). Experimental study of the steady fluid-structure interaction of flexible hydrofoils. Journal of Fluids and Structures, 51, 326–343. https://doi.org/10.1016/j.jfluidstructs.2014.09.009

MODELING OF THE LAKE WAVES FOR THE ENVIRONMENTAL DISTURBANCES SIMULATION OF THE SCALE SHIP MODEL

Anna Miller[1], Andrzej Rak[2]

[1, 2] Department of Ship Automation, Faculty of Electrical Engineering, Gdynia Maritime University, POLAND.

(E-mail: a.miller@we.umg.edu.pl, a.rak@we.umg.edu.pl)

Keywords: environmental disturbances, scale ship model, ship motion simulation, wave modelling,

ABSTRACT

In the development of ship motion control systems, software simulations or scale models experiments in pools or open waters are very often applied at the verification and testing stage. This paper describes the building procedure of a software wave simulator based on the data gathered on the Silm Lake near Iława, Poland, where scale ship models are used for a research and training. The basis of the simulator structure is a set of shaping filters fed by the Gaussian white noise. These filters are built in a form or transfer functions generating irregular wave signals for different input wind forces. To secure simulation for whole range of wind speeds, nonlinear interpolation is used. The lake waves simulation method presented in this paper fills the gap and enables accurate modelling of the environmental disturbances' characteristic for the small lake in the motion control experiments of the scale model ships.

1 INTRODUCTION

One of the main aspects that seems likely to change the modus operandi of the global transportation system the most, over the coming decades, is autonomous vehicles. This includes maritime shipping [19]. In the concept of an autonomous seagoing vessel, one of the vital factors is the motion control system for all phases of the cruise: from berth to berth. This type of voyage, for a fully autonomous ship, includes port maneuvers, as well as moving in restricted water areas at low speed. In such conditions, it is crucial to take into account in the control system the impact of environmental disturbances to ensure the implemented maneuvers are fully safe [7].

Research projects in this context, except the software simulations, frequently include test and verification stages of control systems with scale ships sailing in the open waters like lakes or ponds [1], [3], [13], [18]. Therefore, a model of environmental load of the scale ship caused by the waves and wind blowing over the small inland lake seems to be indispensable. Unfortunately, available models of environmental disturbances, used widely in the simulations of marine control systems, are equivalent to the fully developed ocean or open sea conditions [6], [16]. On the other hand, existing research on lake waves description adopts different types of models and focuses mostly on geophysical and environmental issues [2], [9]. This work describes the design procedure of a unidirectional, nonlinear wave model suitable to simulate the influence of lake surge on a scale ship. Source data for the project were collected over the Silm Lake, Poland, used as a research area for scale ships maneuvering [15]. Introductory analyses of wind and waves phenomena in this place were reported in previous authors' papers [11], [12]. A corresponding elaboration of wind model is being prepared for a separate publication.

2 METODOLOGY

Sea wave can be described as a stationary random process [5]. Thus, reconstruction of it may be achieved by appropriate shaping of frequency components of continuous standard input signal. Among the shaping methods mentioned in the literature [10], for this purpose, most commonly used are forming filters implemented as approximate state-space structures, convolution filters with directly specified power spectral densities (PSD) or compositions of the orthogonal basis functions, typically cosine ones, directly corresponding with the PSD, with variable phase shifts or amplitudes at the boundary of the periodic signal. Shaping filters are usually designed as linear time-invariant (LTI) systems driven by the white noise. It gives good simulation performance, provided a proper PSD approximation by the LTI system.

Based on the ITTC guidelines [16], it was determined in this project to model wave PSD just as an LTI system.

The PSD permits it's approximation by the suitable transfer function, which can be computed from a PSD of measured wave – $S_w(f)$, using least squares method (LSM) according to:

$$\min_{a_k, b_m} \sum_{j=1}^{m} \left(|H(j2\pi f)| - \sqrt{\left(S_w(j2\pi f)\right)^2} \right), \tag{1}$$

where: a_k, b_m – are LTI filter coefficients, $H(2\pi f)$ is a desired frequency response and $m \geqslant k$. Corresponding discrete filter transfer function should be calculated according to:

$$H(z) = \sum_{n=-\infty}^{+\infty} h\,(n) z^{-n}, \tag{2}$$

and has a form of:

$$H(z) = \frac{a_0 + a_1 z^{-1} + \cdots + a_p z^{-p}}{1 + \left(b_1 z^{-1} + \cdots + b_q z^{-q}\right)}. \tag{3}$$

Corresponding analog filter, which reproduces the wave parameters, may be designed using the assumptions of the bilinear transformation method. The following function [8] may be used to convert a digital filter with transmittance $H(z)$ to an analog filter with transmittance $H(s)$:

$$z = \phi(s) = \frac{1 + s\frac{T_s}{2}}{1 - s\frac{T_s}{2}}, \tag{4}$$

where T_s is discrete signal sampling time. Finally, resultant LTI object may be retrieved in a form of a transfer function:

$$T(s) = k\,\frac{b_n s^n + \cdots + b_1 s + b_0}{a_m s^m + \cdots + a_1 s + a_0}. \tag{5}$$

The simulator of the lake waves was designed based on the assumption that all waves are generated by winds. The structure of it is shown in Figure 1, where mean wind speed v_w [m/s] is an input and wave height h_w [mm] is an output signal.

White noise generator is used as a signal source. One can define noise seed, instead of random parameter selection, which leads to the reproducible results of the wave signal specification. "Selector" module rounds wind force to the integers of the BFT scale and acts as a switch for the appropriate pair of LTI forming filters.

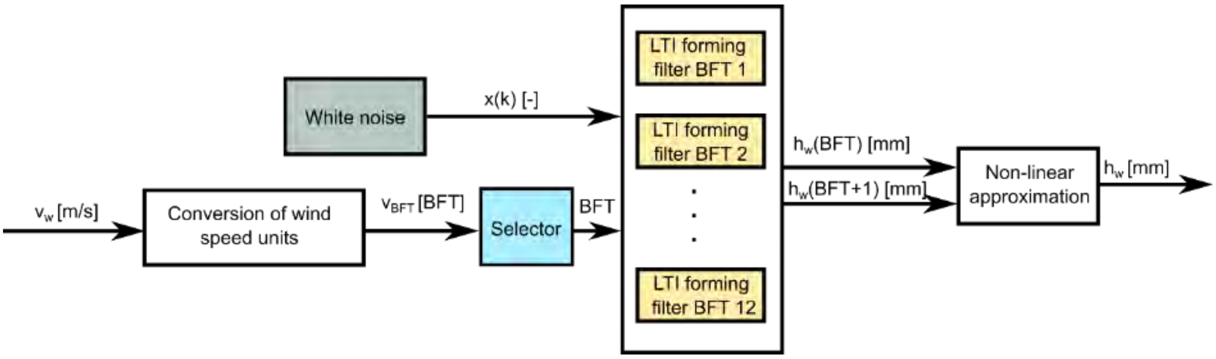

Figure 1. Block diagram of the wave generation algorithm.

The wind speed is recalculated to the BFT in ship model scale to avoid confusion with an assessment of wind impact of two different reference measures in meters per second caused by the ship scaling.

3 RESULTS AND DISCUSSION

Wave height and wind speed measurements were collected in several sessions between spring 2019 and autumn 2021. Measurement equipment was located on the Silm Lake and each measurement session took 12 hours. Detailed acquired data analyses and spectrum modeling results are presented in [12]. The results of these studies confirmed that wave height on a lake is strongly correlated with the wind speed, distribution of the height deviations from mean value and wave amplitudes are Gaussian and Rayleigh respectively and wave PSD function is analogous to the ITTC formulation of the sea waves spectrum. These factors formed the basis for digital wave simulator construction. Measured wave spectrum was modeled as the scaled ITTC spectrum [16] as follows:

$$s(\omega) = A\omega^{-5}exp(-B\omega^{-4}), \tag{6}$$

where:

$$A = 1.51\frac{\bar{H}_{1/3}^2}{\bar{T}_z^4}, \tag{7}$$

$$B = 105.44\bar{T}_z^4, \tag{8}$$

and $\bar{H}_{1/3}$ [mm] is the mean of significant wave height, $\bar{T}_z$ [s] is the mean of significant wave period. Based on the measured $\bar{H}_{1/3}$ and $\bar{T}_z$ values for wind forces of 4 BFT, 5 BFT, 6 BFT, 7 BFT and 9 BFT dependencies for $\bar{H}_{1/3}(BFT)$ and $\bar{T}_z(BFT)$ were extrapolated to get the continuous relationships.

Significant wave height dependence of wind speed, for the fully developed sea wave, is described by the second order polynomial [17]. The same dependence for Lake Erie is described by the square function for wind speeds between 0 and 15 m/s and for higher wind speeds it is linear [4], due to limited lake's depth. On the Silm Lake, fully developed waves are observed for winds less or equal than 6 BFT in the sip's scale, above this value characteristics flattering is observed. Dependence of significant wave height on scaled BFT is described by:

$$\hat{H}_{1/3} = \begin{cases} 0.47v_{BFT}^{2.11} & \text{for} \quad v_{BFT} \leqslant 6BFT \\ -149.4v_{BFT}^{-0.38} + 96.16 & \text{for} \quad v_{BFT} > 6BFT. \end{cases} \tag{9}$$

For the fully developed sea wave significant wave period on wind speed dependence is linear [14]. For the measured Silm Lake waves, as in the case of significant wave height, consistency with general rule is observed for a wind force not exceeding 6 BFT in ship scale. Above this value, due to restricted lake area and depth, again flattering is observed. Dependence of significant wave period on scaled BFT is described by:

$$\hat{T}_z = \begin{cases} 0.045 v_{BFT} + 0.298 & \text{for} \quad v_{BFT} \leqslant 6BFT \\ 0.017 v_{BFT} + 0.474 & \text{for} \quad v_{BFT} > 6BFT. \end{cases} \tag{10}$$

Twelve IIR forming filters, of which parameters were estimated using LSM optimization according to Equation 1, were designed. Those IIR filter's factors, stored in second order section (SOS) matrices, were used to determine the parameters of the discrete transfer functions. Wave height in the real world is modeled as an analogue, continuous signal. To remain consistent with this assumption, continuous transfer functions, according to Equation 5, were computed. The assumption was made to keep the order of the filter transfer functions as low as possible on the cost of acceptable simulator inaccuracy. Therefore, second-order transfer function of general form were proposed:

$$T(s) = k \frac{b_2 s^2 + b_1 s + b_0}{a_2 s^2 + a_1 s + a_0}. \tag{11}$$

The values of the filters' a, b and k (gain) coefficients for each BFT point are shown in Table 1.

Table 1

Coefficients of filters' transfer functions

BFT	k	b_2	b_1	b_0	a_2	a_1	a_0
2	14	0,0065	0,034	$2{,}4\cdot10^{-5}$	1	2,35	161,5
3	6,4	0,36	0,22	0,011	1	2,45	138,1
4	3,2	0,074	0,51	0,0031	1	2,10	116,1
5	3	0,22	1,74	0,028	1	1,86	87,12
6	1,7	0,59	4,83	0,026	1	1,92	80,65
7	1,1	1,02	8,59	0,20	1	1,67	69,44
8	0,6	2	17,00	1,08	1	1,51	65,89
9	0.82	1,47	12,54	0,30	1	1,50	63,52
10	0,75	1,93	16,77	0,13	1	1,54	58,44
11	0,78	1,20	17,57	0,15	1	1,54	56,44
12	0,83	2	17,81	0,024	1	1,58	55,00

The system of forming filters, using a nonlinear interpolation mechanism described in the previous section, was utilized to digitally model the wind generated wave on the Silm Lake.

Digital wave generator as an input takes mean value of wind speed and white noise signal. Based on them wave height, as a time function, was simulated.

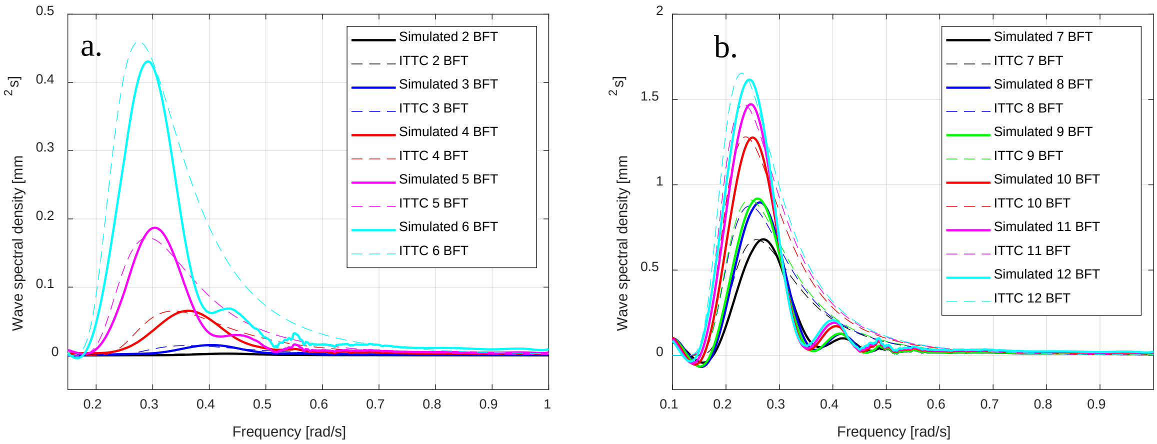

Figure 2 Comparison of simulated and ITTC spectra.

Generator outputs, for the particular BFT, were compared to the ITTC scaled standard wave spectra. Results of this comparison are presented in Figure 2a–b, for winds 2 BFT to 6 BFT and 7 BFT to 12 BFT respectively. The diagram was divided into two parts to ensure the readability of the charts. Simulation results are plotted by the solid line. Corresponding ITTC spectra are indicated by the dashed lines. High convergence of results was obtained over the full range of wind forces. Modal frequency shift toward lower frequencies is observed as wind strength increases, which is consistent with the ITTC spectrum modelling principles. Wave spectral density value also increases as wind BFT advances. Moreover, spectrum narrowing, compared with ITTC wave spectral model, in the higher frequency range is observed.

4 CONCLUSIONS

The following conclusions may be drawn from the research reported in this paper:

- Based on the empirical PSD description of the waves generated by the wind on the small lake, digital simulator of this process may be constructed.
- The structure of the simulator consisting of a group of parallel connected shaping filters dedicated to the reconstruction of the wave signal for particular wind BFT is easy to implement, analyze and verify.
- The relative errors of wave reproduction do not exceed 10%. This is an acceptable level for wave generator application in a ship motion control simulation.
- Dependencies of the significant wave height and the period of the wind force unlike in the open seas do not follow quadratic and linear relationships respectively for all range of force values. They are subjected to flattening.
- Generated time series of irregular waves exhibit properties characteristic of a real wave – proportional increasing height and lengthening period as wind strength increases.

REFERENCES

[1] H. L. Alfheim, K. Muggerud, M. Breivik, E. F. Brekke, E. Eide and Ø. Engelhardtsen, “Development of a Dynamic Positioning System for the ReVolt Model Ship,” IFAC-PapersOnLine, vol. 51, issue 29, pp. 116–121, Sept. 2018, doi: 10.1016/j.ifacol.2018.09.479.

[2] J. C. Allan and R. M. Kirk, “Wind wave characteristics at Lake Dunstan, South Island, New Zealand,” New Zealand Journal of Marine and Freshwater Research, vol. 34, no. 4, pp. 573–591, Mar. 2000, doi: 10.1080/00288330.2000.9516959.

[3] M. Bassam, A. B. Phillips, S. R. Turnock and P. A. Wilson, “Experimental testing and simulations of an autonomous, self-propulsion and self-measuring tanker ship model,” Ocean Engineering, vol 186, pp. 106065, Aug. 2019, doi: 10.1016/j.oceaneng.2019.05.047.

[4] Drews, “Using Wind Setdown and Storm Surge on Lake Erie to Calibrate the Air-Sea Drag Coefficient,” PLOS ONE, vol. 8, issue 8, pp. 1–16, Aug. 2013, doi: 10.1371/journal.pone.0072510.

[5] O. M. Faltinsen, Sea Loads on Ships and Offshore Structures, Cambridge University Press, Cambridge – New York, 1990.

[6] T. I. Fossen, Handbook of Marine Craft Hydrodynamics and Motion Control, John Wiley & Sons, Ltd, 2011, doi:10.1002/9781119994138.

[7] W. Gierusz and M. Rybczak, “Effectiveness of Multidimensional Controllers Designated to Steering of the Motions of Ship at Low Speed,” Sensors, vol. 20, no. 12, p. 3533, Jun. 2020, doi: 10.3390/s20123533.

[8] T. Holton, Digital Signal Processing: Principles and Applications, Cambridge University Press, 2021, doi:10.1017/9781108290050.

[9] K-R. Jin and Z-G Ji, “Calibration and verification of a spectral wind–wave model for Lake Okeechobee,” Ocean Engineering, vol. 28, issue 5, pp. 571–584, May 2001, doi: 10.1016/S0029-8018(00)00009-3.

[10] Klockner, A. Knoblach and A. Hackmann, “How to shape noise spectra for continuous system simulation,” Mathematical and Computer Modelling of Dynamical Systems, vol. 23, no. 3, pp. 284–300, Feb. 2017, doi:10.1080/13873954.2017.1298622.

[11] Miller and A. Rak, “Measurement System for the Environmental Load Assessment of the Scale Ship Model,” Sensors, vol. 23, no. 1, p. 306, Dec. 2022, doi: 10.3390/s23010306.

[12] Miller and A. Rak, “A Measurement System for the Environmental Load Assessment of a Scale Ship Model–Part II,” Sensors, vol. 23, no. 7, p. 3415, Mar. 2023, doi: 10.3390/s23073415.

[13] L.P. Perera, L. Moreira, F.P. Santos, V. Ferrari, S. Sutulo and C. Guedes Soares, “A Navigation and Control Platform for Real-Time Manoeuvring of Autonomous Ship Models,” IFAC Proceedings Volumes, vol. 45, issue 27, pp. 465–470, 2012, doi: 10.3182/20120919-3-IT-2046.00079.

[14] W. J. Pierson Jr. and L. Moskowitz, “A proposed spectral form for fully developed wind seas based on the similarity theory of S. A. Kitaigorodskii,” Journal of Geophysical Research, vol. 69, no. 24, pp. 5181–5190, Dec. 1964, doi:10.1029/JZ069i024p05181.

[15] Shiphandling Research and Trainig Centre. [Online]. Available: http://www.ilawashiphandling.com.pl, [Accessed 15 April 2023].

[16] T. Stansberg, G. Contento, S. Hong, M. Irani, S. Ishida and R. Mercier, “The specialist committee on waves final report and recommendations to the 23rd ITTC,” In: Proceedings of the 23rd ITTC, Venice, Italy, 8–14 Sep. 2002, pp. 505–736.

[17] N. Sugianto, M. Zainuri, A. Darari, S. S. Darsono and N. Yuwono, “Wave Height Forecasting Using Measurement Wind Speed Distribution Equation in Java Sea, Indonesia,” International Journal of Civil Engineering and Technology, vol. 8, issue 5, pp. 604–619, May 2017.

[18] M. Tomera, "Hybrid Switching Controller Design for the Maneuvering and Transit of a Training Ship," International Journal of Applied Mathematics and Computer Science, vol.27, no.1, Mar. 2017, pp. 63–77. doi:10.1515/amcs-2017-0005.

[19] Tsvetkova and M. Hellström, “Creating value through autonomous shipping: an ecosystem perspective,” Maritime Economics & Logistics, vol. 24, issue 2, pp. 255–277 Jun. 2022, doi: 10.1057/s41278-022-00216-y.

UNDERWATER RADIATED NOISE REDUCTION IN LIGHT OF CLASS SOCIETIES INITIATIVES

Marek Narewski [1]

[1] Polish Register of Shipping (PRS).

(E-mail: Marek.Narewski@prs.pl)

Keywords: Hydroacoustics, underwater, radiated noise, URN

ABSTRACT

Underwater radiated noise (URN) generated by commercial shipping and offshore activity has been recognized as a major form of ocean pollution as it has grown significantly over the past few years. Consequently, the International Maritime Organization (IMO) has decided to take measures on raising awareness of the urn issue at international forum. The IMO goal was to issue non-mandatory guidelines with the aim of monitoring the impact and thus ascertaining the efficiency of various mitigation solutions. As one of first steps, IMO agreed in 2009 to start work on the development of non-mandatory technical guidelines. The guidelines were subsequently approved in 2014 (refer to MEPC.1/Circ.833 *guidelines for the reduction of underwater noise from commercial shipping to address adverse impacts on marine life)*. Class societies support IMO efforts and work on development of industry acceptable URN measurements standards that can be used to confirm compliance with IMO guidelines.

1 INTRODUCTION

The IMO 2014 guidelines focused on primary sources of underwater noise such as propellers, hull form, onboard machinery, and covered various operational and maintenance recommendations e.g. hull cleaning. Due to the complexity of the URN issue, the 2014 guidelines did not set future targets for underwater sound levels as there was lack of sufficient research results that were needed on URN measurements as well as on related comparable measurement stds.

In the next years, number of scientific projects has been initiated focused on various aspects of URN, starting from ship design and construction up to in situ URN measurement methodology, data collection and tests onboard real ships. Due to increased marine community interests, IMO agreed in 2021 to review the existing URN guidelines in order to encourage the uptake and awareness of the subject and to ascertain the efficiency of various mitigation solutions. The aim was to provide updated recommendations based on the latest developments in ship design and marine technology, and to address potential obstacles that could prevent general implementation of the recommendations set out in the guidelines. The newly-updated guidelines were finalised during the IMO SDC9 Sub-committee meeting on Ship Design and Construction. The Guidelines may be applied to any ship, taking into account their design, construction and modifications as well as their operation. At the moment, the document waits for approval by the IMO's Marine Environment Protection Committee in June 2023 The draft guidelines are intended to assist relevant stakeholders in establishing mechanisms through which noise reduction efforts can be achieved.

2 MEASUREMENTS

Another important aspect that needs solution is development of internationally accepted standard for measurement of URN and intended to allow ships certification according to the URN emission levels in way acceptable to maritime administrations. Dedicated and accepted by the marine industry technical guidance on ship's generated URN measurements is actually under final development by IACS . The initiative is a result of class accommodated knowledge sharing by class societies that earlier developed own guidance on URN prediction and mitigation measures. The Table 1 below lists the developed and published URN measurement standards already used in the marine industry.

Table 1
Overview of standards for URN measurements

Std ID no	Std name	Application
ICES 209 CRR (1995)	Research Vessel Standard: Underwater Radiated Noise - Cooperative Research Report, No. 209	Fishery research ships
ANSI/ASA S12.64-2009/Part 1 (R2014)	Quantities and procedures for description and measurement of underwater sound from ships - part 1: general requirements	Commercial ships
NATO STANAG 1136 (1984/ 1995/ 2022)	Standards for Use When Measuring and Reporting Radiated Noise Characteristics of Surface Ships, Submarines, Helicopters, etc. in Relation to Sonar Detection and Torpedo Acquisition Risk	Naval ships and military applications
ISO 17208-1:2016	Underwater acoustics — Quantities and procedures for description and measurement of underwater sound from ships — Part 1: Requirements for precision measurements in deep water used for comparison purposes	Commercial shipping and class societies

3 IMO POSITION REGARDING URN

It is globally admitted that maritime activities are tightly linked to the sustainability of sensitive areas including natural habitats and endangered marine species. The underwater noise induced by marine traffic and its impact on the aquatic fauna has increased in proportion to the increase of traffic. The shipping industry is generally aware of this situation and many stakeholders have already taken actions. The International Maritime Organization (IMO)'s consideration on the underwater noise has set up global mitigation dynamics. Since 2014, the IMO's guidelines for the reduction of underwater noise from commercial shipping to address adverse impacts on marine life (MEPC.1/Circ.833) have proposed the basis to address this topic to the maritime industry.

At the 75th Session of the IMO's Marine Environment Protection Committee (MEPC), MEPC75/14 submitted by Australia, Canada and United States clearly raised the same concern about underwater noise from commercial shipping. The proposal was supported by member states of the EU (Ref. to MEPC 75/14/2), in which they also proposed to address underwater radiated noise (URN) on the agenda of the Committee's 76th Session. Scientific evidence of the impact of underwater noise on marine ecosystems is continuously growing, highlighting the need for further collaboration on addressing this issue by the international community. It clearly goes along with all sustainability efforts conducted by IMO, by its member states, also at national level, and by the various associations at international level such as IACS. The whole maritime industry is thus following the dynamics of optimizing the design of future ships and the operations of existing fleet aiming at reducing its footprints under these different drivers, including underwater noise.

4 CLASS SOCIETIES AND IACS POSITION TO LIMIT URN GENERATED BY SHIPPING ACTIVITY

IACS representing 11 leading class societies shares the concern about URN from commercial shipping expressed in MEPC 75/14. IACS has the view that IMO is the appropriate as well as technically competent body to address the mitigation of underwater noise from commercial shipping globally but is working to harmonize URN measurement procedures. Leading class societies already introduced stds for URN measurements however, there is no uniformity of requirements among them and application is related to the contract requirements between shipowner and classification society that performing supervision of design and construction. These discrepancies have led to proposals for rule alignment in order to aid interpretation and comparison of results carried out following different procedures.

Table 2
Overview of classification society "Quiet Class" notations.

Classification society	Name	Year	Driver	Applicable to	Reference
DNV AS (DNV GL)	SILENT (5 class notations)	2018	Environmental concerns	vessels using hydroacoustic equipment; seismic vessels; fishery vessels; research vessels; "environmental"	DNV GL (2018)
Bureau Veritas SA	NR614 Underwater Radiated Noise	2017	MSFD	self-propelled merchant vessels	Bureau Veritas (2017)
Lloyd's Register Group LTD	ShipRight (3 class notations)	2018	IMO and MSFD	merchant vessels	Lloyd's Register (2018)
American Bureau of Shipping (ABS)	Underwater noise (2 class notations)	2018	IMO and MSFD	self-propelled merchant vessels	ABS (2018)
China Classification Society (CCS)	Guidelines for ship underwater radiated noise	2018	Environmental impacts	"ships"	CCS (2018)
RINA Services S.p.A.	RINA DOLPHIN (2 class notations)	2019	Environmental impacts	merchant vessels and yachts	RINA (2017b, 2017a, 2017c)
Korean Register (KR)	Guidances for Underwater Radiated Noise (2 class notations)	2021	Not stated	not stated	Korean Register (2021)

Source EMSA, 2021

IACS highlights that establishing a common means for assessing underwater noise induced by shipping is a key step. A common quantification of the ship underwater acoustics and understanding of the various contributing factors can provide an effective means to drive industry efforts to reduce URN. IACS opinion is that efforts on underwater noise reduction should be put in close parallel with the continuous environmental improvements associated with EEDI and anticipated improvements associated with EEXI, CII and other GHGs emission reduction efforts and potential co-benefits.

IACS, which has already around 20 year return of experience on noise and vibration reduction on-board vessels, through the standardization of comfort consideration, is using its knowledge and expertise to support new measures that are technically feasible and capable of being applied globally and consistently. IACS therefore initiated own internal project and work is ongoing on development of harmonized assessment procedures for URN in order to support the maritime industry in response to the future need for quieter vessels.

5 URN REDUCTION AND CLASS INVOLVEMENT DURING SHIP DESIGN AND CONSTRUCTION

In order to design quiet ship, number of measures must be carried out at design phase as well as during construction of the ships. There are well known procedures to optimize hull design, modify internal arrangements according to ship structure vibration simulations using advance software. The art of building ship free of excessive vibrations noise generated is strictly related to the design an construction of propulsion system and all systems integrated to achieve functionality requested by the ship owner. Finally, when the ship is constructed measurements of URN generated by the ships are to be carried out and those can be supervised by competent class society according to the standards applicable in order to comply with other requirements e.g flag administration – hopefully agreed by bodies involved in URN pollution prevention.

6 CONCLUSION

However, the IMO guidance (once accepted by MEPC) are to be non mandatory, in case of contract obligations and class society supervision for compliance with applicable class society rules over ship construction, confirmation of the compliance with IMO std can have form of the additional class notation mark assigned by class when compliance with applicable URN std is achieved.

PRS already started work to develop own guidance and relevant PRS publication will include new IACS recommendations for URN measurement guidance once its final content will by formally accepted as required by IACS procedures

REFERENCES

[1] **MEPC.1/CIRC.833** *Guidelines For The Reduction Of Underwater Noise From Commercial Shipping To Address Adverse Impacts On Marine Life***).**

[2] Study On Inventory Of Existing Policy, Research And Impacts Of Continuous Underwater Noise In Europe – EMSA Report, 2021

NUMERICAL OPTIMISATION OF POD PROPELLER REVOLUTION FOR A CONTAINER SHIP WITH A HYBRID TWIN-CRP-POD PROPULSION SYSTEM

Hanna Pruszko[1], Maciej Reichel[2] , Krzysztof Czerski[3] and Marek Necel[3]

[1]Gdańsk University of Technology, Faculty of Mechanical Engineering and Ship Technology, POLAND

(E-mail: hanprus1@pg.edu.pl)

[2]Lech Kobyliński Foundation for Safety of Navigation, Ship Handling Research and Training Center, POLAND

(E-mail: maciejr@portilawa.com)

[3]Seatech Engineering, POLAND.

(E-mail: k.czerski@seatech.com.pl, m.necel@seatech.com.pl)

Keywords: CFD, Hydrodynamics, propulsion efficiency, twin-crp-pod

ABSTRACT

The twin-crp-pod propulsion arrangement is an innovative solution that gains from the combination of three well-known systems: twin-propeller, contra-rotating propellers and pod propulsor. Such a propulsion system was analysed for Ultra Large Container Ship with the perspective of increasing propulsion efficiency and improving navigation safety.

This article addresses the problem of finding the optimum position of the aft propulsor and revolution for front and aft propeller. Therefore, the paper shows the results of full-scale Computational Fluid Dynamics numerical simulations that aim to find the self-propulsion point for an Ultra Large Container Ship (ULCS) with a twin-crp-pod propulsion system for various ratios of revolution between the propellers. Moreover, the optimum position was evaluated for one selected propeller's revolution ratio, and the only criterion was the minimisation of power delivered to the propellers.

The calculations were performed using full-scale unsteady RANS simulations. For simplification, only the underwater part of the hull and propulsion system was modelled. Due to the symmetry of the hull and propulsion system, only half of the hull was included in the calculation. The scope of the simulations included four different revolutions of the front propeller and the resulting revolution of the aft propeller. The optimum power distribution was equal to 60%/40% delivered to the front and pod propeller, respectively.

The results of numerical simulations were used as input data for towing tank experiments.

1 INTRODUCTION

Reduction of fuel consumption and minimising greenhouse gas emissions is now vital for the shipping industry. All possible ways to achieve environmental targets should be taken into consideration. Conventional propellers are known to have low efficiency. Most ship propellers on cargo vessels waste about 40 per cent of the energy in the form of rotational losses in the wake, vortex generation, noise production, cavitation, etc. The recovery of such losses is one of the major ways to contribute to a more rational, environmentally friendly use of energy. Ultra-large container ships are those that, on the one hand, have individually the highest carbon footprint.

On the other hand, take advantage of economy of scale and transport vast amounts of goods worldwide. Therefore, this type of ship is a perfect target for taking action to investigate energy-efficient solutions. Twin-crp-pod propulsion arrangement is an innovative solution that gains from three well-known systems: twin-propeller, contra-rotating propellers and pod propulsor. Such a combination should guarantee an increase in efficiency, loss of GHG emissions and improvement of manoeuvrability and ship handling abilities.

Some designs combine two of mentioned solutions, e.g. hybrid crp-pod, where a single pod propulsor is placed behind a conventional propeller and works on the contra rotation principle [1;4;5;6]. Such a configuration has been introduced to high-speed vessels, like ro-pax [7]. The comparison of the self-propulsion performance of the CRP-POD vessel and single screw ship was presented by [8]. Moreover, the design optimisation, such as the propeller design parameters and clearance between the propellers, was investigated [9]. However, the concept of the hybrid twin-crp-pod for Ultra Large Container Ships has not been introduced.

This article addresses the problem of the relation between the front and aft propeller revolution and total delivered power. The investigation aimed to determine the optimum RPM of propellers and by means of full-scale CFD simulations. The scope of simulations included performing calculations for four different combinations of propeller revolutions. The following sections presents the methodology, results and discussion of the current findings.

2 METHODOLOGY

The case study vessel was an Ultra Large Container Ship. The hull was redesigned, starting from the single screw ship. In Table 1the main particulars of the case study vessel are presented.

Table 1
Main particulars of the case study vessel.

Name	Symbol	Value
Length overall	L_{OA}	399.90 m
Length between perpendiculars	L_{PP}	378.40 m
Breadth moulded	B	53.60 m
Draught (scant.)	T_{SCAN}	16.00 m
Drought (design)	T_{DESIGN}	14.00 m
Displacement	Δ	214120 t
Service speed	v	21 kn

The decision process and redesigning objectives to obtain the twin screw model of the single screw hull were described in detail by [3]. In Figure 1, the 3D model of the twin-screw bare hull and aft part of the ship equipped with the pods and propellers are presented.

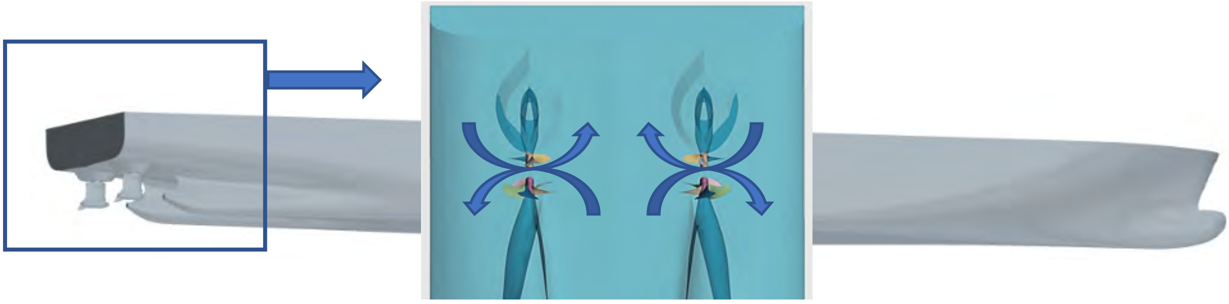

Figure 1 Twin-crp-pod propulsion for Ultra Large Container Ship.

The pod housing was designed based on the analysis of the currently available market solutions. The choice of the propeller geometry parameters was based on the literature review and case study propellers were chosen from the stock propellers database of Foundation for Safety of Navigation and Environment Protection and Gdańsk University of Technology.

In Table 2, the geometry parameters of the front and pod propellers are presented.

Table 2
Propeller geometry parameters.

Name	**Symbol**	**Front propeller - Outward rotation direction**	**Rear propeller - Inward rotation direction**
Diameter	D	7.68 m	6.90 m
Number of blades	Z	5	4
Pitch Ratio	P/D	1.0221	1.016
Expanded area ratio	A_E/A_0	0.8014	0.5184

The revolutions of the front propeller were kept constant. At the same time, the revolution of the aft-propeller was changed in a way to obtain the required thrust and, therefore, to find the self-propulsion point. Simulations were performed using an unsteady RANS approach. The finite volume method was applied for solving the governing equations of mass and momentum conservation, and Star CCM+ software was used.

The numerical set-up for self-propulsion is as follows. The length of the computation domain was 1600 m, the breadth was 600 m, and it was 600 m high. The velocity inlet condition was applied to the upstream and bottom boundary. The symmetry condition was applied to the top and side boundaries. The pressure outlet condition was assigned to the downstream boundary. It was decided that only half of the model would be taken for the computations (symmetry plane condition). The computations were performed for single-phase flow only with the underwater part of the hull modelled. The mesh size was equal to 9M of elements, and the sliding mesh approach with a rotating local coordinate system was used for the direct modelling of the propeller. The flow was turbulent with the k-ω SST turbulence model applied. The second-order implicit temporal discretisation scheme was applied. The time step was equal to 0.005 s. which corresponded to 114 time steps per one propeller rotation for the highest value of analysed aft propeller RPM. The same numerical conditions were presented in [2]

For the first round of the calculations, four different front propeller revolutions were used and corresponding to it two values of aft propeller. One set of parameters corresponded to thrust deficit relating to the resistance, and the second to thrust overload. The self-propulsion point was found using linear interpolation.

For a selected combination of front-aft propeller revolutions, the position of the pod housing was changed to find the best position from the total resistance point of view. All computations were performed for the design speed (21 knots) and draft (14 m). Table 3 presents the summary of the computation cases.

Table 3
Computation matrix.

Case No.	Front Propeller RPM	Aft propeller RPM (point 1)	Aft propeller RPM (point 2)
1	81	105	114
2	83	105	114
3	85	99	105
4	87	96	102

The values that were evaluated from the numerical simulations were the total resistance of the hull, pod housing and propellers, thrust and torque of both propellers and net force (calculated as the difference between total resistance and combined thrust of propellers).

3 RESULTS AND DISCUSSION

For each case using the linear interpolation the self-propulsion point was found –i.e. the point in which the resistance was balanced by the thrust of the propellers. The results of the propeller revolution optimization are presented in Table 4.

Table 4
Computation results - optimisation of power distribution.

RMP_{FRONT}	RPM_{AFT}	T_{FRONT} [kN]	T_{AFT} [kN]	Q_{FRONT} [kNm]	Q_{AFT} [kNm]	Q_{TOTAL} [kNm]	$P_{D\ FRONT}$ [MW]	$P_{D\ AFT}$ [MW]	$P_{D\ TOTAL}$ [MW]
81	109.3	762.76	743.49	1111.5	806.27	3835.5	18.86	18.46	37.32
83	106.3	654.89	861.02	1249.6	683.57	3866.3	21.72	15.22	***36.94***
85	102.8	985.99	525.45	1397.5	568.41	3931.8	24.88	12.24	37.11
87	99.1	1129.2	387.13	1567.6	445.30	4025.8	28.56	9.24	37.81

It can be noticed that the smallest value of total delivered power for both propellers is obtained when the revolution of the front propeller is equal to 83 RPM. Then the self-propulsion point is obtained when the aft propeller rotates at 106.3 RPM. According to Table 4, the power distribution between the propellers in this case is equal to 59% / 41%.

In Figure 3 the velocity field function in the longitudinal direction for the stern region of propellers is presented. The dark blue colors represents the areas of increased velocity in the direction of flow. It can be noticed that it occurs around the propellers and behind them.

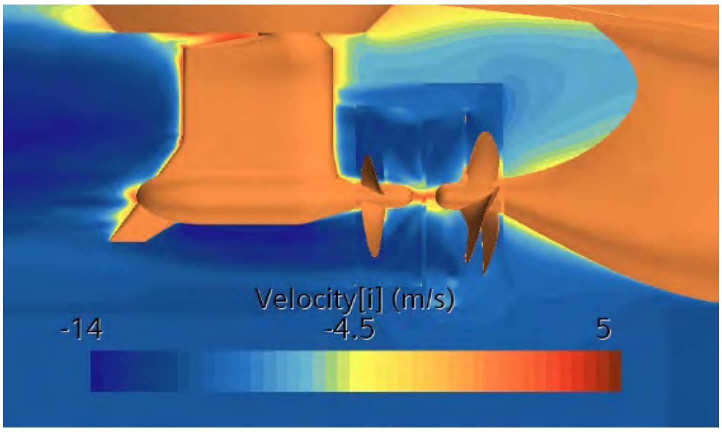

Figure 2 Velocity flow field.

Figure 3 presents the results of this study. On the left is the relation between the front propeller RPM and Total Delivered Power to the propeller P_D.

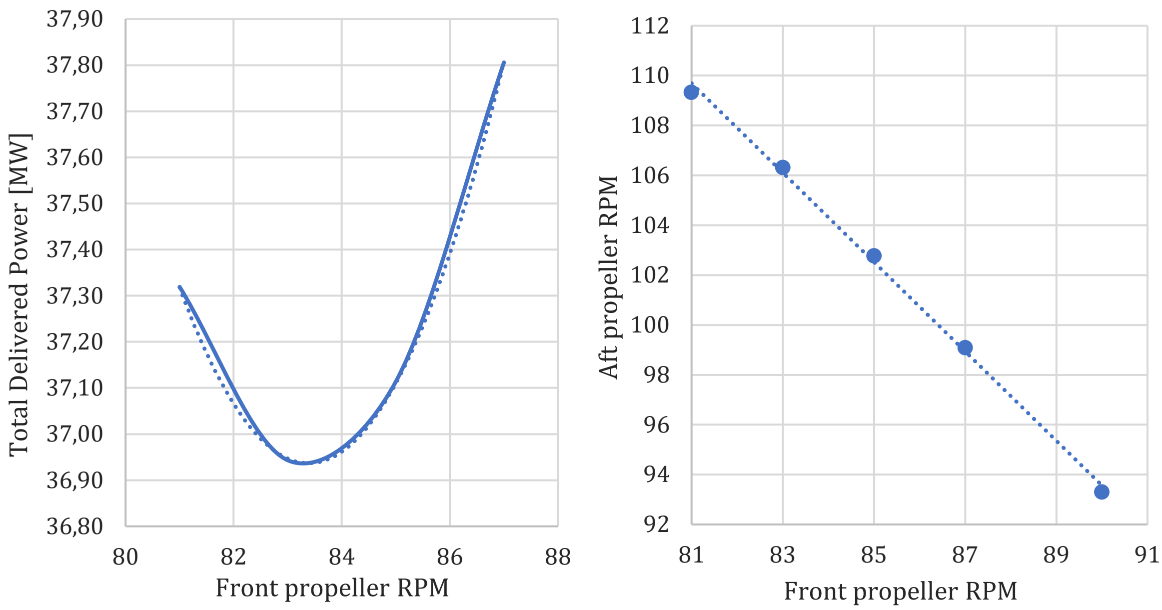

Figure 3 Results of revolution optimisation.

The minimum is very well recognizable. On the right-hand side is the relation between the RPM of the front and aft propeller. The linear relation could be noticed, which might indicate the high credibility of the presented results.

4 CONCLUSIONS

This article addresses the problem of the relationship between the front and aft propeller revolution and total delivered power. The aim of this investigation was to determine by means of full-scale CFD simulations the optimum RPM of propellers. For selected constraints, the optimum propeller revolution combination was established. Therefore, the aim of the article was achieved. The results of the simulations were used as input for towing tank experiments.

The future works will include performing the numerical simulation with the consideration of the free surface effects, the establishment of the scale effect and validation of numerical simulations.

ACKNOWLEDGMENT

This work was supported by MarTERA and co-financed by Polish National Centre for Research and Development (NCBR) and Development (NCBR) under the grant agreement MARTERA-2/twin-crp-pod ULCS/1/2020 and the German Federal Ministry of Economic Affairs and Energy (BMWi).

Calculations were carried out at the Centre of Informatics Tricity Academic Supercomputer & Network.

REFERENCES

[1] Petteri, Ämmälä. 2004. "CRP Azipod Propulsion Concept-Advanced Cost-Effective Solution." *Journal of The Japan Institute of Marine Engineering* 39 (9). https://doi.org/10.5988/jime.39.544.

[2] Pruszko, H., Reichel, M., Czerski, K., Necel, M., Schmale, J., Brüns, S., Modelling ship contra-rotating propellers – confronting virtual disc model with direct propeller computation, Numerical Towing Tank Symposium, Zagreb, Croatia, 2022

[3] Reichel M., Pruszko H., Czerski K., Necel M., Innovative twin-crp-pod propulsion system for Ultra Large Container Ships - challenges and opportunities., 15th International Symposium on Practical Design of Ships and Other Floating Structures PRADS 2022 Dubrovnik, Croatia, October 9th – 13th, 2022

[4] Quereda, R., Mariano P., González-Adalid, J., and Soriano, C.. 2017. "Conventional Propellers in CRP-POD Configuration . Tests and Extrapolation ." Proceedings of the Fifth International Symposium on Marine Propulsors, no. June. 2017

[5] Sánchez-Caja, A., Pérez-Sobrino, M., R Quereda, M Nijland, T Veikonheimo, J González-Adalid, Ilkka Saisto, and A Auriarte. 2013. "Combination of Pod, CLT and CRP Propulsion for Improving Ship Efficiency: The TRIPOD Project." In *Proceedings of the Third International Symposium on Marine Propulsors SMP '13*.2013

[6] Sasaki, Noriyuki, Mariko Kuroda, Junichi Fujisawa, Takanori Imoto, and Masaharu Sato. 2009. "On the Model Tests and Design Method of Hybrid CRP Podded Propulsion System of a Feeder Container Ship." In *First International Symposium on Marine Propulsors*.2009

[7] Ueda, Naoki, Akira Oshima, Takashi Unseki, Shigetomo Fujita, Shingen Takeda, and Tohru Kitamura. 2004. "The First Hybrid CRP-POD Driven Fast ROPAX Ferry in the World." *Technical Review* 41 (6).2004

[8] Wang, Zhan-zhi, Min Shao-song, Peng Fei, and Shen Xing-rong. 2021. "Comparison of Self-Propulsion Performance between Vessels with Single-Screw Propulsion and Hybrid Contra-Rotating Podded Propulsion." *Ocean Engineering* 232. https://doi.org/https://doi.org/10.1016/j.oceaneng.2021.109095.

[9] Ying, Xiong, Zhang Ke, Wang Zhan-zhi, and Qi Wan-jiang. 2016. "Numerical and Experimental Studies on the Effect of Axial Spacing on Hydrodynamic Performance of the Hybrid CRP Pod Propulsion System *." *China Ocean Eng* 30 (4): 627–36. https://doi.org/10.1007/s13344-016-0040-8.

OPEN WATER MODEL TESTS OF BRASS AND 3D-PRINTED COMPOSITE PROPELLER: FDM AND SLS

Piotr Pruszko [1] Maciej Reichel [,2]

[1,] Institute of Ocean Engineering and Ship Technology, Gdańsk University of Technology.

(E-mail:)

[2] Ship Handling Research and Training Centre, Foundation for Safety of Navigation.

(E-mail:)

Keywords: Towing tank tests, propeller's hydromechanical characteristics, 3D printed propeller, blade deformation, B-Wageningen serial propeller

ABSTRACT

This paper aims to present the results of a comparative study of propellers with the same geometry, but differing in stiffness depending on the material and manufacturing technique of the propeller. There is currently a very strong development in 3D printing technology. The appropriate use of the solutions available through these techniques makes it possible to reduce the cost of making a propeller. However, each solution is characterized by different strength parameters. Consequently, each propeller is characterized by a different state of blade deformation under hydromechanical loads. This has the effect of changing the hydromechanical characteristics of the propeller compared to a non-deformable object. Knowing how the design of the propeller affects the efficiency of the propulsion system also makes it possible to reduce the vessel's operating costs.

During the research, thrust and torque were measured, and the efficiency of each propeller was determined on this basis. The serial propeller under consideration belongs to the B-Wageningen series, and the techniques used to make the models were milling in brass, 3D printing using the additive printing technique with PLA (polylactic acid) plastic with continuous carbon fiber reinforcement and 3D printing using the selecting laser sintering technique with powdered nylon. The tests were carried out in the towing tank of the Gdansk University of Technology at the Institute of Ocean Engineering and Ship Technology. A propeller dynamometer was used to measure the forces and the measurements were made in accordance with the recommendations of the International Towing Tank Conference (ITTC).

On this basis, hydromechanical characteristics were determined for the three tested propellers. In addition, blade deformation tests under static loading were carried out. A comparative analysis of the results leads to an estimation of how the stiffness of the propeller blade and thus the deformations occurring during operation affect the overall efficiency of the propeller.

SIMPLIFIED METHOD TO ANALYSE THE WHIPPING-INDUCE VIBRATIONS IN CONTAINER SHIPS

Emil Roch[1] and Krzysztof Woloszyk[2,1]

[1] Faculty of Mechanical Engineering and Ship Technology, Gdansk University of Technology

(E-mail: emil.roch@pg.edu.pl)

[2] Research and Development Department, Polish Register of Shipping

(E-mail: k.woloszyk@prs.pl)

Keywords: Whipping, Container ships, Finite Element Method, Slamming, Vibrations

ABSTRACT

This work aimed to analyse, using the finite element method, the influence of dynamic-induced dumped hull oscillations, named "whipping" on structure strength. The presented results are part of the project carried out in the Research and Development Department of the Polish Register of Shipping. The review of existing techniques to determine the ship hull structural response due to the hydrodynamic forces is outlined. Additionally, the necessity to consider the dynamic hull vibrations in assessing the hull girder strength has been addressed. A series of models were prepared to investigate the effect of hull stiffness, added mass and forces modelling on the received global bending moment values. The bow flare slamming loading was determined using the simplified method. The obtained results are discussed, and future works are outlined.

1 INTRODUCTION

Due to the increasing size of container ships recently, phenomena that were not considered previously need to be captured in their structural design. Due to their specific hull structure (low stiffness) and relatively high speeds, there are prone to significant dynamic loading. The high slamming loads in the bow flare region could result in the transient response of the entire hull girder, commonly known as the "whipping" phenomenon. Such a phenomenon can be observed in Figure 1, where stresses observed on the deck are presented [1]. It is noted that whipping-induced stresses are of much higher frequency than quasit-static stresses due to bending on waves. Therefore, a dynamic solver is needed to investigate that problem in the time domain.

The analysis of the whipping phenomenon is quite complex since it needs to be considered as a fluid-structure interaction problem. A comprehensive review of existing numerical methods available to solve this problem can be found in [2]. Different modelling techniques are available in terms of seakeeping analysis, slamming load and structural response. Finally, two types of coupling between structural response and hydrodynamic loading exist. The first is one-way coupling, where initially calculated hydrodynamic loads are applied and structural response is observed. The second one, more accurate, is two-way coupling. It considers that the hydrodynamic loads will depend on the hull deformations in a particular moment of time and are updated in each time step.

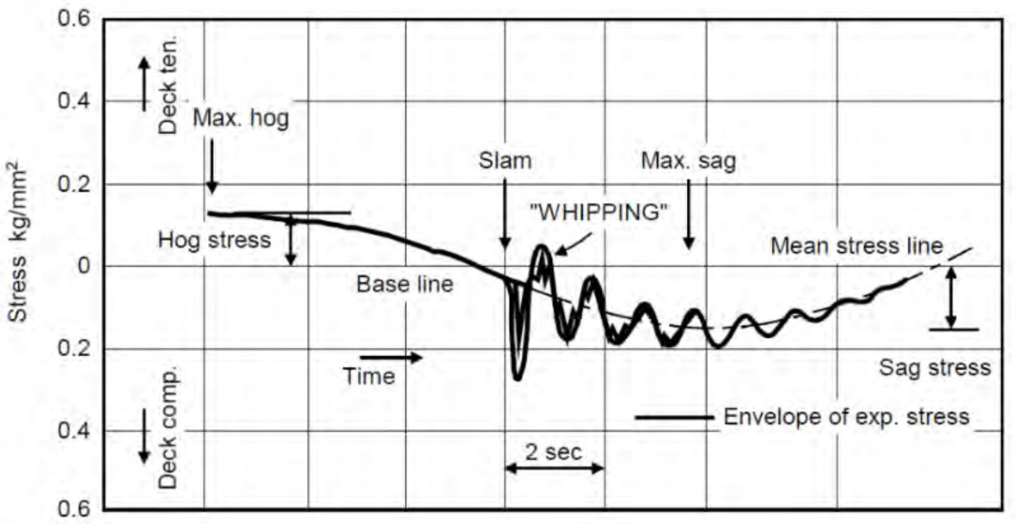

Figure 1 The changes in stresses observed in the deck due to the "whipping" phenomenon [1].

The results of the ongoing research project in Polish Register of Shipping are presented in the work. Although the two-way coupling methodology is more accurate, the presented work focused on a simplified one-way coupling method that allows estimating the impact of whipping into the total bending moment of the ship hull girder with less modelling and computational effort.

2 METHODS AND CASE STUDY

2.1 Analysed ship

As a reference model for the whipping analysis, the 14500 TEU container ship has been chosen. The ship dimensions are: length between perpendiculars of 347 m, breadth of 48.2 m, depth of 29.85 m and the general arrangement of the ship is presented in Figure 2.

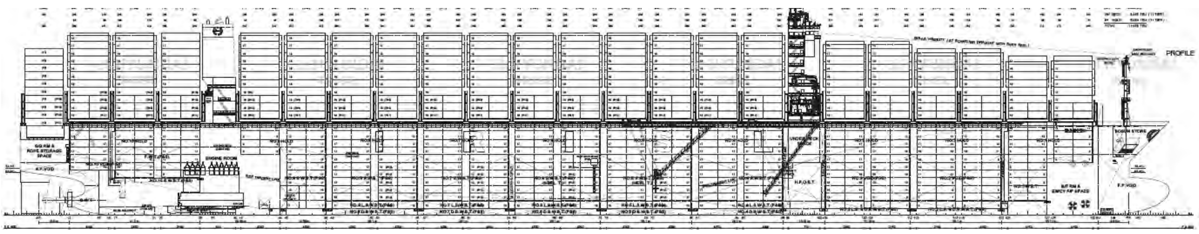

Figure 2 The general arrangement of the container ship.

2.2 Calculation of the slamming force

The slamming force was estimated as proposed in [1]. In order to calculate the bow impact velocity, which is used for the calculation of bow slamming load, the simplified ship motion analysis was conducted as suggested in [3]. Various significant wave heights depending on the wave frequency were investigated considering the 25-year return period. The most severe conditions were considered in further calculations (significant wave height of 5.6 m and wave period of 5.5 sec), which resulted in a bow impact velocity equal to 7.46 m/s. The estimated maximum bow slamming load was equal to 30.47 MN. Two types of load modelling techniques were employed. In the first one, the load increases linearly during the slamming phenomenon and drops to 0 instantly (one-step approach). In the second one, the load increases and then decreases linearly within the same time periods (two-step approach).

2.3 FE modelling

The beam on the spring foundation was used as a structural model. Then, the cross-section characteristics (cross-sectional area, moments of inertia, etc.) were calculated based on the structural drawings. Two model types were adopted at this stage, i.e. prismatic beam (cross-section characteristics are constant within the length and are considered as for the midship section) and 5-segment beam with the variation of characteristics depending on the hull region.

The spring foundation was adopted to model the hull and surrounding water interaction. Each node was supported vertically by the spring having stiffness and damping. Finally, the added mass was modelled by mass points located on each node. Two types of added mass calculations were performed, i.e. using the formulation presented in [4] and PRS publication [5], respectively.

Since presented computations were performed in the xy plane, the other degrees of freedom were suspended. Thus, the translation along the z-axis and rotations around the x- and y-axes were blocked for all nodes. Having a defined function in time, the slamming force was applied in a single node in the region where the bow slamming force is acting. Finally, the explicit dynamic computations were performed, and the integration step was adjusted based on the calculation of frequencies of normal modes of the ship structure.

3 RESULTS AND DISCUSSION

The example of calculated bending moments performed on a prismatic beam (one set of characteristics of cross-section) considered in three cross-sections is presented in Figure 3. It is noted that the bending moment has a first peak in the bow region (0.75 L) and then 'travels' towards the aft region (0.25 L). In addition, it is noted that multiple modes of vibrations superimpose into the resulting time function.

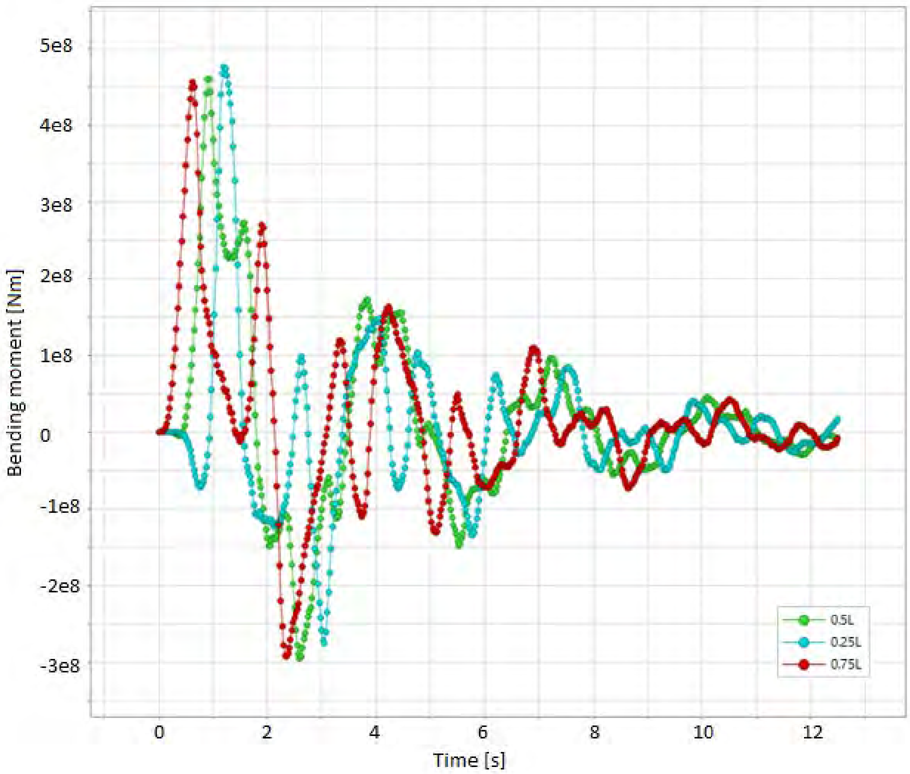

Figure 3 Bending moments in prismatic beam.

Table 1
Summary of the whipping-induced bending moments

Number of segments	Force excitation function	Added mass calculation method	Maximum sagging moment [MNm]	Maximum hogging moment [MNm]
1	One-step	Publication [4]	485	353
1	One-step	Publication [5]	484	349
5	One-step	Publication [4]	862	593
5	Two-step	Publication [4]	875	619

Table 1 presents the summary of maximum whipping-induced bending moments for various models considered. It is noted that from various parameters, the number of considered segments has a crucial influence on the resulting bending moments. There is also observed some influence of the type of excitation force function. However, the type of added mass calculations shows very little impact on resulting bending moments.

4 CONCLUSIONS

The presented approach provides a fast method to assess the impact of whipping-induced vibrations on hull girder strength. When compared with quasi-static wave bending moments, the whipping-induced moment oscillates between 15% and 24% of that values for the 5-segment model. Thus, it is observed that this phenomenon cannot be neglected even in the design stage. In further studies, the more discretised model (more segments) could be used to see if there is further change in resulting bending moments. The beneficial would also be validating the presented approach with some advanced models, i.e., a fully coupled approach and determination of wave loads using the panel method. This will be the next step in the research project conducted in the Polish Register of Shipping.

REFERENCES

[1] American Bureau of Shipping, Guidance notes on whipping assessment for container carriers, 2010.

[2] Ergin, A., Alley, E., Brandt, A., Drummen, I., Hermundstad, O., Huh, Y. C., ... & Zhang, G. Committee II. 2: Dynamic Response. In Proceedings of the 20th International Ship and Offshore Structures Congress (ISSC 2018) Volume 1 (pp. 255-333). IOS Press, 2018.

[3] Jensen, J. J., Mansour, A. E., & Olsen, A. S., Estimation of ship motions using closed-form expressions, Ocean Engineering, Vol. 31(1): 61-85, 2004.

[4] Więckowski , J., Mechanika Konstrukcji Okrętowych, Wydawnictwo Politechniki Gdańskiej, 1985.

[5] Polski Rejestr Statków, Publikacja 2/I. Zapobieganie drganiom na statkach, Gdańsk, 2004.

TIME-DOMAIN NUMERICAL EVALUATION OF SHIP RESISTANCE AND MOTION IN REGULAR WAVES BY USING THE CFD URANS METHOD

Mohammad Sadeghi[1], Hamid Zeraatgar[2], Mohammad Hossein Ghaemi[3*], Mojtaba Barjasteh[4]

[1, 2,4] Faculty of Maritime Technology, Amirkabir University of Technology, IRAN

(E-mail: sadeghi.mohamad324@gmail.com, hamidz@aut.ac.ir, barjasteh@aut.ac.ir)

[3] Faculty of Mechanical Eng. and Ship Technology, Gdańsk University of Technology, POLAND

(E-mail: ghaemi@pg.edu.pl)

Keywords: Added Resistance, CFD URANS methods, Seakeeping, Ship Motion, Ship Resistance, Wave-Induced Resistance

ABSTRACT

Taking into account the International Maritime Organisation's (IMO) strategy to radically reduce the GHG emitted by the shipping industry towards zero emission operation, today's assessment of ship behaviour in waves, its seakeeping characteristics and resistance and their interrelation with fuel consumption and emissions are one of the most attended research subject. There are three methods to conduct this analysis, which are Experimental Fluid Dynamics (FED), numerical methods e.g. Computational Fluid Dynamics (CFD) and empirical analysis. This study shows the results of time-domain analysis of ship motions and resistance in head sea waves by using the CFD method, which is then verified using the experimental results. The tests were run for different wavelengths for a KCS model. Numerical results, which are based on solving Unsteady Reynolds-Averaged Navier-Stokes equations (URANS) show that the CFD method applied by using STAR CCM+ can be reliable for evaluating the ship seakeeping characteristics and resistance in waves.

1 INTRODUCTION

To reduce air pollutants and Greenhouse Gases (GHG), recently the International Maritime Organization (IMO), has required all vessels to provide solutions to increase energy efficiency by mandating EEDI (Energy Efficiency Design Index), EEXI (Energy Efficiency Existing Ship Index), CII (carbon intensity indicator) and SEEMP (Ship Energy Efficiency Management Plan) as the adoption of amendments to MARPOL Annex VI. Among different solutions reduction of fuel consumption plays a fundamental role. In this relation, International Towing Tank Conference (ITTC) has recently initiated a deep investigation into the added resistance induced by waves. Understanding and analysis of the instantaneous values of the total resistance in waves in combination with the interaction of hull, propeller and engine can make a clear picture of the fuel consumption profile and pave the road for elaborating better control strategies for ship motion to reduce the emissions.

The three approaches for analysing the added resistance in waves are Experimental Fluid Dynamics (FED), numerical methods e.g. Computational Fluid Dynamics (CFD) and empirical analysis. So far, many studies and research have been done in the field of testing and calculating the added resistance in the head sea wave. One of the first researchers were Storm-Tejsen et al., who identified effective parameters in the added strength of 60 series ships by EFD method [1].

For the S175 container ship, Fuji and Takahashi, [2], and Nakamura and Naito, [3], conducted additional resistance tests at different speeds. Kashiwagi et al., [4], and Kashiwagi, [5], calculated the added resistance for several different ships.

Since the KVLCC2 ship is a model with available results, many researchers have used it for further resistance tests. Guo and Steen, [6], evaluated the added resistance of KVLCC2 in short waves. Park et al., [7], studied the uncertainty of added resistance tes~~ting~~ results in seafaring conditions. Lee et al., [8,9], conducted a series of experiments to understand how different hull shapes affect the added resistance in waves. Other tests have been done on the KCS model to estimate the added resistance, [10-12].

The majority of the above-mentioned studies analyse the added resistance in head waves. The findings show that the number and the range of studies conducting the oblique sea condition are much less than those studies that address the head sea condition. In this regard, Fuji and Takahashi, [2], investigated the added resistance of a ship ~~at~~ in a range of incident wave angles with 30^{o} increment. Kashiwagi et al., [4], investigated the experimental results of added resistance for a model in oblique waves. Recently, Valanto and Hong, [13], measured the added drag in an HSVA cruise ship wave and discussed the effect of Parametric Roll (PA) on the added drag. Stocker, [12], presented data on the added resistance of a KCS vessel in 45° incident waves.

Nowadays, the analysis of added resistance using CFD has become more widespread. The added resistance is defined as subtraction of the calm water resistance from the average of total resistance in waves for a given time length. Orihara and Miyata, [15], solved the Reynolds-averaged Navier-Stokes equation (RANS) using the CFD method and concluded that the added resistance in the wave can be analysed with relative accuracy. Guo et al., [15], studied the added resistance of the KVLCC2 ship using the RANS equation and confirmed the analysis results in general. Sadat Hosseini et al., [16], compared experimental and CFD results of the added resistance under head wave conditions. Yang and Kim, [17], analysed the effective components of the added resistance of KVLCC2 by the Cartesian method. The results of this research show that CFD is satisfactory in estimating the added resistance in head wave condition. However, in oblique sea conditions, it is not straightforward to obtain CFD results due to the computational burden.

As far as empirical analyses are considered, there are many available studies, too. In short waves, Fuji and Takahashi, [2], used some coefficients to derive empirical formulas. Faltinsen et al., [18], developed other empirical formulas. MARIN (Netherlands Marine Research Institute) presented the STAwave method for calculating the added resistance in waves [19]. Also, NMRI proposed an improved formula based on Fuji and Takahashi's formula [20-22], whereby the coefficients were modified using experimental data. Liu and Papanikolaou, [23,24], proposed a new and updated empirical formula to estimate the added resistance. It is stated that in the case of oblique waves, the Faltinsenet al. formula, [18], for short waves may not be appropriate because both diffraction and radiation components are important. A related study can be found in MPEC 70/INF30 (2016), [25], where empirical formulas for radiation and diffraction components in oblique waves have been delivered. Yang et al. (2018), [26], also modified the formula of Faltinsen et al., [18], by considering three aspects in their formulation: the range of the ship's intake, the ship's speed, and the top form of the broken water surface.

It should be mentioned that generally, there are two groups of formulae for calculating the added resistance. The first one, Far-Field Formula (FFF), uses the conservation of momentum and the second one, the Near-Filed Formula (NFF), is based on pressure integration. FFF was developed by Maruo, [27], and was further developed by Newman, [26]. NNF was ~~used~~ employed by Faltinsen et al., [18]. Both formulas were then developed using Narrow-Body Theory (NBT).

By improving the computing ability and capacity of new computers, both FFF and NFF were implemented in software using the 3D Panel Method (3DPM). A comparison between the results by using FFF or NFF can be found in Joncquez, [29]. He studied the added resistance using both methods based on the RANKIN panel method. Kim and Kim, [30], and Kim et al., [31], also used both methods to evaluate the added resistance. Sadeghi and Zeraatgar [32], investigated the ship behaviour in regular and irregular waves to assess the effect of anti-pitch fins on sea-keeping parameters.

In this study, a CFD tool (SRAR CCM+) is utilized by applying URANS equations in combination with free surface modelling by the Volume of Fluid (VoF) method to evaluate the added resistance of a KCS model in four different wavelengths. Next, to validate the results, they have been compared with the experimental results in the time domain. The results include the pitch and heave motion, and time-series of total resistance in waves. The main difference between this work with other similar works is to focus more on the time series ship resistance in different wavelengths.

2 METHODOLOGY

The concept of the study is using implemented URANS equations in a CFD tool to numerically analyse the added resistance of a model ship in head regular waves with different wavelength, and then the results are compared with the EFD results to make a general conclusion about the extent of capability of CFD method to predict the instantaneous added resistance. Here, the ship's motion is described by heave and pitch. The other ship’s motion components are not relevant. Such a conclusion will help to a better understanding of the interaction of hull-propeller-engine leading to the elaboration of new strategies for ship control in waves and consequently reduction of fuel consumption. In this regard, a CFD software called STAR CCM+ was utilized to assess the added resistance of a KCS model under various conditions. The URANS equations were applied in conjunction with a Volume of Fluid (VoF) method for free surface modelling.

2.1 Governing Equations

The URANS equations that can be found in Pletcher, [33], are applied here considering viscous incompressible flow for a ship in waves. Additionally, the Reynolds decomposition of turbulent quantities is considered [34]. For modelling the turbulence $k-\omega$ SST (Shear Stress Transport) model is used. This model calculates the stress Reynolds in laminar and turbulent flows and its solver is changeable between them as the flow regime. Also, this model has an extra term which makes the waves do not be dissipated, [35-37]. It combines the standard $k-\varepsilon$ and $k-\omega$ models by rewriting both k and ω equations in terms of ω, [38]. The argument for combining both models is that the $k-\omega$ model is superior to the $k-\varepsilon$ model in the boundary layer, but it fails for flows with pressure-induced separation. In addition, the ω equation is sensitive to the free stream outside the boundary layer [39]. Thus, by combination, the best qualities of each model are used.

2.2 The Case Study

In this study, the KCS model is utilized to assess the time series of resistance, heave and pitch motion. The parameters of the KCS model are presented in Table 1.

Table 1
KCS model parameters

Parameters (unit)	Value
Overall length (LOA) (m)	2.500
Waterline length (L_{wl}) (m)	2.325
Breadth (m)	0.322
Draught (m)	0.108
Displacement (kg)	52.03
Block coefficient (-)	0.644
Midship section coefficient	0.953
LCG from aft waterline perpendicular (m)	1.132
VCG from draught (m)	-0.005
Pitch radius of Gyration (%L)	25

The accuracy of the numerical results depends on the mesh, time step and inner iteration. In addition, the dimension of volume controls and related boundary conditions are another effective parameter in the CFD method. The dimensions of domains are selected based on the ITTC recommendation [40]. In this study to simulate better ship dynamics and control the meshes, the overset technique is utilized. In this technique, there is a background domain in which waves are generated there and overset domain which is around the model to record better dynamics of the model and resistance. To control the grids of volume control, background and overset regions being gridded by trimmer mesh. Trimmer mesh is a controllable gridding technique which divides the control volume into small cubical regions. For comparing the effect of the number of grids, heave and pitch and resistance in waves are compared for coarse, medium and fine meshes. Figure 1 shows the heave and pitch motion, as well as resistance in waves for these three cases of meshing.

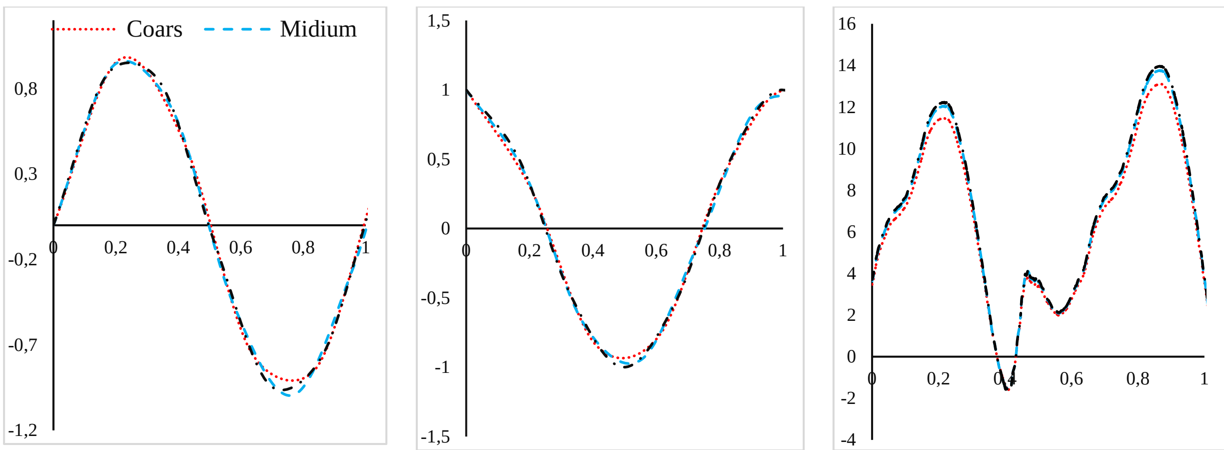

(a) (b) (c)

Figure 1 Non-dimensional heave (a), pitch (b) motion, and resistance in waves (c) (results for three meshing modes: coarse, medium and fine)

3 RESULTS AND DISCUSSION

To determine the added resistance in waves the calm water resistance is subtracted from the averaged time series of total resistance in waves at the same forward speed. Table 2 shows the resistance of the KCS model both for EFD and CFD at Fn=0.26. The acceptable range for Y+ is 30-60, and Figure 2 shows that Y+ is acceptable for this simulation.

Table 2
Calm water resistance of KCS model (Fn=0.26)

EFD	CFD	%Difference
3.177 (N)	3.106 (N)	2.6

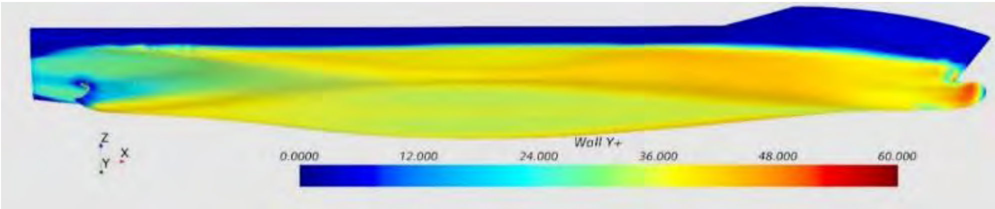

Figure 2 Distribution of Y+ on the KCS hull skin

Table 4 shows the regular wave parameters which are used in the present study. All tests are conducted at Fn=0.26.

Table 3
Wave parameters for 4 different options

Option	Wave period (s)	Wavelength/L_{wl}	Wave height (mm)
C1	0.858	0.49	56
C2	1.051	0.74	56
C3	1.302	1.14	56
C4	1.695	1.93	56

Figure 3 shows the time series of CFD analysis in comparison to the EFD results for options C1 to C4 for heave and pitch motion, and the resistance, respectively.

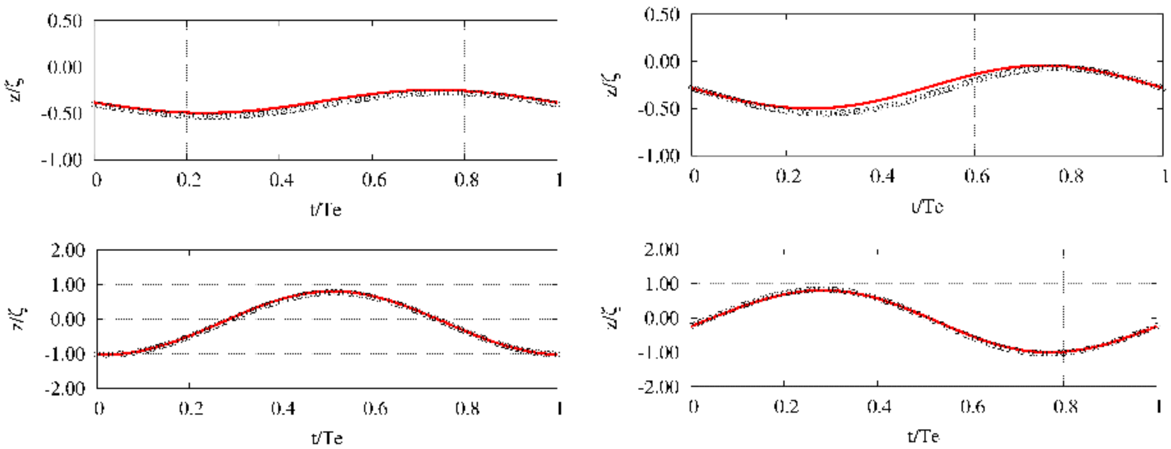

(a) CFD and EFD results of heave motion for options C1 to C4

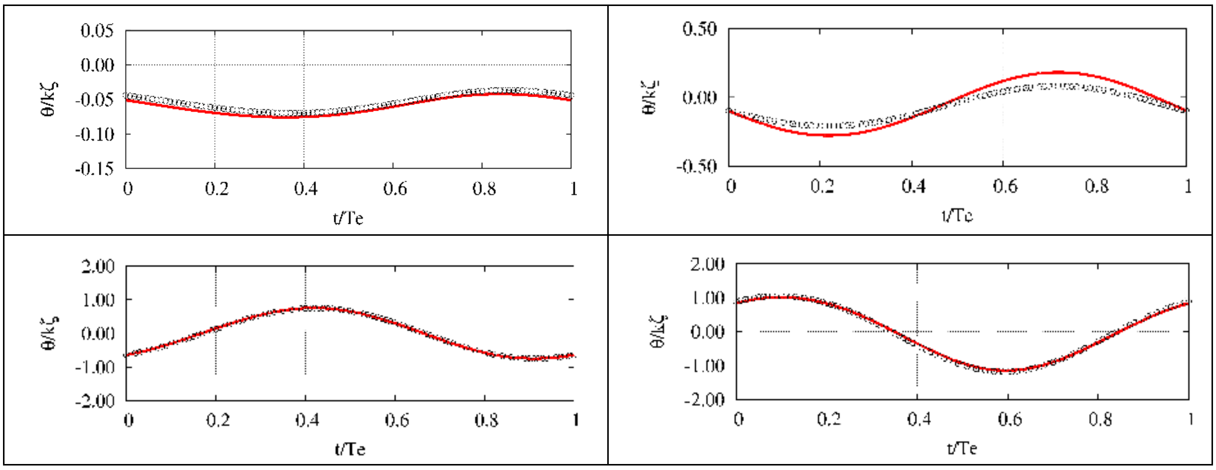

(b) CFD and EFD results of pitch motion for options C1 to C4

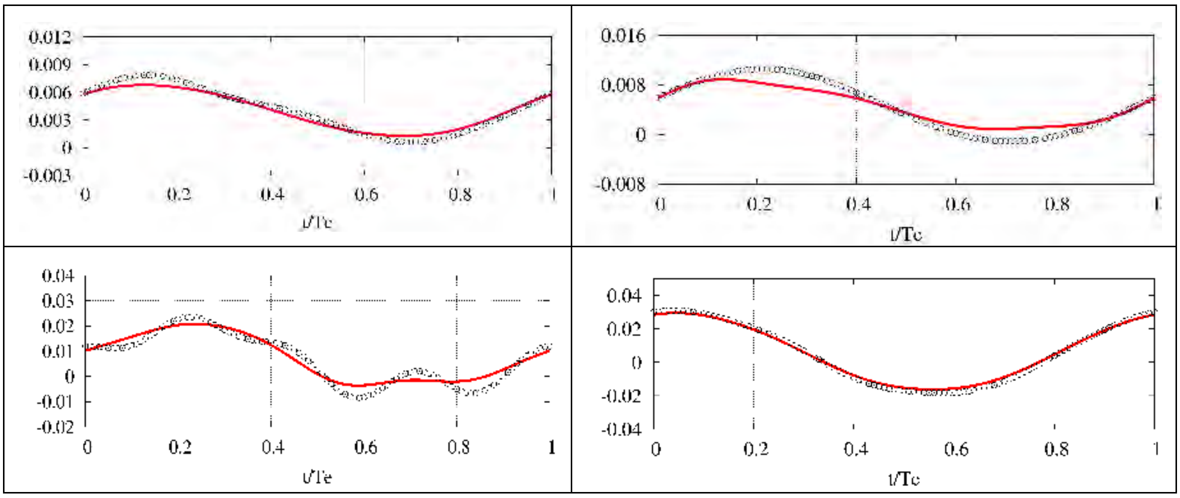

(c) CFD and EFD results of ship's resistance for options C1 to C4

Figure 3 CFD and EFD results of ship's motion and resistance for different options

Finally, Table 4 shows the non-dimensional heave and pitch amplitudes, and added-resistance in waves, where the CFD and EFD results are compared and the relative difference between them are given.

Table 4
Non-dimensional results

Variable	λ/L_{wl}	EFD	CFD	%Difference
z/ζ	0.49	0.1475	0.1147	-22.22
	0.74	0.2622	0.2295	-12.5
	1.14	0.8688	0.9180	5.66
	1.93	0.9344	0.9016	-3.50
$\theta/k\zeta$	0.49	0.0196	0.0295	50.14
	0.74	0.1475	0.1762	19.7
	1.14	0.7475	0.7573	1.31
	1.93	1.1114	1.0721	-3.53
$R/\rho g\zeta^2 B^2/L_{wl}$	0.49	2.812	2.126	-24.23
	0.74	3.217	2.969	-7.70
	1.14	9.968	8.963	-10.08
	1.93	2.617	2.561	-2.14

4 CONCLUSIONS

In this study, CFD tools have been employed to numerically investigate the ship motion (heave and pitch) and resistance in head wave condition in four different wavelengths, and the results are compared with EFD results for validating purposes. As far as the requirement for CFD analysis is considered, the numerical results are acceptable and the CFD tool is properly applied for solving the problem. Additionally, comparing the CFD and EFD results show that the generally estimated added resistance by using the CFD tool is lower than the values predicted by EFD by 2.1% to 24.2%, depending on the wavelength ratio (λ/L_{wl}). In the case of heave motion, the range of difference between CFD and EFD results is almost the same, from 3.5% to 22.2%, but not necessarily the CFD results are lower for all wavelengths. For pitch motion, the range of difference is even higher up to ac. 50%. However, it should be mentioned that for wavelength higher than unity, the agreement between the CFD and EFD results is acceptable and the relative difference does not exceed 10%. The presen~~ted~~ study and the results pave the road for a wider parametric analysis of added resistance and ship motion in waves in the time domain and consequently provide an initial picture of ship behaviour in waves leading to a better understanding and investigating fuel consumption and GHG emissions.

REFERENCES

[1] Storm-Tejsen, J., Yeh, H.Y.H., Moran, D.D., Added resistance in waves. Trans. - Soc. Nav. Archit. Mar. Eng. 81, 250–279, 1973.

[2] Fujii, H., Takahashi, T., Experimental study on the resistance increase of a ship in regular oblique waves. In: Proceedings of the 14th ITTC, pp. 351–360. Ottawa, 1975..

[3] Nakamura, S., Naito, S., Propulsive performance of a containership in waves. J. Soc. Nav. Archit. Jpn. 15, 24–48, 1977.

[4] Kashiwagi, M., Sugimoto, K., Ueda, T., Yamasaki, K., Arihama, K., Kimura, K., Yamashita, R., Itoh, A., Mizokami, S., An analysis system for propulsive performance in waves. J. Kansai Soc. Nav. Architect. 241, 67–82, 2004.

[5] Kashiwagi, M., Hydrodynamic study on added resistance using unsteady wave analysis. J. Ship Res. 57, 220–240, 2013.

[6] Guo, B., Steen, S., Evaluation of added resistance of KVLCC2 in short waves. J. Hydrodyn. 23 (6), 709–722, 2011.

[7] Park, D.M., Lee, J., Kim, Y., Uncertainty analysis for added resistance experiment of KVLCC2 ship. Ocean Eng. 95, 143–156, 2015.

[8] Lee, J., Park, D.M., Kim, Y., Experimental investigation on the added resistance of modified KVLCC2 hull forms with different bow shapes. J. Eng. Marit. Environ. 231 (2), 395–410, 2017.

[9] Lee, J.H., Kim, B.S., Kim, Y., Study on steady flow effects in numerical computation of added resistance of ship in waves. In: 10th International Workshop on Ship and Marine Hydrodynamics, Keelung, Taiwan, 5-8 November, 2017.

[10] Joncquez, S.A.G., Second-order Forces and Moments Acting on Ships in Waves. Ph. D. Thesis. Technical University of Denmark, Denmark, 2009.

[11] Simonsen, C.D., Otzen, J.F., Nielsen, C., Stern, F., CFD prediction of added resistance of the KCS in regular head and oblique waves. In: 30th Symposium on Naval Hydrodynamics, Hobart, Tasmania, Australia, 2-7 November 2014.

[12] Stocker, M.R., Surge Free Added Resistance Tests in Oblique Wave Headings for the KRISO Container Ship Model. M.S. Thesis. The University of Iowa, 2016.

[13] Valanto, P., Hong, Y., Experimental investigation on ship wave added resistance in regular head, oblique, beam and following waves. In: Proceedings of the 25th International Ocean and Polar Engineering Conference, Big Island. Hawaii, USA, 21- 26 June 2015.

[14] Orihara, H., Miyata, H., Evaluation of added resistance in regular incident waves by computational fluid dynamics motion simulation using an overlapping grid system. J. Mar. Sci. Technol. 8, 47–60, 2003.
[15] Guo, B.J., Steen, S., Deng, G.B., Seakeeping prediction of KVLCC2 in head waves with RANS. Appl. Ocean Res. 35, 56–67, 2012.
[16] Sadat-Hosseini, H., Wu, P., Carrica, P.M., Kim, H., Toda, H., Stern, F., CFD verification and validation of added resistance and motions of KVLCC2 with fixed and free surge in short and long head waves. Ocean Eng. 59, 240–273, 2013.
[17] Yang, K.K., Kim, Y., Numerical analysis of added resistance on blunt ships with different bow shapes in short waves. J. Mar. Sci. Technol. 22, 245–258, 2017.
[18] Faltinsen, O.M., Minsaas, K.J., Liapis, N., Skjørdal, S.O., Prediction of resistance and propulsion of a ship in a seaway. In: Proceedings of the 13th Symposium on Naval Hydrodynamics, Tokyo, Japan, pp. 505–529, 1980.
[19] MARIN, “Recommended Analysis of Speed Trials”, Sea Trial Analysis JIP, 2006.
[20] Kuroda, M., Tsujimoto, M., Fujiwara, T., Ohmatsu, S., Takagi, K., Investigation on components of added resistance in short waves. J. Jpn. Soc. Nav. Archit. Ocean Eng. 8, 171–176, 2008.
[21] Kuroda, M., Tsujimoto, M., Sasaki, N., Ohmatsu, S., Takagi, K., Study on the bow shapes above the waterline in view of the powering and green-house gas emissions in actual seas. J. Eng. Marit. Environ. 226 (1), 23–35, 2012.
[22] Tsujimoto, M., Shibata, K., Kuroda, M., Takagi, K., A practical correction method for added resistance in waves. J. Jpn. Soc. Nav. Archit. Ocean Eng. 8, 141–146, 2008.
[23] Liu, S.K., Papanikolaou, A., On the prediction of added resistance of large ships in representative seaways. Ships Offshore Struct. 12, 690–696, 2017.
[24] Liu, S.K., Papanikolaou, A., Approximation of the added resistance of ships with small draft or in ballast condition by empirical formula. Proc. IME M J. Eng. Marit. Environ. 1–14, 2017.
[25] MPEC 70/INF.30, Air Pollution and Energy Efficiency, Supplementary Information on the Draft Revised Guidelines for Determining Minimum Propulsion Power to Maintain the Manoeuvrability of Ships in Adverse Conditions. IMO Report, 2016.
[26] Yang, K.K., Kim, Y., Jung, Y.W., Enhancement of asymptotic formula for added resistance of ships in short wave. Ocean Eng. 148, 211–222, 2018.
[27] Maruo, H., The drift of a body floating on waves. J. Ship Res. 4, 1–10, 1960.
[28] Newman, J.N., The drift force and moment on ships in waves. J. Ship Res. 11, 51–60, 1967.
[29] Joncquez, S.A.G., “Comparison Results from S-OMEGA and AEGIR.” FORCE Technology Report No. FORCE107-24345, p. 21, 2011.
[30] Kim, K.H., Kim, Y., Numerical study on added resistance of ships by using a time-domain Rankine panel method. Ocean Eng. 38, 1357–1367, 2011.
[31] Kim, K.H., Seo, M.K., Kim, Y., Numerical analysis on added resistance of ships. Int. J. Offshore Polar Eng. 21, 21–29, 2012.
[32] Sadeghi. M, Zerratgar.H, Investigation on the effect of anti-pitch fins for reducing the motion and acceleration of ships using computational fluid dynamics. Ocean Engineering 267 (2023) 112965. https://doi.org/10.1016/j.oceaneng.2022.112965, 2023.
[33] Pletcher, R. H., J. C. Tannehill, and D. A. Anderson, Computational Fluid Mechanics and Heat Transfer. 3rd ed. Boca Raton, Fla: CRC Press, 2013.
[34] Tennekes, H. and J. L. Lumley, A First Course in Turbulence. Cambridge, Massachusetts: The MIT Press. Chap. 2 and 5, 1972.
[35] Choi, J., Yoon, S.B., Numerical simulations using momentum source wave-maker applied to RANS equation model. Coast. Eng. 56, 1043–1060, 2009.

[36] Park, J.C., Kim, M.H., Miyata, H., Fully non-linear free-surface simulations by a 3D viscous numerical wave tank. Int. J. Numer. Methods Fluid. 29, 685–703, 1999.
[37] Peric, R., Abdel-Maksoud, M., Reliable Damping of Free Surface Waves in Numerical Simulations, 63. Ship Technology Research, 2016.
[38] Tucker, P., Turbulence. In Advanced Computational Fluid and Aerodynamics (Cambridge Aerospace Series, pp. 260-361). Cambridge: Cambridge University Press. doi:10.1017/CBO9781139872010.006, 2016.
[39] Menter, F. R., M. Kuntz, and R. Langtry, Ten years of industrial experience with the SST turbulence model. In: Turbulence, Heat and Mass Transfer 4(1), pp. 625–632, 2003.
[40] Procedures, I.T.T.C., Guidelines, Uncertainty Analysis in CFD Verification and Validation, 7, 5-03-01-01, 2008.

HYDROACOUSTICS TESTING LABORATORY – RESEARCH CAPABILITIES AND COMPETENCES

Aleksander M. Schmidt[1]

[1,] Hydroacoustics Testing Laboratory, Gdańsk University of Technology, Faculty of Electronics, Telecommunications and Informatics.

(E-mail: firstauthorsname@aaaa.bbb, secondauthorsname@aaaa.bbb)

Keywords: hydroacoustic, transducer, antenna, sonar, underwater acoustic device

ABSTRACT

The Hydroacoustics Testing Laboratory was established by the Decree of the Rector of the Gdańsk University of Technology on December 1, 2012, as a unit depending directly on the Dean of the ETI Faculty of GUT. The Laboratory continues the research tradition of the Sonar Systems Department of WETI in the field of electrical and acoustic measurements of various underwater acoustic devices and systems - from elementary hydroacoustic transducers to complex, multi-element hydroacoustic antennas, mounted on ships or hydrotechnical structures. The Laboratory disposes of the equipment necessary to conduct research, including high-class measuring hydrophones from leading manufacturers, such as Brüel & Kjær or RESON. This equipment allows for conducting hydroacoustic tests in a very wide range of signal frequencies - from a few Hz up to 1 MHz. In 2016, the Laboratory confirmed its research competence by obtaining the accreditation of the Polish Center for Accreditation, which it maintains to this day.

INVESTIGATION OF MEWIS DUCT AS ENERGY SAVING DEVICE USING COMPUTATIONAL FLUID DYNAMICS -AN OVERVIEW

Prashant Singh

Department of Ocean Engineering and Naval Architecture, Indian Institute of Technology, Kharagpur, INDIA

(E-mail: singh.prashantbhadauria@kgpian.iitkgp.ac.in)

Keywords: Computational Fluid Dynamics, Energy Saving Devices, Mewis Duct, Pre Swirl Device, Shipflow

ABSTRACT

Due to a significant increase in oil prices in the past, achieving optimal fuel utilization has become a critical factor for the operating economy of all ships today. In response to this need, technology has been developed to reduce the bunker cost of both existing and upcoming ships in both developed and developing countries. As part of its technical measures to decrease greenhouse gases from ships, IMO has introduced Energy Efficiency Design Index (EEDI) and Energy Efficiency Existing Ship Index (EEXI) for ships, which indicate their energy efficiency. To improve energy efficiency, hull forms have been refined and propulsive devices such as pre or post swirl ducts and hull vanes have been introduced.

Model tests have shown that Mewis duct show that power saving of 5-8% is achieved but the position of duct can be optimised for the best posible efficiency. The paper deals with the simulations in CFD using Mewis duct, the problems encountered while using CFD tools for full scale fuller ships running at low Froude numbers and the best possible fixed position of the duct.

1 INTRODUCTION

The conventional ducted propeller is a significant technological solution for enhancing propulsive performance. While ships equipped with conventional ducted propellers were able to achieve power savings, they also encountered a significant issue of cavitation erosion on the duct's inner surface. As a consequence, this led to costly repairs and negative impacts on the operation of the ship. The design goal of the Mewis Duct, is to mainly improve two loss sources-losses in the ships wake by the duct and rotational losses in slipstream by the fins.

2 METHODOLOGY

Ship's hull geometry and propeller appendages are modelled along with suitable Mewis Duct. The CFD-calculations are performed by solving RANS equations using finite volume methods in Flowtech software "Shipflow".

The goal of the optimization process is to customize the duct to the specific hull shape and wake characteristics, and to choose a duct design that results in the greatest possible power savings for the given vessel. The wake pattern on the propeller is analyzed to examine the influence of interactions between the hull and propeller, and a self-propulsion test is conducted on the propeller to determine the values of propulsive coefficients.

3 RESULTS AND DISCUSSION

XCHAP simulations were run on the bare hull. The experimental results for coefficient of total resistance (C_T) obtained from literature review is shown in Figure. The CFD results obtained from Shipflow was compared to the experimental results for validation of the bare hull. The wave height profile along the length of hull in fig 1.

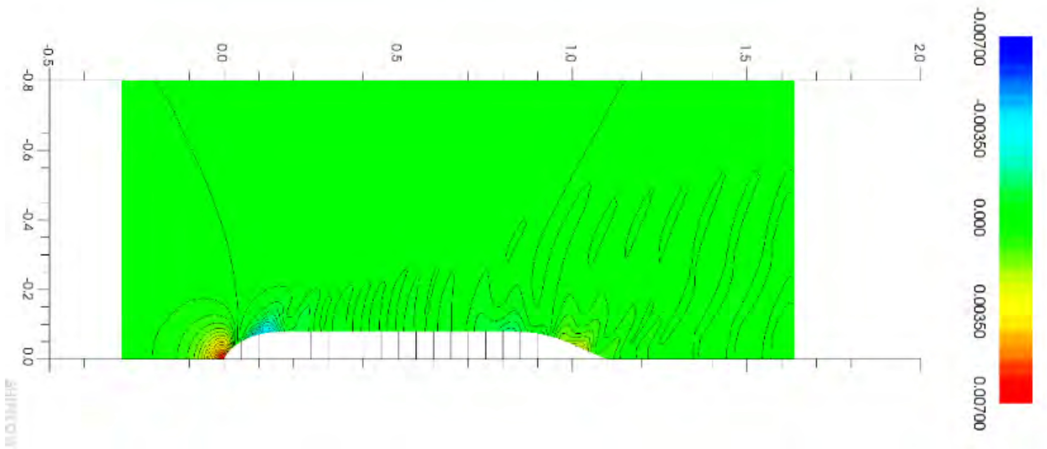

Figure 1 Wave Height along the length of hull

Self Propulsion Tests were conducted on both the models (with and without ducts) in order to determine Mean Axial Wake, Torque Coefficient, Thrust Coefficient, Advance Coefficient and other propulsive coefficients. The effective wake is plotted over a propeller disc (figure 2 & 3) and a considerable improvement in wake characteristics was observed.

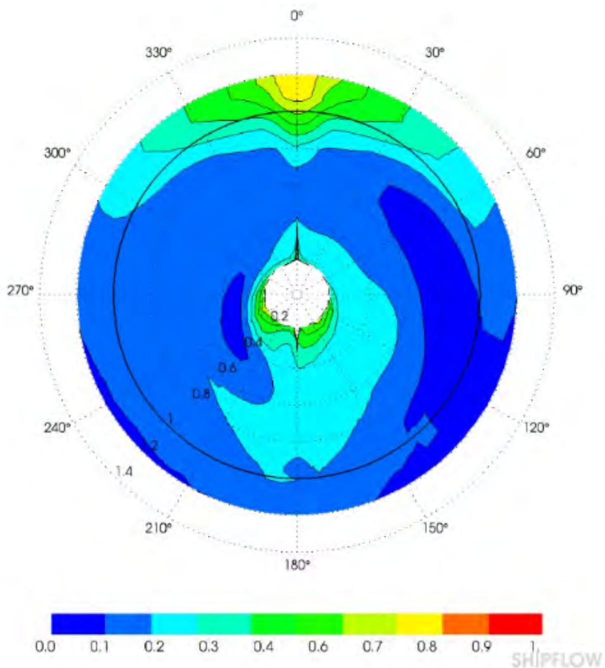

Figure 2 Total wake fraction in propeller disc without duct

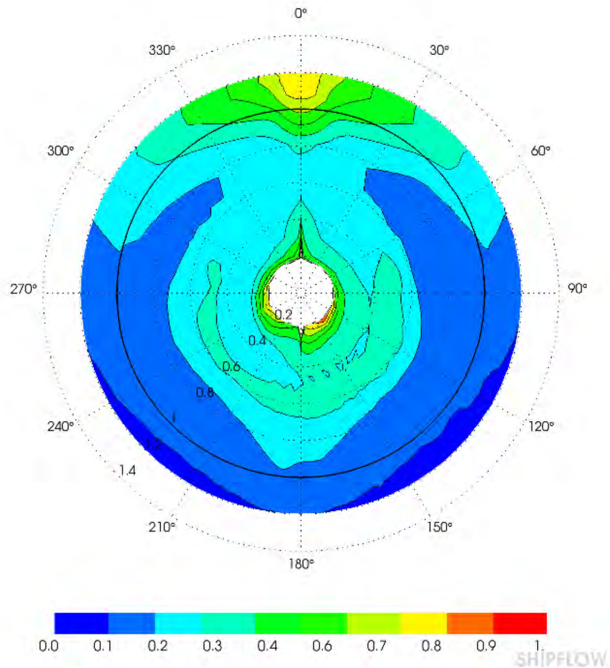

Figure 3 Total wake fraction in propeller disc with duct

The location of duct is varied for in order to obtain an optimum position to fix the duct to get the maximum energy saving. The viscous flow computational grids are similar to the grids used in finding out resistance. The overlap between hull, ducts and its brackets are calculated by the XCHAP module. The locations (non dimensionalised form) are shown in table 1.

Table 1
Varied locations of duct

Location	Distance from Propeller (X/Lpp)
Location 1	0.9930
Location 2	0.9937
Location 3	0.9923
Location 4	0.9945

The computations were done for wake fraction, advance coefficient, thrust and torque coefficients and it was found that location number 2 was best suitable for positioning the duct. The plot of results for mean wake and advance coefficients are shown in the plots drawn in figure 4 & 5.

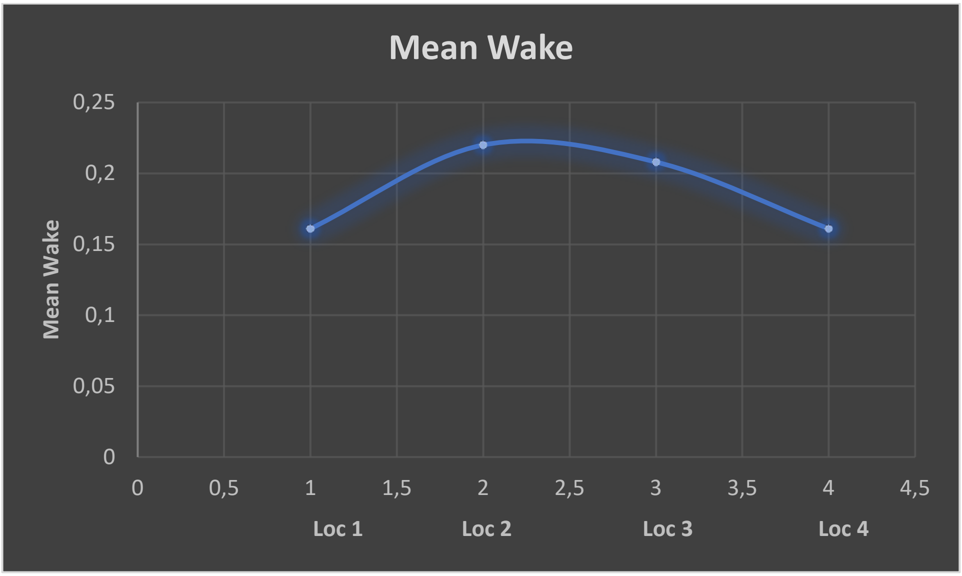

Figure 4 Plot of Mean Wake at various locations

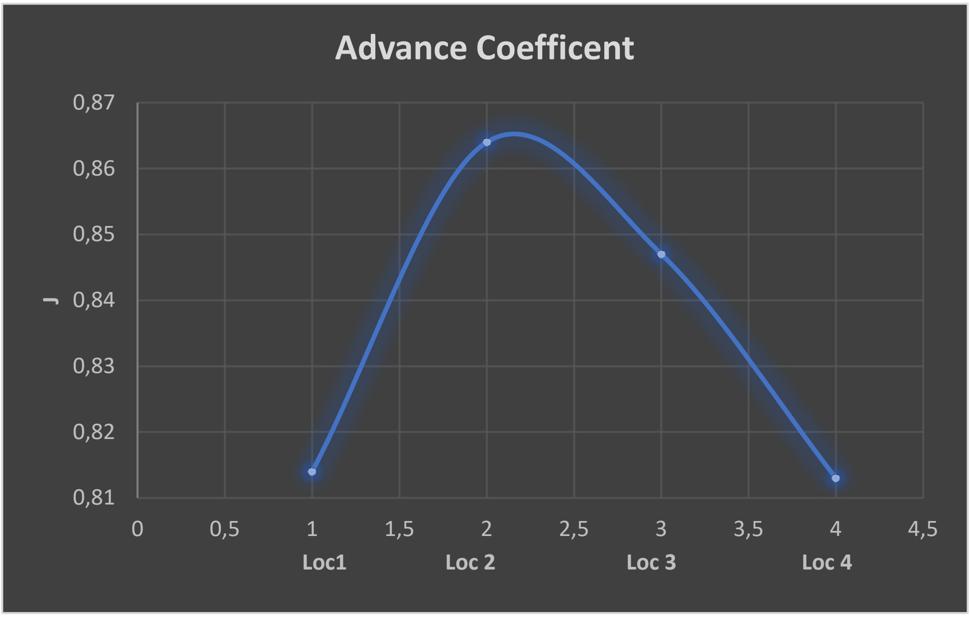

Figure 5 Plot of Advance Coefficient at various locations

4 CONCLUSIONS

After carrying out resistance and Self Propulsion Test, the effect on total Power Delivered was observed and tabulated. It was found that at Froude number of 0.14, 6.2% reduction in Delivered Power was observed. The plots were plotted for a range of Froude Number with or without Mewis Duct as ESD was drawn as:-

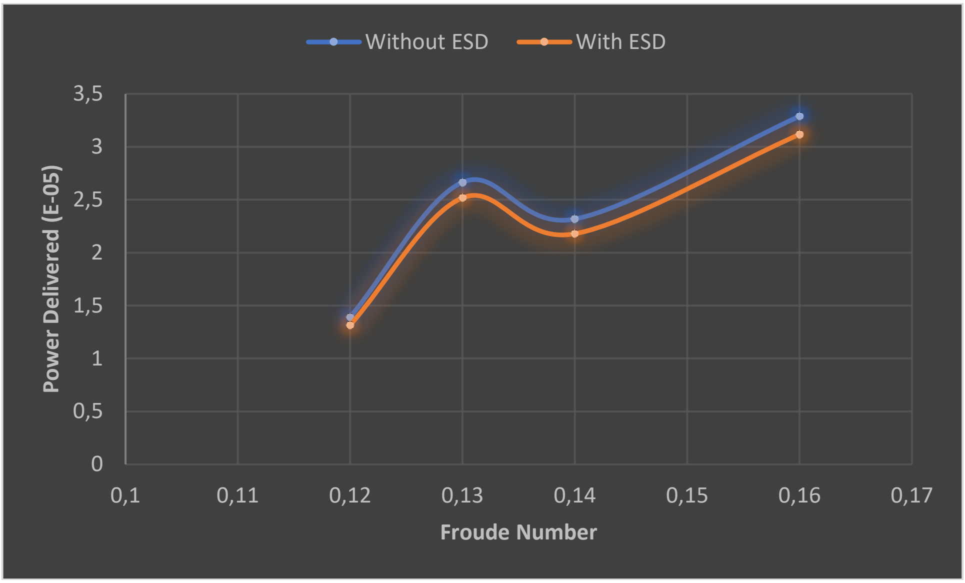

Figure 6 Plot of Total Energy Saving for a range of Froude Number

REFERENCES

[1] Tom van Terwisga, "On the working principles of Energy Saving Devices", Third International Symposium on Marine Propulsors smp'13, Launceston, Tasmania, Australia, 2013.

[2] F. Celik and M. Guner, "Energy saving device of stator for marine propellers", Ocean Engineering 2007.

[3] Friedrich Mewis and Thomas Guiard, "Mewis Duct® – New Developments, Solutions and Conclusions", Second International Symposium on Marine Propulsors smp'11, Hamburg, Germany, 2011.

[4] H. Narita, H. Yagi, H. D. Johnson and L. R. Breves, "Development and Full-Scale Experiences of a Novel Integrated Duct Propeller", SNAME Transactions, Vol. 89, 1981, pp. 319-346.

[5] L.X. Hou, C.H. Wangn , A.K. Hu and F.L. Han, "Wake-adapted design of fixed guide vane type energy saving device for marine propeller", Ocean Engineering 2005.

[6] Kadir Burak Korkmaz, "CFD Predictions of Resistance and Propulsion for the JBC with and without an Energy Saving Device", Sweden 2015.

[7] Shuling Chen, Beilei Zou, Changzhi Han and Shiqiang Yan, Comparative Study on Added Resistance and Seakeeping Performance of X-Bow and Wave-Piercing Monohull in Regular Head Waves, 2022.

[8] Zhirong Shen and Richard Korpus, "Numerical Simulations of Ship Self-Propulsion and Maneuvering Using Dynamic Overset Grids in OpenFOAM", Tokyo 2015.

[9] Keunjae Kim, Michael Leer-Andersen and Michal Orych , "Hydrodynamic Optimization of Energy Saving Devices in Full Scale", Australia 2014.

[10] Michal Orych , Sofia Werner and Lars Larsson, "Validation of full-scale delivered power CFD simulations", Sweden 2021.

[11] Michal Orych , Sofia Werner and Lars Larsson, "Roughness effect modelling for wall resolved RANS – Comparison of methods for marine hydrodynamics", Sweden 2022.

[12] Friedrich Mewis , “Six Years Mewis Duct® - Six Years of Hydrodynamic Development”, Sweden 2022.

[13] Jie Dang, “An Exploratory Study on the Working Principles of Energy Saving Devices (EDSs), CFD Investigations and ESD Design Guidelines”, Brazil 2012.

[14] Nobuyuki Hirata , “JBC Test Data in NMRI”, Tokyo 2015

[15] Callum Stark ,Yunxin Xu, Ming Zhang, Zhiming Yuan, Longbin Tao and Weichao Shi, “Study on Applicability of Energy-Saving Devices to Hydrogen Fuel Cell-Powered Ships” , Glasgow 2022.

SECURING CARGO IN CONTAINERS IN RELATION TO THE REQUIREMENTS OF THE CSC CONVENTION

Jarosław Soliwoda, dsc eng.

Polish Register of Shipping, POLAND, Gdynia Maritime University, POLAND

(E-mail: j.soliwoda@prs.pl, j.soliwoda@wn.umg.edu.pl)

Keywords: Cargo transport, Container, Safety of transport

ABSTRACT

The globalization of transport with the simultaneous containerization of transport generates a huge number of situations that result in cargo damage. The following article addresses the problems of structural uniformity of regulations and requirements for the transport of cargo in containers as well as ISO conventions and standards for container design. Possibilities of harmonization of regulations and requirements for securing cargo in a container to increase transport safety have been proposed.

1 INTRODUCTION

Changes in the transport structure of the last thirty years have resulted in the popularization of cargo transport in transport units such as containers. They dominated the transport of general cargo as well as are used in the transport of bulk cargo. Containerization of transport is dictated by the shortening of the time of reloading operations in container terminals and, in principle, the reduction of the costs of safe cargo storage. In addition, containerization transfers the responsibility for the correct placement of the cargo in the container and its fastening from the carrier to the packer of container. Each container should therefore be safe for all systems operating containers, such as ships, cars and semi-trailers, trains and reloading devices. On the other hand, the container should allow safe transport of cargo inside it. Therefore, it must be equipped with a load securing system.

This means that each cargo container approved for transport will be safe within the strength limits defined by its strength tests. Each transport container is also subject to regular inspection of its structure. In the event of damage exceeding the permissible size, the container cannot be used further without making the required repairs.

The confirmation of the technical condition of the container is the CSC plate placed on its door along with the date of its inspection.

The analysis of container transport and cargo damage shows that a significant percentage of containers (about 15%) transport cargo that is incorrectly fastened and a significant amount of cargo damage in containers (about 28%) is caused by their incorrect fastening. ("Container focus Preventing the loss of containers at sea", The Swedish Club, 2020). This is mainly due to two reasons: the desire to reduce the cost of cargo transport by reducing the cost of securing and the lack of knowledge about the possibility of securing the cargo inside the container.

2 LEGAL REQUIREMENTS

The 1972 International Convention on Safe Containers (CSC'72) introduced a framework of safety standards for the design, construction and use of containers for sea and land transport.

The CSC convention is supplemented by the ISO 1496 and ISO 1161 standards describing the strength parameters of the container structure. In addition, each state party to the convention may introduce separate regulations for containers in transport (Container Construction Regulations, PRS 2014, Supervision Regulations for Containers in Operation, PRS 2012).

Each container used in sea and land transport for the transport of cargo must be authorized by a designated institution. In Poland, it is the Polish Register of Shipping. Authorization includes consideration of the container documentation, supervision of prototype strength tests and acceptance of each manufactured container. Each container prototype receives a "Container Construction Type Approval Certificate".

In case of modification of existing containers, it may be subjected to further strength tests confirming its condition. An additional plate is placed on the container informing about the modification of the container.

The ISO 3874 standard presents the possibilities of handling the container in transport and methods of its attachment to the means of transport. It also contains basic information about the need to secure the load inside it and the required location of the center of mass.

In 1997, the International Maritime Organization (IMO), together with the International Labor Organization (ILO) and the United Nations Economic Commission for Europe (UNECE), provided guidelines for packing transport units (CTUs). In 2014, updates to the 1997 guidelines were presented. The updates were defined as a code of practice for the handling and packaging of cargo transport units intended for sea and land transport (CTU Code, MCS.1/Circ.1497). The CTU Code is an optional document, but in practice used as a basis for the safe transport of cargo in containers.

The CTU Code provides information and references on all aspects of loading and securing cargo in containers and in intermodal transport, taking into account the requirements of all types of sea and land transport. The CTU Code applies to transport operations in the entire intermodal transport chain and is a guideline not only for those responsible for packing and securing cargo, but also for those receiving and unpacking such units. The Code of Conduct also covers issues such as training and packaging of dangerous goods.

The CTU Code was supplemented with a document containing information and supplementary materials to the CTU Code (MCS.1/Circ.1498).

The CTU'2014 Code contains information on the strength of the container structure based on the scope of prototype strength tests performed in accordance with the CSC'1972 Convention.

3 CONTAINER STRENGHT TESTS

The CSC'72 Convention, Annex II, presents the requirements for the safety of container structures and the scope of strength tests to which the prototype is subjected. The prototype container is tested at an authorized Test Station under the supervision of a designated institution. The strength tests of the container are carried out with a load exceeding the permissible weight of the container with cargo. Depending on the test, the container is loaded from 1.6 to twice its permissible weight. Therefore, the strength limits of a transport container are defined by its GROSS WEIGHT. In the CSC and ISO standards, the maximum container weight is defined as Rating (R).

The scope of strength tests of the cargo container in relation to the possibility of securing the cargo includes:

1. Lifting test at the top and bottom corners with a total load of 2R.
2. Wall strength tests, frontal with a load of 0.4P (Payload), side with a load of 0.6P.
3. Floor load with a pressure of 7260 kg on the forklift axle.
4. Tests of cargo securing systems with a load of 150% of the nominal load.

The container passes the tests if it does not experience permanent deformations that prevent its safe transport. This means that the tests are performed for the plastic deformation limit of the container structure.

4 CARGO TRANSPORT UNIT CODE

The Cargo Transport Unit Code (CTU Code) presents the minimum requirements for the lashing system in accordance with the ISO 1496 standard. These requirements include the minimum number of lashing points in a given type of container and their minimum strength. In the used containers, there are the number of lashing points provided for by the standard and with higher strength in relation to the upper lashing points.

Over the years of the application of the CSC Convention and ISO standards, the permissible weight of containers has increased. Initially, it was 20,480 kg, while from 2022 it is 36,000 kg. Increasing the permissible weight of the transport container did not increase the strength of the fastening points inside it.

The CTU Code contains tables with recommended accelerations to which the load will be subjected during transport by various means of transport. The acceleration tables have been developed for three transport regions:

1. Region A - for waves with a significant height of up to 8 m, applies to the Baltic Sea, the Mediterranean Sea, the Black Sea, the Persian Gulf and the oceanic belt between the latitudes of 30°N and 35°S.
2. Region B - for a wave with a significant wave height of 8 m to 12 m, applies to the North Seas including the Skagerrak, Okhotsk, Japanese, English Channel and the oceanic belt between 35°S and 40°.
3. Region C – for a significant wave above 12 m, applies to other oceanic regions.
4. The load transported in the CTU should meet the conditions foreseen for the most unfavorable transport area.

The CTU Code presents the recommended methods of securing cargo in containers:

1. Blocking the load against the container structure using its frame and side, front and door walls,
2. Friction (press) fastening using the Top-Over method,
3. Lashing using methods: Spring, Straight and Half-Loop.

The person who packs the container should prepare such a fastening system that will optimally use the parameters of the container and the possibilities of the fastening system while protecting the load against damage. Unfortunately, a large variety of cargo transported in containers and a very large number of companies responsible for their packaging make it impossible to develop a uniform fastening scheme and the lack of real possibility to control the quality of cargo securing. The solution to this problem is to develop a clear scheme for the correct loading and securing of cargo in containers. The existing solutions proposed in the CTU Code do not solve this problem effectively enough.

The algorithm for verifying the correctness of loading the container should be two-stage. The first step is to check the load on the container, the second is to secure the load. In order to determine the loads and resulting forces, the means of transport of the container and its geographical region must be strictly defined. In the CSC convention, with regard to the strength tests of the container prototype, the maximum loads to which it is subjected are defined. The CTU Code presents these values as limit values. Strength tests are carried out under static loads, while the transport of the container is carried out under dynamic influences. With regard to the strength of the container frame, there is a safety factor of 2 (sf = 2) because the tests are carried out for loads twice as large as its permissible load. However, in relation to the walls of the container, such a load is used during the tests that will be used during the blocking of the load. The safety factor is 1. In addition, the wall load test is carried out with its even distribution. During the operation of the container, the walls are used to block the load significantly exceeding the loads that were used during strength tests. This results in frequent deformations of the container walls and weakening of their structure.

In the last decade, cargo in a container has been secured mainly by the use of webbing lashings, usually made of polyester. These are disposable belts cut to the appropriate length. This type of fastening allows for quick and effective fastening of various types of cargo in containers and at the same time does not cause damage to the cargo. However, it is characterized by a significant maximum stretchability of up to 7%. When tightening the lashing strap, it stretches up to 4%. This means that there is still the possibility of stretching the strap during the forces acting on the load. It is therefore a flexible fastening which may temporarily increase the load on the container walls if the load has been blocked against them.

5 PROPOSED REQUIREMENTS FOR SAFE CARGO TRANSPORTATION

In order to safely transport cargo in a container, two stages of actions presented below should be performed

Stage I - checking the container loads

1. Total load on the container – the weight of the cargo, dunnage and lashings must be less than the load capacity of the container – a requirement from the CSC convention.
2. Longitudinal bending moment of the container – the obtained bending moment of the entire container with cargo in its center must be lower than the allowable resulting from the strength tests carried out, from the test of lifting the container by the corners.
3. Transverse bending moment of the floor stiffeners – the obtained bending moment acting on the transverse elements stiffening the floor should be lower than the allowable resulting from the strength tests carried out, the corner lifting test and the floor loading test.
4. Local load on the floor – the load pressure must be lower than the permissible one resulting from the strength tests carried out, from the floor loading test. The load weight resulting from the maximum vertical accelerations during transport should be used for calculations.
5. Loading of the container walls – load pressure must be lower than the permissible one resulting from the strength tests carried out, from the load test on the side walls. The load pressure should be calculated on the actual contact surface of the load with the container wall.

Stage II - checking the securing of the load

1. Determination of the friction force, taking into account the material from which the container floor is made and the base of the load received into it, as well as vertical acceleration of the load, especially in sea transport.

2. Determination of the forces securing the movement in the longitudinal and transverse directions by using lashings.
3. Determination of the locking forces from the container walls when used to lock the load.
4. Determination of anti-tipping moments from the weight of the load, taking into account vertical accelerations.
5. Determination of anti-tipping moments by using lashings.

Problems to solve in order to improve the safety of cargo transport in containers

1. The load locally overloads the container floor
2. The permissible bending moment of the entire container is exceeded
3. Load securing is insufficient due to the limited strength and number of attachment points.
4. Lashing straps with a strength exceeding the strength of the lashing points in the container are used for lashing. The tensioning force of the lashing straps reaches or even exceeds the permissible load on the lashing points.
5. The walls of the container are used for fastening up to the strength limit tested during the container prototype tests.
6. The load is spread against the walls of the container leaning against them locally with much greater force than in the prototype
7. The load is blocked using the corrugation of the container walls.
8. The load is blocked by means of securing devices nailed to the floor of the container
9. The coefficient of friction between the load and the floor is not fully verified.

Table 1

Verification parameters of the permissible load of the container from the cargo for an example of a standard 40' AAA, 42G1 container:

No	Description	Condition	Strength parameters
1.	Payload	$p \leq P$	28.20 t
2.	Linear floor load	$q_l \leq q_{lperm}$	2.88 t/m
3.	Floor area load	$q_a \leq q_{aperm}$	1.44 t/m^2
4.	Container longitudinal bending moment	$BM_L \leq BM_{Lperm}$	48.00 tm
5.	Transverse bending moment of floor stiffeners	BMB_1m ≤BMBperm_1m	2.25 tm
6.	Strength of front and door walls	$q' \leq q_{perm}$	1.44 t/m^2
7.	Sidewall strength	$q' \leq q_{perm}$	0.43 t/m^2
8.	Strength of lashing points	LC≤MSL	1 t/point

The solution to the presented problems may be the implementation of the following recommendations:

1. Defining the safety factors in relation to loading of the container structure by cargo during its transport.
2. Introduction of changes in ISO Standards regarding the strength of fastening systems, introduction of systems with greater strength.
3. Introduction of internal marking of the container (on the door) informing about the strength of the fastening systems and information about friction coefficients.
4. Introduction of internal marking of the container (on the door) informing about the permissible floor load in relation to its local strength and the entire container structure.

Fulfillment of the above requirements will make it possible to standardize the processes of designing loading and securing cargo in containers. It will also reduce the cost of cargo damage. It will also reduce the chances of damage to the containers themselves

REFERENCES

[1] Code of Practice for Packing of Cargo Transport Units (CTU Code)'2014, IMO/ILO/UNECE,

[2] International Convention for Safe Containers (CSC)'72, IMO 1972.

[3] Norm ISO EN 668.

[4] Norm ISO EN 1496.

A 3D ANALYTICAL MODEL FOR THE INTERACTION OF WATER WAVES WITH AN OSCILLATING BREAKWATER

Sebastian Sorek[1] and Wojciech Sulisz[2]

[1, 2] Department of Wave Mechanics and Structural Dynamics, Institute of Hydro-Engineering of Polish Academy of Sciences, POLAND.

(E-mail: s.sorek@ibwpan.gda.pl, sulisz@ibwpan.gda.pl)

Keywords: 3D models, analytical models, hydrodynamics, wave flume verification, wave modelling,

ABSTRACT

An analytical 3D model of nearshore hydrodynamics was derived. A shore protection structure working as an oscillating-type breakwater capable of energy production was defined and implemented into the solution. The model was used to obtain incident, reflected, and transmitted waves and hydrodynamic loads acting on the device. Experiments conducted in a wave flume validated the kinematics predicted by the model.

1 INTRODUCTION

Modelling hydrodynamics and wave-structure interactions is essential for coastal and offshore engineering. Many numerical models can be applied to solve these problems. However, 3D analytical solutions to this problem are very rare. A solution to this problem is of significant importance to engineers and scientists because it can be applied to describe wave interaction with wave energy converters or novel-type breakwaters for shore protection.

In this work, a 3D boundary-value problem for the interaction of water waves with an oscillating breakwater is formulated and an analytical solution is achieved. The derived model is applied to predict near- and far-field solutions. Hydrodynamical force and momentum are calculated. Model kinematics are verified in wave flume experiments. Finally, the prospects of further developing the model are discussed.

2 METHODOLOGY

The analytical model is derived on the basis of the potential wave theory, with all its assumptions [1], [2]. The boundary conditions for the model comprise the kinematic and dynamic boundaries at the still water level, the kinematic boundary condition at the structure and at the sea floor, and the radiation boundary conditions. To obtain a solution, the Taylor series expansion technique and the perturbation method are applied [3]. In further analysis, only the first-order solution of the perturbation method and the spatial variables are used. The geometry and parameters of the breakwater structure are defined. The equation of motion of the device is formulated and implemented into the model. The incident, transmitted, and reflected velocity potentials are derived.

To verify the model, laboratory experiments were conducted in the wave flume of the Institute of Hydro-Engineering of the Polish Academy of Sciences in Gdańsk. A wave gauge was installed in the wave flume to measure free-surface oscillations. A set of 5 regular waves of lengths from 1.6 to 7.2 m and wave periods from 2.15 to 5.03 s were generated for water depth settings of h = 0.4 m and h = 0.6 m. The Fourier analysis was applied to the obtained experimental data to compare them with those calculated in the model.

3 RESULTS AND DISCUSSION

The derived original 3D analytical solution was applied to determine the amplitudes, hydrodynamic force, and momentum acting on the oscillating device. The loads were calculated by integrating the dynamic pressure acting on the structure for a broad spectrum of wave conditions and a wide range of mass and stiffness of the device. The results show that the wave loads and amplitudes increase with increasing wave lengths. In general, the stiffness of the system has a significant effect on the wave loads and amplitudes, while the effect of mass is less pronounced. Wave loads increase and structure oscillation amplitudes decrease with the increasing stiffness, while with the increasing mass of the structure, wave loads decrease and structure oscillation amplitudes increase.

The radiated waves predicted by the analytical model were compared with experimental results. The difference between the theoretical results and experimental data was less than 5 % in all but one instance. The theoretical model predicts experimental results with sufficient accuracy. According to widely validated and recognized Haskind relations [4], this outcome also verifies forces obtained from the derived model.

The future development of the model is discussed. The stage of implementation of an inclined sea bottom, wave breaking, and wave runup into the model is described. The method of verification and the first results are presented.

4 CONCLUSIONS

An original 3D analytical model for wave interaction with a novel oscillating-breakwater was presented. The derived model is applied to predict near- and far-field solutions. The wave loads acting on the structure were determined. Laboratory experiments were conducted in a wave flume to verify the derived analytical model. The obtained results provided sufficient validation of the model. Further opportunities for developing the model are identified and discussed.

REFERENCES

[1] Wehausen J.V., Surface Waves, Handbuch der Physik 9, Springer-Verlag, Berlin, 1960, 446-778.

[2] Kinsman B., Wind Waves, Prentice-Hall Inc., Englewood Cliffs, New Jersey, 1965.

[3] Sulisz W., Application of Boundary Element Method to the modeling of wave powered plant, Proc. of Annual Symposium of the International Association for Boundary Element Methods, Santiago, 2013.

[4] Haskind M.D., The exciting forces and wetting of ships in waves, Izv.Akad.Nauk SSSR, Otd.Tekh.Nauk, 7(7), 1957, 65-79.

UNDERWATER NOISE GENERATED BY SHIP TRAFFIC IN THE POLISH BALTIC WATERS – RESULTS OF THE BIAS EU PROJECT

J. Tęgowski[1] and K. Trzcińska[1]

[1] Faculty of Oceanography and Geography, University of Gdańsk, POLAND

(E-mail: j.tegowski@ug.edu.pl, karolina.trzcinska@ug.edu.pl)

Keywords: Baltic Sea, ship traffic, underwater noise

ABSTRACT

This paper presents the results of a study of underwater noise emitted by ships in the Baltic Sea in 2014. In the framework of the "Baltic Sea Information on the Acoustic Soundscape - BIAS" project, 38 hydroacoustic recorders measuring sound pressure levels were submerged by six Baltic countries. Regions of high anthropogenic sound intensity at 63 Hz and 125 Hz were mapped and underwater noise statistics were determined for the entire Baltic Sea area.

1 INTRODUCTION

Since the end of World War II, underwater noise levels in the oceans have increased significantly, mainly due to increased shipping. In enclosed seas such as the Baltic Sea, the intensity of noise caused by ship traffic has a major impact on the vital functions and behaviour of marine animals, possibly leading to changes in their behaviour and even to death. Reducing the intensity of underwater noise generated by ships is of interest to the European Commission, which has issued a Marine Strategy Framework Directive recommending monitoring of underwater noise at regional scales. Underwater noise has become the focus of numerous international organizations (e.g., HELCOM and IMO). The International Maritime Organization is working to introduce regulations for ship construction and navigation leading to a reduction of the level of underwater noise generated by ships. The EU Life+ BIAS project has mapped underwater noise of anthropogenic origin throughout the Baltic Sea. The knowledge gained in the project enables organizations that monitor marine pollution to introduce regulations that reduce the level of underwater noise generated by ship traffic.

2 METHODOLOGY

The BIAS project [1, 3] deployed a total of 38 acoustic recorders throughout the Baltic Sea to measure underwater noise levels throughout 2014. In the area of the Polish exclusive economic zone, 5 recorders (Fig.1) SM2M from Wildlife Acoustics were submerged at depths of 12m to 85m, measuring ambient noise continuously at sampling frequencies of 24kHz and 96kHz and a dynamic range of 16 bits. The recorded signals were filtered through one-third octave bandpass filters at 63Hz and 125Hz to detect ship noise, according to EU recommendations. Wind speed and direction were also measured for the two deployment sites. In addition, ship traffic information from AIS and VMS systems was taken into account, making it possible to separate shipping noise from noise generated by geophysical phenomena in the sea.

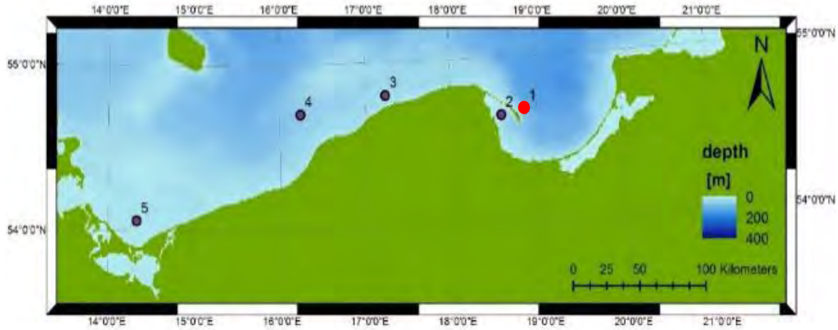

Figure 1 Deployment of hydroacoustic recorders in the Polish Baltic Sea area.

3 RESULTS AND DISCUSSION

An example of continuous underwater ambient noise registration lasting 12 hours and 25 minutes by recorder number 1 (Figure 1, red dot), on June 11th, 2014 is shown in Figure 2.

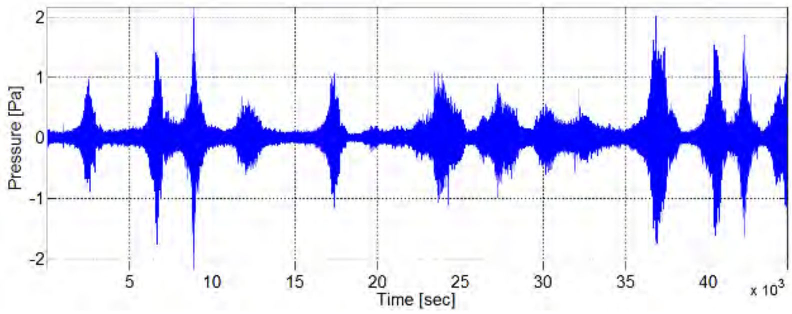

Figure 2 Example of continuous underwater ambient noise registration by recorder number 1 on June 11th 2014.

More than a dozen ships passing at different distances were recorded near hydroacoustic buoy No. 1, causing the sound pressure to rise to 2 Pascals. The signal spectrum from Fig.2 is shown in Fig.3 with the 63 Hz and 125 Hz frequencies well extracted. These are the evident frequencies

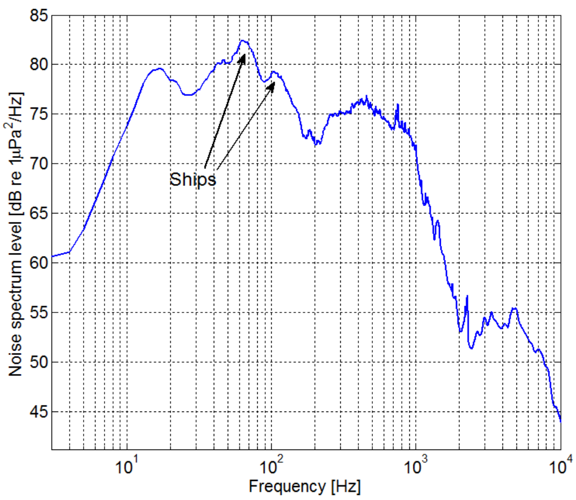

Figure 3 Averaged underwater noise spectrum as seen from Fig.2 with 63 Hz and 125 Hz frequencies emitted by passing vessels indicated.

corresponding to the noise emitted by moving ships.

The main metric in the measurement of underwater noise levels is the Sound Pressure Level (SPL) calculated for 1/3 octave bands, where in our case the center frequencies of the filter were 63 Hz and 125 Hz [2], as follows:

$$SPL = 10 \cdot log_{10} \frac{1/_T \int_0^T p(t)^2 dt}{p_0^2} = 10 \cdot log_{10} \left(\frac{p_{rms}}{p_0}\right)^2 = 20 \cdot log_{10} \left(\frac{p_{rms}}{p_0}\right) \quad [\text{dB re } 1\ \mu\text{Pa}],$$

where p(t) – sound pressure in [Pa], T – integration time in [s], p_0 = 1 μPa – reference pressure.

The main source of natural environmental sounds in the seas is a noise generated by breaking waves. At sea states greater than 3B, underwater noise generated by waves increases. However, noises emitted by ships at certain characteristic frequencies (e.g., 63 Hz and 125 Hz) are louder than natural ambient noise. This is evidenced by the results of the measurements shown in Figure 4. It presents sequentially the results of wind speed measurements in the vicinity of the hydroacoustic recorder 1 (Fig.1.) at Hel Marine Station, the number of ships within 5 km, 10 km and 15 km of the hydroacoustic buoy, $SPL_{63\text{Hz}}$ and $SPL_{125\text{Hz}}$.

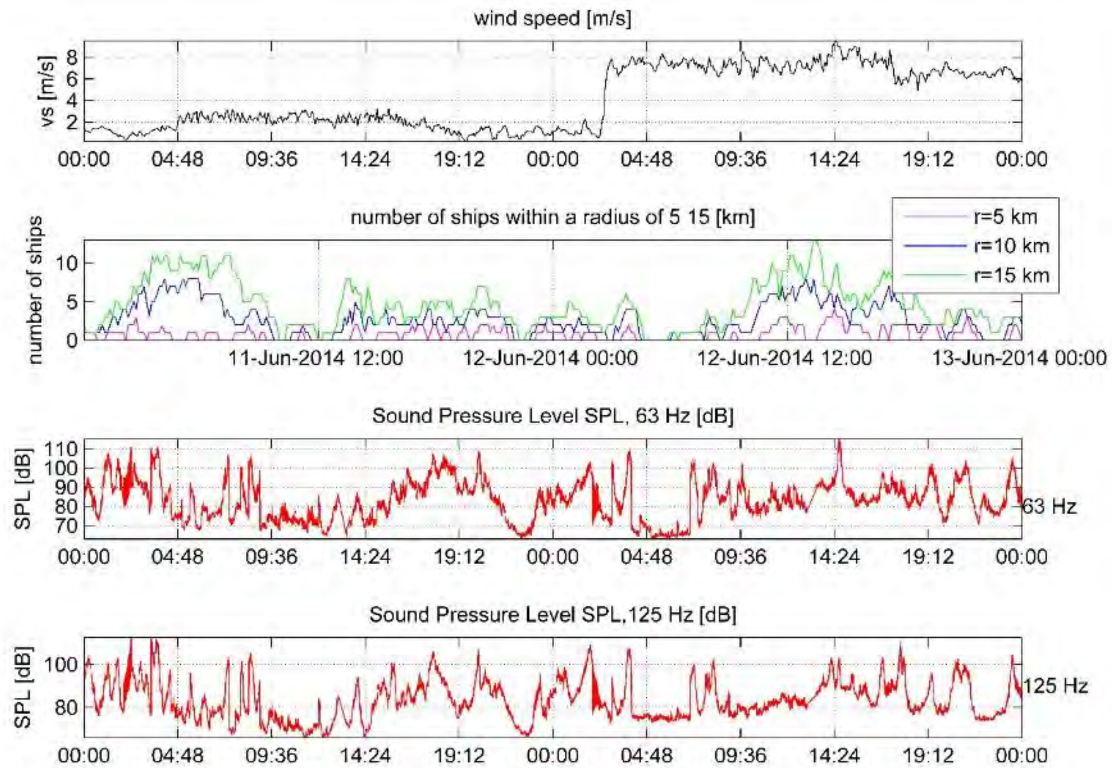

Figure 4 Averaged underwater noise spectrum as seen from Fig.2 with 63 Hz and 125 Hz frequencies emitted by passing vessels indicated.

The results showed here represent a 48-hour recording conducted over two days on June 11-12th, 2014. During the first measurement period up to about 2:00 a.m. on June 12th, the wind speed did not exceed 2 m/s, and then rapidly increased to a constant speed of about 8 m/s and remained at such level until the end of the measurement period. At the same time, the number of ships passing at different distances from the acoustic recorder fluctuated from 0 to 12.

The values of $SPL_{63\text{Hz}}$ and $SPL_{125\text{Hz}}$ depend strongly on the intensity of ship traffic and overall sea state. When the wind speed increases then after a few hours there is an increase in wave action, which generates an increase in noise of natural origin. However, despite the strong background noise, the 63Hz and 125Hz frequencies clearly show an increase in sound pressure when ships pass nearby.

4 CONCLUSIONS

The presented results of underwater sound measurements proves that underwater noise emitted by ships in the Baltic Sea is propagated over long distances and, despite the high level of natural sounds, is detected by hydroacoustic recorders. It can be a disturbing factor in the life processes of marine animals, and hence its reduction is the subject of work of international organizations involved in the reduction of marine pollution.

ACKNOWLEDGMENT

This work has been conducted under EC LIFE+ project No. LIFE11 ENV/SE/000841 and Polish National Fund for Environmental Protection and Water Management (NFEP&WM).

REFERENCES

[1] Sigray, P., Andersson M., Pajala, J., Laanearu J., Klauson, A., Tęgowski, J., Boethling, M., Fischer, J., Tougaard, J., Wahlberg, M., Nikolopoulos, A., Folegot, T., Matuschek, R., Verfuss, U., BIAS: A Regional Management of Underwater Sound in the Baltic Sea, Chapter in The Effects of Noise on Aquatic Life II, Advances in Experimental Medicine and Biology, Vol. 875, 1015-1023, 2016.

[2] Mustonen, M., Klauson, A., Andersson, M., Clorennec, D., Folegot, T., Koza, R. Pajala, J., Persson, L., Tegowski, J., Tougaard, J., Wahlberg, M., Sigray, P., Spatial and temporal variability of ambient underwater sound in the Baltic Sea, Scientific reports 9 (1), 1-13; 2019.

[3] Tęgowski J., Koza R., Pawliczka I., Skóra K., Trzcińska K. and Zdroik J., Statistical, spectral and wavelet features of the ambient noise detected in the southern Baltic sea, Vol.1, 1-6., Proc. of 23rd International Congress on Sound and Vibration (ICSV23), Athens, Greece, 10-14 of July, 2016.

NUMERICAL MODELING OF CONTAINERSHIP BEHAVIOUR ON WAVES TAKING INTO ACCOUNT THE WHIPPING AND SPRINGING PHENOMENA

M. Warmowska-Gadzińska, K. Wołoszyk

Research and Development Division, Polish Register of Shipping, POLAND
(E-mail: m.warmowska@prs.pl, k.woloszyk@prs.pl)

Keywords: hydrodynamics, simulation of ship motion, whipping and springing, elastic vibration of ship

ABSTRACT

The article describes simulations of ship motions on waves, taking into account whipping and springing phenomena, which have particular influence on the safety of container ships navigation. It indicates the selection methods of parameters of sea waves, which may cause the dangerous phenomena. The article presents the determination methods of the extent of the ship structure displacements during the ship motion on waves in result of free surface impact on ship's bow flare region or flat surface of stern. Simplified method describing forced vibrations of ship structure apply the forces determined by simulations with the use of time-domain seakeeping code.

1 INTRODUCTION

In the case of containerships moving with higher speeds, whipping and springing are dangerous phenomena which may lead to permanent deformation of ship structure or even hull girder collapse. Discussions are conducted in the international forum on the effects of those phenomena, of particular importance for a classification societies, such as Polish Register of Shipping (PRS). Up to now, some methods of prediction of those phenomena and their description were developed. The structural strength verification is performed on the basis of carried out numerical calculations. Complex simulations are being performed of the ship motion on waves with simultaneous analysis of structure vibrations due to rhythmic slamming of bow or stern elements on wave surface. The experimental studies are performed as well, to validate the proposed numerical tools.

Also PRS aims to create own tools and methods for modeling of such phenomena. In the years 2020-2022, PRS has performed analyses of the whipping phenomenon impact into vertical bending moment of the ship hull [1]. At the Gdańsk University of Technology, the master's thesis has been developed by a PRS employee [2], which was based on the performance of a series of calculations of the ship structure behaviour. To this end, dynamic analysis tool for FEM models was employed (Timoshenko beam model, explicit time-domain code, simplified description of strength parameters for five cross-sections of the ship). However, the slamming forces were calculated using simplified methods, without performing seakeeping analysis. Consideration of whipping forces accurately in simulation procedures and establishing own procedures for the description of forced vibrations of the hull structure has been the subsequent step.

2 METHODOLOGY

Simulations of ship behaviour on waves have been carried out for a head regular wave with the use of PRS own program – *ShipSimuationCalc*. Ship motion equations, which are the basis for the program procedures, are developed for the gravity centre of the ship in the inertial system moving with an average forward speed of the ship u_1. The ship is regarded as a rigid body [3]. During simulations, deformations of the ship structure due to forced vibrations are not taken into account. Calculations are carried out with the use of time-domain integration procedure, considering the use in future procedures for ship motion in irregular waves and possible including in equations non-linear phenomena associated with vibrations of the ship structure.

During numerical simulations of ship behaviour on waves, any information pertaining to forces and moments acting on the ship in particular cross-sections, has been recorded. Information on the motion components and waving parameters in the time domain has also been kept.

In the first step, analyses of natural vibrations of structure for the uniform beam model have been carried out. The ship has been analysed with the use of a beam of constant cross-section (the values of mass m, added mass $a33$, inertia moment of the structure cross-section I were independent of the beam cross-section's horizontal position). The issue has been precisely described in reference [4]. In this paper, only natural-frequency of two-node bending mode has been assumed.

Subsequently, the values of forces due to wave free surface impact on bow and stern, gained during simulation of ship motion on waves, have been taken into account in consideration of forced vibrations of the ship structure.

3 RESULTS AND DISCUSSION

Table 1 presents main data adopted in calculations made for a containership.

Table 1
Ship structure parameters

L_s – ship length [m]	B_s – ship breadth [m]	T_s – ship draft [m]	u_1 –ship velocity [knots]	E – Young module [N/m^2]
360	48.2	14.5	19	2.06E+11

For the analysis of whipping and springing phenomena, parameters defining structure strength (Young's modulus E, distribution of I section moments of inertia and m mass, an added mass a_{33} for zero wave period) were needed for ship description. Table 2 shows the mass and moments distribution for the ship divided into nine compartments with different average strength parameters of cross-sections.

Table 2
Distribution of mass, added mass and moments of inertia
of the cross-section for particular compartments

No	I [m4]	m [kg/m]	a_{33} [kg/m]
1	338,3	67610	40564
2	627,6	331158	72013
3	910	588712	114991
4	988,1	709990	119883
5	1040	736642	126099
6	1040	736054	125822
7	883	687101	118578
8	606,4	530711	100180
9	362,7	207375	37078

where *No* – number of compartment, *I* – an average value of the moment of inertia of cross-section in the compartment, *m* – mass in the compartment per a length unit, a_{33} – added mass of compartment per a length unit for infinite wave frequency.

3.1 Simulation of ship movement

The simulation of ship behaviour as a rigid body has been performed for the model depicting the ship hull surface with the use of about fifty thousand panels. For the head wave, the equations have simplified to three degrees of freedom: surge, heave and pitch.

The motion equations (1) consider external forces: F_K – Froud- Krylov force, F_D – diffraction force, F_R – radiation force

$$Mu'' + Bu' + Ku = F_K + F_D + F_R \tag{1}$$

where: M – mass matrix, B – damping matrix, K – stiffness matrix, u” – acceleration of the ship gravity centre, u’ – the vector of ship velocity, u – the vector of ship displacements and rotation.

Other forces, such as F_d – the force due to water on deck, F_s – the force acting on rudder, have been neglected in the motion equations.

Figure 1 shows the time history of the values of ship motion components for harmonic wave with period of *T*=15,44s and wave height of *H*=10m, velocity of ship *u1*=0[knots].

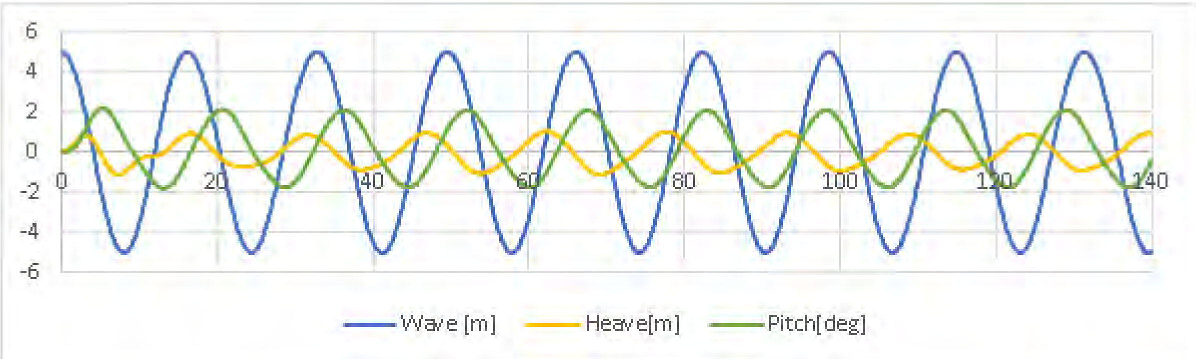

Figure 1 Components of ship motion in time domain, obtained in simulation

3.2 Analysis of natural vibrations for Euler beam

In the first step, the analysis of equations for natural vibrations of structure has been performed.

Assuming that the ship freely immersed in water will be described with the use of an uniform beam, i.e. with parameters: *m* – body mass per unit, a_{33} – infinite frequency of added mas in heave, *EI* – bending stiffness, that are constant in time and are independent of *x* – longitudinal coordinate of ship, the vertical deformations of beam *z*(*t,x*) are described by the equation:

$$(m + a_{33})\frac{\partial^2 z}{\partial t^2} + \frac{\partial^2}{\partial x^2}\left(EI\frac{\partial^2 z}{\partial x^2}\right) = 0 \tag{2}$$

Function *z*(*x,t*) of vertical deformation of the beam is to comply with boundary conditions of zeroing forces and moments at both ends of the beam.

Using the method of separating variables (assuming that displacement *z* is a product of two functions: amplitude function *a*(*t*) depending only on time and function *ψ*(*x*) depending only on longitudinal coordinate *x*):

$$z(t,x)=a(t)\ \psi(x) \tag{3}$$

general form of the equation solution (2) is received as follows:

$$\psi(x) = (\cosh(kL) + \cos(kL))\,(\cos(kx) + \cosh(kx)) + (\sinh(kL) + \sin(kL))(\sin(kx) + \cosh(kx)\,),$$

$$a(t) = \cos(\omega t).$$

At the adopted assumptions, the equation (2) defines the relation between the figure k and the frequency ω of natural vibrations of structure. The relation is defined by the formula:

$$(m + a_{33})\omega^2 = EIk^4 \tag{4}$$

The figure k is the own value of equation (4) and has to fulfill the equation (it follows form (2) and boundary conditions):

$$\cosh(kL) * \cos(kL) = 1 \tag{5}$$

There is not only one solution k of equation (5). In the paper it is assumed only two-node bending mode vibrations, with the highest vibration period T_d. Such two-node vibration occurs when:

$$kL = 1{,}50562\ \ldots\ [\text{rad}].$$

For the examined container ship length L equals to length of ship Ls and k is equal to about 0,013[rad/m].

Taking for the consideration the average values of: moment of inertia of cross-section I equal to 660m^4 and the sum of ship mass m and added mass a_{33} equal to 551604kg/m, the value of the two-node natural vibrations period T_d is equal to about 2,318 s, for the examined container ship.

From the formula (4), in the case of moment of inertia I changes within the range of 660-1060m^4, the natural vibrations period T_d takes values from 1,8s to 2,3s. For the cross-section moment of inertia I equal to 660m^4, increase or decrease of the value of the sum of mass and added mass by 20% caused that the period of natural vibrations has also changed to the range from 2,1s to 2,5s.

For the examined container ship, the value of the two-node natural vibrations period T_d may be taken as ca. 2,318s.

3.3 Forces of bow slamming on wave surface

The springing phenomenon is caused by oscillating slamming of water on the ship surface. Resultant forces depend on the position of ship panel in relation to water surface, position of the panel speed vector in relation to wave surface and the position of vector tangent to the wave in relation to ship panel surface.

Slamming forces are directly proportional to the square of vector being the projection of difference of panel and water particles speed to the direction of the vector normal to the panel. The forces depend also on the panel size. During the simulation, the slamming forces were calculated only for those panels which in the specified time step were above the wave surface, and in the following time step were at least partly covered by waves.

The ship structure has been divided along horizontal axis into 140 segments. For each of them, the values of forces resulting from free surface slamming by structure panels (the structure has been divided into 50 thousand panels) were summed up.

The period of wave T equal to 2s does not force significant motions of such big ship, what was proved by simulations. According to probability distribution of waves occurrence on the North Atlantic [5], the significant wave height for the mean period of zero-crossing equal to 2s is not higher than 1m.

The water speed u_w on water surface of regular wave can be obtained from equation:

$$|u_w| = \frac{2\pi}{T} A \tag{6}$$

For harmonic wave of amplitude A equal to 0,5 m and wave period T equal to 2 s, water speed u_w on water surface (6) does not exceed 1,6 m/s.

With the ship moving with a speed of 19 knots on a head wave with wave period equal to 5,24 s, the encounter period of wave would be equal to natural vibration period. In such case, wave of maximum height of 3 m may be expected, therefore the speed of particles on the surface of free wave may be estimated to 1,8 m/s.

In the case of reducing ship speed, the period of the wave, whose encounter period will be equal to the natural vibration period, will also reduce. In result, the value of maximum amplitude of wave and the speed of bow slamming onto the wave will reduce.

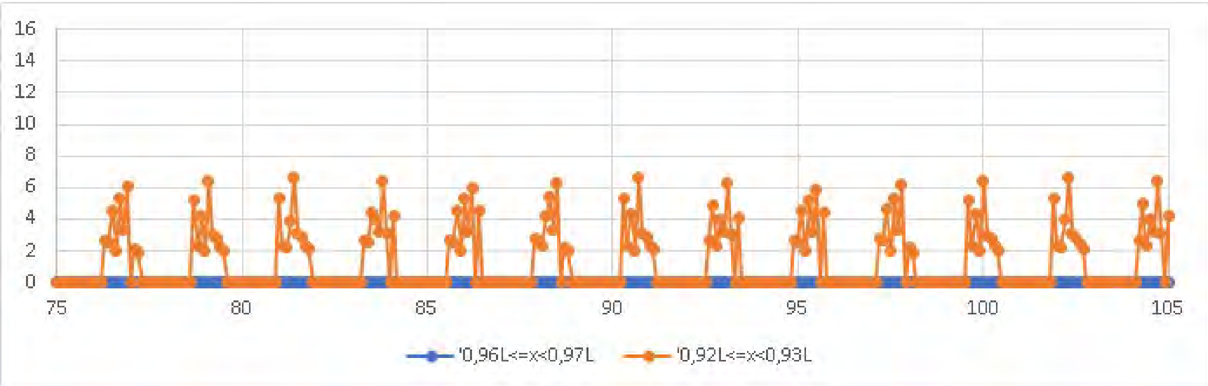

Figure 2 Distribution of the sum of forces [kN] acting on two forward parts of the ship, u_1=19knots, T=5,24s, H=3m

Unfortunately, in result of introduction of forward speed, the equations describing the elastic vibration issue will take more complex formula [4].

Calculations for the ship of zero mean forward speed have been also performed. High values of forces due to bow slamming on wave will occur for waves of length within 1,1 to 1,4 of ship's length, when the ship will perform fast and sudden moves. Simulations for waving period equal to 5-period of natural vibrations, ca 13,93 s, have been performed. For such wave, waves even up to 12 m high may be observed and, in result, water particles on free surface move with a speed of above 2,71 m/s. When comparing Figure 2 and Figure 3 it may be found that the forces have increased even by 5 times.

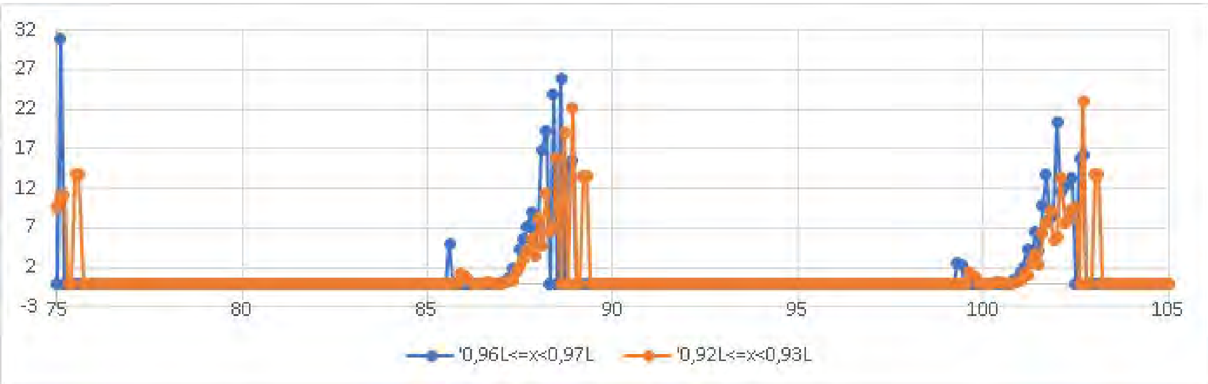

Figure 3 Distribution of sum of forces [kN] (in time domain) acting on two forward parts of ship, u_1=0 knots, T=13,93, H=12m.

3.4 Forced vibrations due to external forces

When considering non-uniform mode for a uniform beam:

$$(m + a_{33})\frac{\partial^2 z}{\partial t^2} + \frac{\partial^2}{\partial x^2}\left(EI\frac{\partial^2 z}{\partial x^2}\right) = f_v(x,t) \tag{7}$$

At the right-side of equation (7), non-zero external forces $f_v(x,t)$ appear, which define forces due to wave slamming and pressure onto ship's bow.

In this case, assuming that the solution $\psi(x)$ of structure two-node natural vibrations is known, see equation (3), the solution for function $a(t)$ shall be found

$$\frac{\partial^2 \mathrm{a}}{\partial \mathrm{t}^2} + \omega^2 \mathrm{a} = \mathrm{F_v(t)} \tag{8}$$

where function F_v is derived from the formula:

$$\mathrm{F_v(t)} = \frac{\int \mathrm{f_v(x,t)}\psi(\mathrm{x})\,\mathrm{dx}}{\int(\mathrm{m}+\mathrm{a}_{33})\psi^2(\mathrm{x})\mathrm{dx}} \tag{9}$$

After applying the values of forces f_v acting on the ship's bow or stern, calculated in simulations, the values of deformations caused by natural vibrations of structures due to bow and stern slamming onto head wave may be obtained. It is, however, not easy to predict when the structure can be subject to such enforcements.

For the already considered case when the ship will move at a speed of 19 knots on the wave of wave period 5,24s, the forces due to bow slamming onto wave appears by ca. 0.25 of natural vibration period T_d and may cause natural vibrations (Figure 4). In the second case (ship motion with zero speed and wave period equal to six times of natural vibration period), the time of slamming is too long to induce natural vibrations of structure, although the slamming force is much greater (Figure 5).

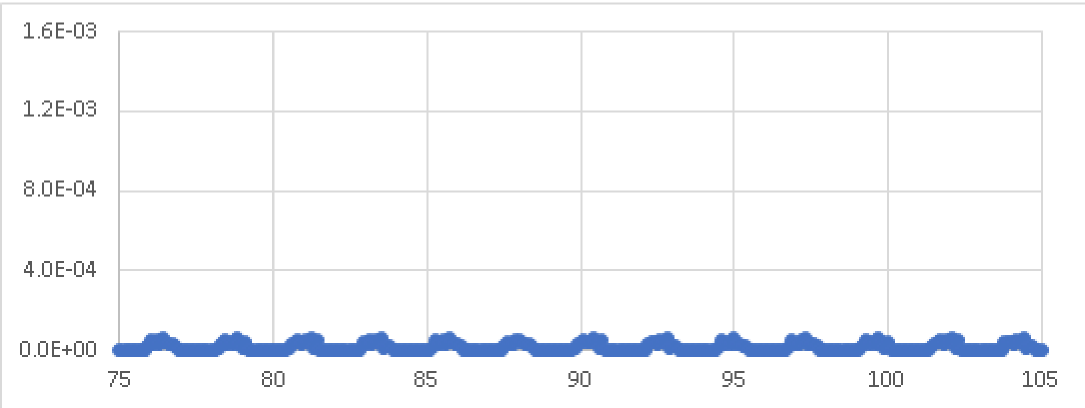

Figure 4 Change in time-domain of the values of $\mathrm{F_v}$ acting on ship's bow in the case of harmonic waves of wave period T=5,24 s and at wave height H=3m, and ship speed u_1=19 knots.

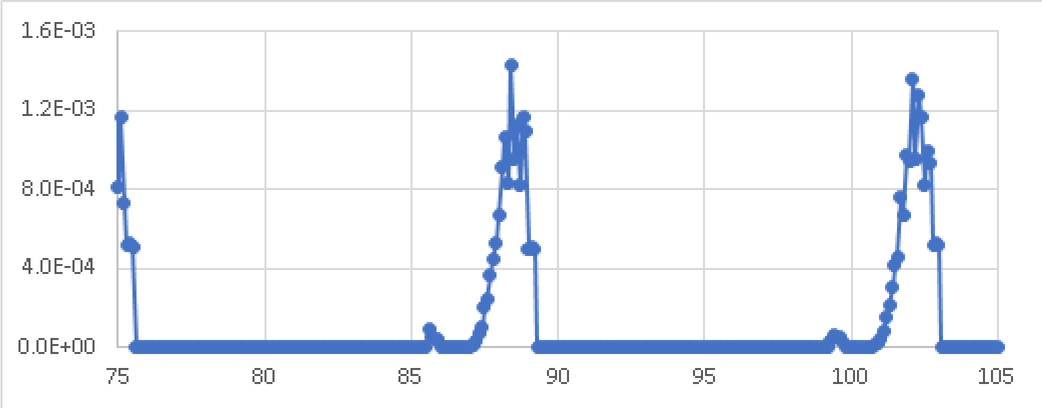

Figure 5 Change in time-domain of the values of forces Fv acting on ship's bow in the case of harmonic waves of wave period T=13.93 s and at wave height H=10m, and ship speed u_1=0 knots.

The obtained from numerical calculations forces, due to slamming onto ship's bow, are the basis for definition of the values of structure deformations when simple models describing natural vibrations issues are applied. It's obvious, that with considered simplifications, the deformation values are significantly overestimated. The vibrations will be damped by changes of strength parameters of structure and changes in time-domain of the value of added mass and in occurrence of irregular wave.

4 CONCLUSIONS

Performed calculations prove the possibility of appearing springing phenomenon at ship service, which causes considerable increase of bending moments acting on ship structure. The cases of fast move of ship on wave with encounter frequency close to ship natural vibration frequency are particularly dangerous. In such cases, relative speed of wave motion against ship hull increases, and it in result increases the force of wave slamming onto the structure elements.

Introduction of structural changes in the ship's plating increasing hull bending rigidity will only slightly affect the values of natural vibrations but it has effect on the size of hull structure deformations. The forces of slamming onto the hull structure do not depend on used structure materials. Similarly, immersion of the ship will cause the change of its added mass, but the changes will not considerably influence the values of the structure natural vibrations frequency.

Procedures have been developed for determination of structure deformation caused by natural vibrations in the case of applied Euler-Bernoulli beam model and taking simplified assumptions. Calculations of forces acting on the items of ship's bow or stern and the values a_{33}, performed during simulations, were used as parameters for the calculation of natural vibrations. Slamming of wave free surface on ship's bow, observed during simulations, may result in enforcing natural vibrations.

In the next step, the forces acting on the whole ship at its motion in waves changing in time-domain shall be considered in equations for vibrations of hull structure. The last step will consist in including procedures for calculation of structure deformations due to the structure natural vibrations in simulations of ship's motions in waves and estimating differences in the values of gained stresses in structural components.

ACKNOWLEDGMENT

The article has been developed within internal activities carried out in the Research and Development Division of Polski Rejestr Statków.

REFERENCES

[1] Jankowski, J., Bogdaniuk M., Wołoszyk K., Whipping contribution to the vertical bending moment, PRS Internal Report, 2021

[2] Roch E., Analysis of ship hulls vibrations of springing and whipping types, Master's thesis, Gdańsk University of Technology, 2021

[3] Pawłowski, M., Równania ruchu okrętu (Ship Motion Equations), PRS Technical Report, 2002

[4] Faltisen O., Hydrodynamics of High-Speed Marine Vehicles, Cambridge University Press, 2009.

[5] IACS Unified Recommendation Rec 34 Standard Wave Data – Rev.2 Dec 2022 Complete Revision.

[6] Qibin Wang i inni, Hydroelastic analysis of CSSRC 20,000 TEU ultra large containership in time domain, Conference material, 2017

UNDERWATER NOISE ISSUES

M. Weryk[1]

[1] Maritime Advanced Research Centre (CTO S.A.), POLAND.

(e-mail: mateusz.weryk@cto.gda.pl)

Keywords: Underwater noise, environmental issues

ABSTRACT

The problem of the environmental impact of transportation is, nowadays, a crucial topic. In the maritime industry the assessment of the noise impact of ships is quite a new challenge especially for non-military vessels. The effects that the underwater noise emissions can have on the marine fauna are proven to be significant. This aspect is directly correlated to the increase of the diffused background noise in the oceans due to the widespread increase of the shipping traffic. This topic is well known to Classification Societies which establish and apply technical requirements for the design, construction and operational maintenance of ships and marine structures. As a next step IMO has been working on the draft guidelines for minimizing underwater radiated noise (URN). The draft revised guidelines provide an overview of approaches applicable to designers, shipbuilders and ship operators to reduce the underwater radiated noise of any given ship. They are intended to assist relevant stakeholders in establishing mechanisms and programmes through which noise reduction efforts can be realized.

1 INTRODUCTION

Underwater noise pollution is a growing concern that is often overlooked. Anthropogenic noise, caused by human activities such as shipping, construction, and military sonar, can have negative impacts on marine life. These impacts include behavioral changes, hearing damage, and even death. The objective of this study is to investigate the current standards set by classification societies for reducing underwater noise pollution and to suggest future work in this area.

2 CLASSIFICATION SOCIETIES - STANDARDS

Classification societies have set standards to limit the noise generated by vessels and offshore structures. These standards include guidelines for designing quieter ships, reducing underwater noise from drilling and seismic surveys, and reducing noise from shipping operations. There is a number of EU Projects which were established for underwater noise emission reduction (i.e. AQUO, SILENTV, etc). One example is the International Maritime Organization's (IMO) guidelines on reducing underwater noise from commercial shipping. These guidelines include measures such as reducing ship speed, improving hull design, and using sound-absorbing materials. Another example is the American Bureau of Shipping (ABS) classification society, which has developed noise emission standards for offshore platforms. Bureau Veritas established additional class notation URN related with underwater radiated noise emitted by any self-propelled ships. It aims at managing and mitigating acoustical impact on marine fauna. This notation covers both shallow and deep waters.

3 FUTURE WORK

Despite the progress made by Classification Societies, more work needs to be done to reduce underwater noise pollution. One area for future work is the development of quieter propulsion systems, such as electric or hybrid engines, for use in ships and offshore structures. Another area is the improvement of acoustic monitoring and modeling tools, which can help to identify noise sources and predict the impact of noise on marine life. Additionally, there is a need for continued research on the effects of underwater noise on marine ecosystems and the development of effective mitigation measures.

4 CONCLUSIONS

Underwater noise pollution is a growing concern that can have significant impacts on marine life. Classification societies have set standards to limit the noise generated by vessels and offshore structures, but more work is needed to reduce noise pollution. Future work in this area includes the development of quieter propulsion systems, improvement of acoustic monitoring and modeling tools, and continued research on the effects of noise on marine ecosystems. By working together, we can create a quieter and healthier underwater environment for marine life.

REFERENCES

[1] Weryk, M., Kozaczka, E.,Grelowska G., Study of Noise Propagation for Small Vessels, Archives of Acoustics, Vol. 40, No. 2, pp. 267–272 (2015).

[2] Weryk, M., Szkudlarek, W., Underwater Radiated Noise Measurements in Shallow Waters., European Acoustic Association - Forum Acusticum, Krakow, Poland, 2014, pp. 52–62.

[3] Bureau Veritas, Underwater Radiated Noise (URN), July 2018, Rule Note NR 614 DT R02 E

Polish Register of Shipping

Head Office:

Polski Rejestr Statków S.A.
al. gen. Józefa Hallera 126
80-416 Gdańsk, Poland

tel: +48 58 346 17 00
+48 58 751 11 00
fax: +48 58 344 99 33
e-mail: mailbox@prs.pla

Gdańsk University of Technology

Faculty of Mechanical Engineering and Ship Technology:
Gdańsk University of Technology
ul. Gabriela Narutowicza 11/12
80-229 Gdańsk, Poland

tel: +48 58 347 20 32